AN ALGORITHM FOR DESIGNING NONLINEAR SPRINGS, OR NONLINEAR DAMPERS, USING A MECHANICAL FORCE GENERATOR AND ITS APPLICATION TO AN AIRCRAFT LANDING GEAR

A THESIS SUBMITTED TO
THE GRADUATE SCHOOL OF NATURAL AND APPLIED SCIENCES
OF
MIDDLE EAST TECHNICAL UNIVERSITY

BY

FATİH YILDIZ

IN PARTIAL FULFILLMENT OF THE REQUIREMENTS
FOR
THE DEGREE OF MASTER OF SCIENCE
IN
MECHANICAL ENGINEERING

DECEMBER 2021

Approval of the thesis:

DESIGN AND ANALYSIS OF AIRCRAFT LANDING GEAR BY USING DYNAMICALLY FAVOURABLE OVER-CONSTRAINED MECHANISMS

submitted by **FATİH YILDIZ** in partial fulfillment of the requirements for the degree of **Master of Science** i**n Mechanical Engineering Department, Middle East Technical University** by,

Prof. Dr. Halil Kalıpçılar
Dean, Graduate School of **Natural and Applied Sciences** _____

Prof. Dr. M. A. Sahir Arıkan
Head of the Department, **Mechanical Engineering** _____

Prof. Dr. Reşit Soylu
Supervisor, **Mechanical Engineering, METU** _____

Examining Committee Members:

Assoc. Prof. Dr. Ergin Tönük
Mechanical Engineering, METU _____

Prof. Dr. Reşit Soylu
Mechanical Engineering, METU _____

Prof. Dr. Yiğit Yazıcıoğlu
Mechanical Engineering, METU _____

Assist. Prof. Dr. Osman Gökhan Özgen
Mechanical Engineering, METU _____

Assist. Prof. Dr. Kutluk Bilge Arıkan
Mechanical Engineering, TED University _____

Date: 03.12.2021

I hereby declare that all information in this document has been obtained and presented in accordance with academic rules and ethical conduct. I also declare that, as required by these rules and conduct, I have fully cited and referenced all material and results that are not original to this work.

Name, Surname: Fatih Yıldız

Signature:

ABSTRACT

AN ALGORITHM FOR DESIGNING NONLINEAR SPRINGS, OR NONLINEAR DAMPERS, USING A MECHANICAL FORCE GENERATOR AND ITS APPLICATION TO AN AIRCRAFT LANDING GEAR

Yıldız, Fatih
Master of Science, Mechanical Engineering
Supervisor: Prof. Dr. Reşit Soylu

December 2021, 186 pages

The landing gear system is one of the most critical aircraft sub-systems that takes part in the landing, taxi and take-off phases of every aircraft. Its main function is the absorption of part of aircraft's kinetic energy during landing. There are different types of shock absorbers to perform this task. The performance of the shock absorbers has developed a lot after the invention of air-oil type shock absorbers. However, increasing the performance of these shock absorber elements is still a field of research followed by companies and institutions.

Mechanical Force Generators, on the other hand, are novel over-constrained mechanisms that are known for low friction and shaking force properties. A very important property of Mechanical Force Generator is being flexible to be designed for any required force characteristic.

This thesis study consist of mainly three sections. Firstly, a design methodology for Mechanical Force Generator design is developed. For this design methodology, Mechanical Force Generator has been considered for two different purposes: a non-linear equivalent spring and a non-linear equivalent damper. Then, spring mass

damper model was developed for landing gear modeling. This model is validated against the results of a test performed by the National Advisory Committee for Aeronautics. Using a spring mass damper model, an optimization is sought on the landing gear used in this test. The methods and approaches to find the optimum spring and damper characteristics are explained. In the last, using the optimum spring damper characteristics determined in the optimization, the design of Mechanical Force Generator is followed for the landing gear. The applicability and feasibility of the design on landing gear are presented and discussed. Throughout the study, special properties of Mechanical Force Generator are investigated, and different areas it may be utilized are evaluated and recommended at the end of the study.

Keywords: aircraft landing gear, shock absorber efficiency, mechanical force generator

ÖZ

MEKANİK KUVVET JENERATÖRÜ KULLANILARAK LİNEER OLMAYAN YAY VE LİNEER OLMAYAN DAMPER TASARIM ALGORITMASI VE UÇAK İNİŞ TAKIMINA UYGULANMASI

Yıldız, Fatih
Yüksek Lisans, Makina Mühendisliği
Tez Danışmanı: Prof. Dr. Reşit Soylu

Aralık 2021, 186 sayfa

İniş takımı sistemi, çoğu uçakta bulunan ve uçağın iniş, taksi ve kalkış aşamalarında görev alan, en kritik uçak alt sistemlerinden biridir. Bu sistemin ana fonksiyonlarından biri, iniş sırasında uçağın kinetik enerjisinin bir bölümünü sönümlemektir. Bu görevi yerine getirmek için farklı tiplerde şok sönümleyiciler bulunmaktadır. Şok sönümleyicilerin performansı, hava-yağ tipi şok sönümleyicilerin bulunmasından sonra çok gelişmiştir. Buna rağmen, şok sönümleyicilerin performansının artırılması bugün hala endüstride ve akademide araştırmalara konu olmaktadır.

Mekanik Kuvvet Jeneratörleri düşük sürtünme ve sarsma kuvvetleri ile bilinen ve yakın zamanda bulunmuş olan aşırı-kısıtlı mekanizmalardır. Mekanik Kuvvet Jeneratörlerinin en önemli özelliklerinden biri istenilen herhangi bir kuvvet karakteristiği için tasarlanabilme esnekliğine sahip olmalarıdır.

Bu tez çalışması ana hatlarıyla üç kısımdan oluşmaktadır. Başlangıçta, Mekanik Kuvvet Jeneratörleri için bir tasarım yöntemi önerilmiştir. Bu tasarım yöntemi için Mekanik Kuvvet Jeneratörü iki farklı amaçla değerlendirilmiştir: lineer olmayan yay

ve lineer olmayan damper. Sonrasında, iniş takımı modellemek için bir yay-damper modeli geliştirilmiştir. Geliştirilen bu model National Advisory Committee for Aeronautics tarafından gerçekleştirilmiş test sonuçları ile doğrulanmıştır. Bu yay-damper modeli kullanılarak, testte kullanılmış olan iniş takımı optimize edilmiştir. Bu optimizasyon sırasında kullanılan metotlar ve yaklaşımlar açıklanmıştır. Son kısımda, optimizasyonda belirlenen optimum yay ve damper karakteristikleri kullanılarak Mekanik Kuvvet Jeneratörü tasarımı yapılmıştır. Mekanik Kuvvet Jeneratörünün iniş takımı üzerinde uygulanabilirliği ve fizibilitesi sunulmuş ve tartışılmıştır. Tez boyunca Mekanik Kuvvet Jeneratörlerinin özel nitelikleri araştırılmış, farklı kullanım alanları değerlendirilmiş ve tezin sonunda önerilmiştir.

Anahtar Kelimeler: uçak iniş takımı, şok sönümleyici verimliliği, mekanik kuvvet jeneratörü

To my family…

ACKNOWLEDGMENTS

Firstly, I would like to express my deepest gratitude to my supervisor Prof. Dr. Reşit Soylu, for his guidance, advice, criticism, encouragement, and insight throughout the thesis and my academic life. He has been not only an advisor but also a mentor during all my studies.

I would like to express my thanks to my manager Ali Akçay and my colleagues Öner Altınbağ and Hasan Akman for their support and advice during the thesis study.

I am very grateful and would like to express my special thanks to my colleagues Burak Güzeller and Paul Antony Shaw for sharing their experience in the aviation industry and helping me construct the basis of the thesis study with this knowledge.

I would like to thank my dear friends Berk Özyurt, Selin Akıncı, Can Coşkun, Duygu Akyürek and my love Müge Şahin for being there for me when I needed the most.

Last but not least, I would like to express my grateful thanks to my parents Hatice and İsmail, and my dear brothers Yavuz and Enes Emre from deep inside of my heart. They have always been by my side and been the light of my life.

TABLE OF CONTENTS

LIST OF TABLES

TABLES

LIST OF FIGURES

FIGURES

LIST OF ABBREVIATIONS

ABBREVIATIONS

2D	2 Dimensional
A/C	Aircraft
ALE	Acceleration Loop Equation
AVS	Air Vehicle Systems
C.G.	Center of Gravity
DoF	Degree of Freedom
GA	Genetic Algorithm
HSLDS	high-static-low-dynamic-stiffness
LGS	Landing Gear System
LCE	Loop Closure Equation
MFG	Mechanical Force Generator
MFG-4-gr	Mechanical Force Generator when Link 4 is ground
MFG-no-gr	Mechanical Force Generator with no grounded links
MFGD	Mechanical Force Generator Damper
MFGS	Mechanical Force Generator Spring
MR	Magnetorheological
NACA	National Advisory Committee for Aeronautics
SA	Shock Absorber
VLE	Velocity Loop Equation

cha	Chamber
com	Compression
def	Deflection
dmp	Damper
opt	Optimum
spr	Spring
tc	Tension/Compression
ten	Tension
w.r.t.	with respect to

LIST OF SYMBOLS

SYMBOLS

$\vec{\imath}$	The unit vector in the direction of x axis
$\vec{\jmath}$	The unit vector in the direction of y axis
$\vec{k}$	The unit vector in the direction of z axis
$\vec{x}^{(i)}$	The x axis of $\mathcal{F}_i$
$\vec{y}^{(i)}$	The y axis of $\mathcal{F}_i$
$\vec{z}^{(i)}$	The z axis of $\mathcal{F}_i$
O_i	Origin of $\mathcal{F}_i$
$\mathcal{F}_i$	ith reference frame
η_{SA}	Shock absorber efficiency
$b_{"abb"}$	Damping coefficient of the “abbreviated” damper
c_{frc}	Influence of force on the main optimization objective
c_{str}	Influence of stroke on the main optimization objective
d_{cle}	Minimum distance of slot centerline from link edge
$E_{MFG,spr}$	Energy stored at the MFGS
$F_{cha,spr}$	Spring force created inside the chamber of MFGS
$F_{MFG,spr}$	Equivalent spring force of MFGS
$F_{cha,dmp}$	Damper force created inside the chamber of MFGD
F_{LIFT}	Lift force action on the aircraft during landing
$F_{MFG,dmp}$	Equivalent damper force of MFGD

$F_{SA,dmp}$	Damper force created by the shock absorber
$F_{SA,spr}$	Spring force created by the shock absorber
F_{abb}	Force created at the “abbreviated” element
g	Gravitational acceleration
$k_{"abb"}$	Spring coefficient of the “abbreviated” element
$\hat{k}_{"abb"}$	Spring stiffness of the “abbreviated” element
k_{tire}	Spring coefficient of the tire
$l_{0,MFG}$	Fictitious free length of MFGS
$l_{f,"abb"}$	Free length of the “abbreviated” spring
L	Vertical distance between O_2 and m_L
m_1	Mass of the upper weight
m_2	Mass of the lower weight
m_L	Mass of load placed on Link 2
r_r	Roller radius
r_{tire}	Tire outer radius
s_i	Position of ith link
$\dot{s}_i$	First derivative of s_i with respect to time (velocity)
$\ddot{s}_i$	Second derivative of s_i w.r.t. time (acceleration)
s_{cha}	Stroke of chamber
s_{def}	Deflection of the tire
Δs_{MFG}	Total change in the MFG stroke
s_{SA}	Distance between upper mass and lower mass

$\hat{s}_{SA}$	Change of s_{SA} from the initial contact, the stroke
t_0	The time where the initial contact does occur
t_f	The time where $\hat{s}_{SA} = \hat{s}_{SA,max}$
t_s	The time where the dynamic system oscillation settles
$\vec{v}_i$	Velocity of ith link
V_V	Vertical speed at the initial contact
$W_{MFG,dmp}$	Work done (energy absorbed) by MFGD

CHAPTER 1

INTRODUCTION

In this chapter, basic information regarding a Mechanical Force Generator (MFG) and a landing gear shock absorber (SA) are provided. The organization and scope of the thesis are presented at the end of the chapter.

1.1 Introduction to Mechanical Force Generator

An MFG is an over-constrained mechanism proposed by Soylu [1] which transforms force or motion in one direction into force or motion in another direction. (see Figure 1.1) This mechanism has many benefits, such as having small friction forces and shaking forces due to the symmetry of the mechanism [1],[2],[3].

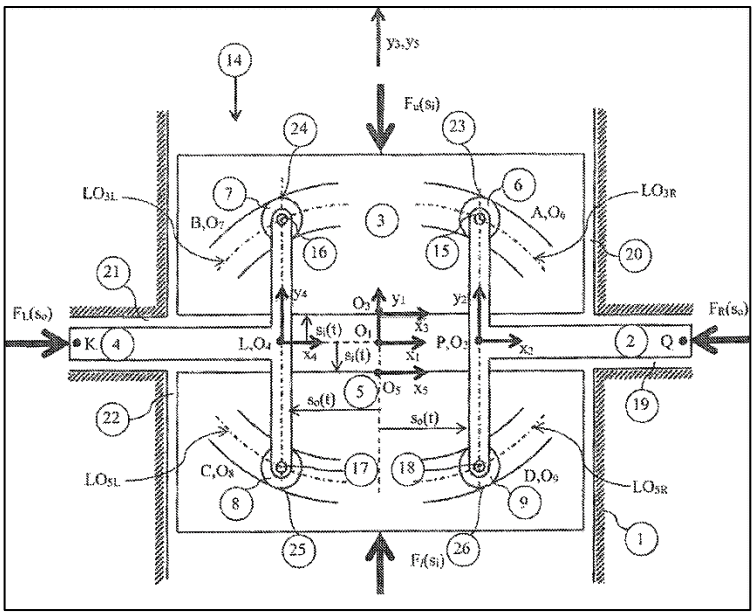

Figure 1.1. Mechanical Force Generator [1]

Previous studies on MFG have concentrated on using an MFG to increase the energy efficiency of an already existing machine [2], [3]. Alternatively, the maximum force or maximum torque requirement of the driving actuator may also be reduced [2], [3]. In his study, Mencek [4] showed that MFGs provide, theoretically, a substantial improvement in the energy efficiency of an already existing machine. However, the actual performance of the system may not be as good as theoretically predicted [4].

Another study performed by Erdinç [3] focused on using an MFG to reduce the energy consumption of an existing machine for a given periodic task. In this study, the use of MFG resulted in a significant reduction in the machine's energy consumption [3].

Ekinci [2] improved the previously developed methods to determine the optimum power profiles. Supporting his simulations with experiments, Ekinci demonstrated that combining an MFG within an existing machine could improve the machine's performance by minimizing the maximum torque required to run the task [2].

The aforementioned studies on MFG are primarily focused on the optimization of the power characteristic and energy consumption of an existing system. This thesis study, on the other hand, is focused primarily on creating an equivalent nonlinear spring and an equivalent nonlinear damper by using a linear spring and a linear damper within MFG.

1.2 Introduction to Landing Gear Shock Absorbers

Aircraft design is a multi-disciplinary process that includes aerodynamics, structures, avionics, software, and Air Vehicle Systems (AVS). This multi-disciplinary design process is broken down into levels to facilitate the design more efficiently. The Landing Gear System (LGS) is one of the most critical sub-systems under AVS.

The purpose of employing a landing gear on an aircraft is to support the aircraft on the ground during take-off, landing; and to decelerate the aircraft safely. The landing gear damps the kinetic energy and reduces the structural loading experienced by the

airframe during landing. Early and lighter aircraft designs generally used landing gears that were fixed (non-retractable). However, modern, and heavier aircraft designs generally use retractable landing gears in order to improve the aircraft's aerodynamic efficiency. Aircrafts with different landing gear configurations are presented in Figure 1.2 and Figure 1.3.

Figure 1.2. An aircraft with non-retractable landing gears [5]

Figure 1.3. An aircraft with retractable landing gears [6]

The coordinate system used for the aircraft design is presented in Figure 1.4. The installation of the landing gear is performed such that wheel rolling direction is parallel to aircraft longitudinal, i.e., forward-aft, direction.

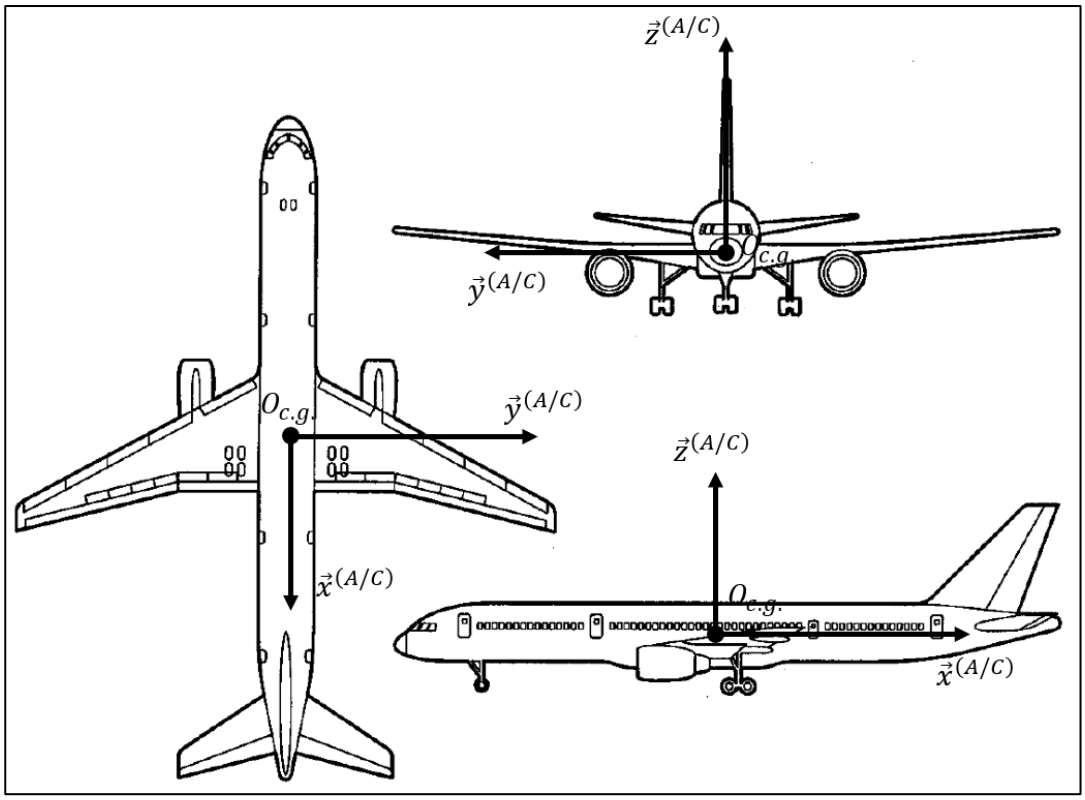

Figure 1.4. The coordinate system used for aircraft (A/C) design [7]

A description of the components of typical landing gear is presented in Figure 1.5. Some of the components in this figure are only designed for specific types of aircraft. For example, gravel deflectors are specific to the aircraft operating off an unpaved runway to avoid foreign object damage. Some of the generic components applicable to most modern retractable aircraft landing gears are listed below.

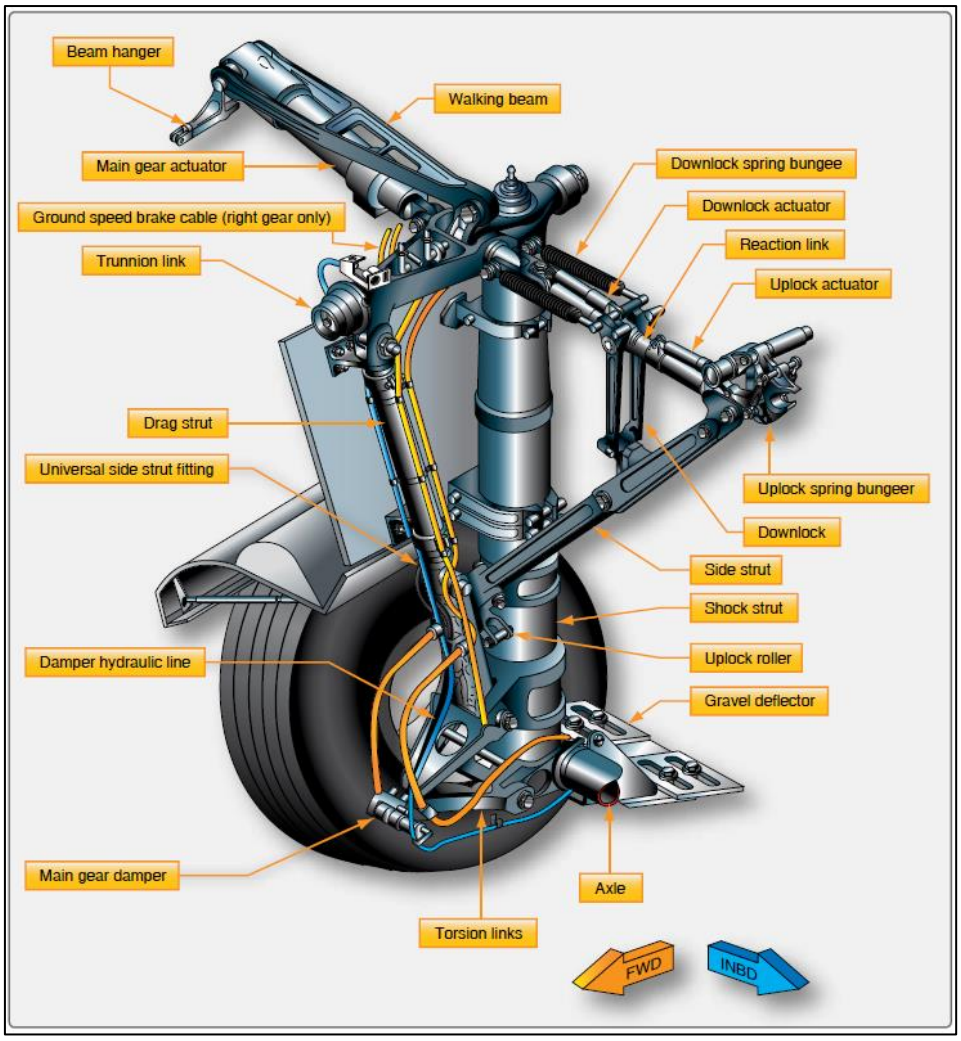

Figure 1.5. Nomenclature of landing gear components [8]

- The trunnion is a structural component of landing gear, which mainly carries the vertical loads on the aircraft, such as the vertical reaction load during landing or taxying.
- Drag strut is another structural component of the landing gear that mainly carries the loads along the longitudinal direction, such as spin-up and spring-back loads during landing and braking loads.
- Side strut is another structural component of the landing gear that mainly carries the loads along the lateral direction, such as drift landing loads.

- A shock absorber is the most characteristic landing gear component, which transfers the ground reaction forces onto the aircraft. Shock absorbers in earlier aircraft were made of steel springs or rubbers. However, modern aircraft are usually employed with oleo-pneumatic type shock absorbers due to their high efficiency.
- Downlock mechanism provides locking of the retractable gear in the extended position to prevent it from collapsing when the aircraft is on the ground.

Shock absorber design of a landing gear is, still, a very important research field. Early landing gear designs, such as the ones that exist in World War II aircraft, incorporated shock absorbers of different types such as steel spring, rubber spring, air type, and liquid spring type [9]. However, development of new technologies on changed the trend towards using oleo-pneumatic type shock absorbers, where the air is used as spring and oil is used for damping. The advantages of the oleo-pneumatic type shock absorbers against earlier design methods are presented in Figure 1.6.

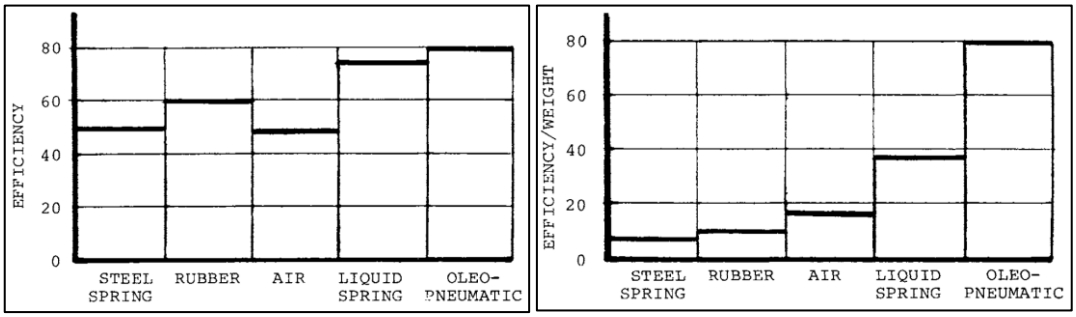

Figure 1.6. Comparison of different types of shock absorbers: efficiency (left), efficiency/weight ratio (right) [9]

In Figure 1.6, the efficiency of different types of landing gears is presented. On the right, the figure shows ratings of different types of landing gears, which are obtained by dividing efficiency by the dimensionless weight parameter.

Typical design configurations of an oleo-pneumatic shock absorber can be seen in Figure 1.7. The oil and gas are separated in configurations A and A'. The remaining configurations B, C, C', D, and E are mixed type shock absorbers (gas and oil are

mixed). The differences in the mixed type of shock absorber configurations are dependent on the design details such as sealings, structural layout, and oil/air volume.

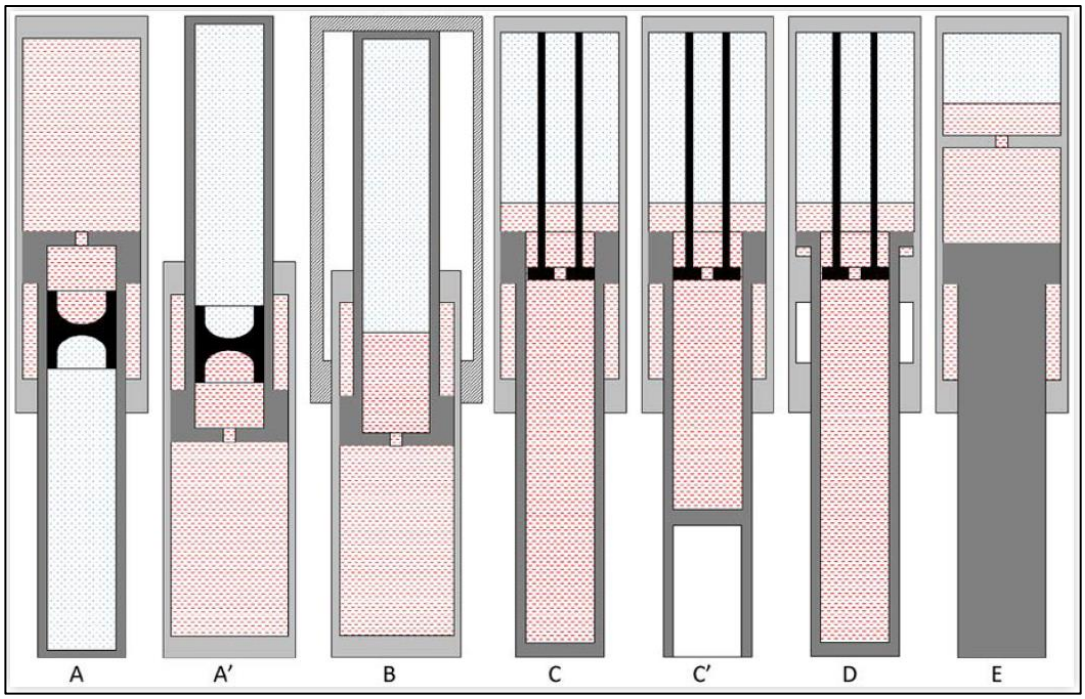

Figure 1.7. Cross-sectional view of oleo-pneumatic shock absorber configurations (oil: red, gas: blue) [10]

1.3 Introduction to Landing Gear Drop Test

Aircraft landing gear design is a critical system of the aircraft. Failure of the landing gear is not acceptable for the sake of the lives of the flight crew and passengers. Thus, the fail-safe principle is followed during the landing gear design so that the gear continues functioning until the aircraft comes to the end of its life [11]. In order to satisfy the requirements of the aircraft design, loads and conditions that the landing gear may encounter during operations of the aircraft are implemented into the design. These loads and conditions are mainly the landing loads, the taxying loads, and the steering loads. Landing loads are the primary loads for the design, which affects the design significantly; however, the secondary loads also do affect the detailed design

of the gear. The taxying and steering loads are the most important input for the fatigue life calculations of the landing gear.

The primary loads must be defined and tested before the aircraft flies for the first time, so that the design of the landing gear complies with the aircraft [12]. The so-called drop test procedure is followed to check the validity and correctness of the design.

The drop test, as the name implies, is performed by dropping the landing gear (that is supported with a structure) from a height with a mass at the top of the gear. The conditions of the drop test (drop mass, drop height, tire rotation speed) are defined in accordance with aircraft landing conditions to simulate the same conditions during landing. The scope of the test is limited from the initial touchdown to the settling of the dynamic system.

A landing gear drop test is usually performed for two purposes: validation of simulation models and qualification of the design. A generic drop test setup is presented in Figure 1.8 [13].

Figure 1.8. Drop test setup of a landing gear [13]

The advantage of a drop test is that it enables the landing gear design to be isolated from the aircraft parameters, such as the flexibility of the aircraft fuselage. Thus, it enables the standalone model of landing gear to be integrated into the aircraft model.

Although it is a physical test procedure, modeling a drop test is also a design process before realizing a landing gear design. A mathematical model helps to simulate the same environment in order to design and optimize a shock absorber for the landing gear.

A drop test result is mainly evaluated for its three properties: maximum force at the shock absorber ($F_{SA,max}$), maximum stroke change of the shock absorber ($\hat{s}_{SA,max}$) (see Figure 1.9), and efficiency (η_{SA}). The descriptions of these properties are presented in detail in Chapter 4.

A typical evaluation of a drop test can be observed in Figure 1.9. The initial contact starts at t_0. The final time, t_f is defined as the time where the stroke change, $\hat{s}_{SA}$, reaches its maximum. The dynamic motion continues until the oscillation of the system is damped, where time is t_s. The results between t_f and t_s is usually checked for the realizability of the design, such as the prevention of a rebound where the contact between the tire and the ground is lost. The efficiency of the shock absorber is evaluated in the time interval $t_0 \leq t \leq t_f$ (see Section 4.2.1).

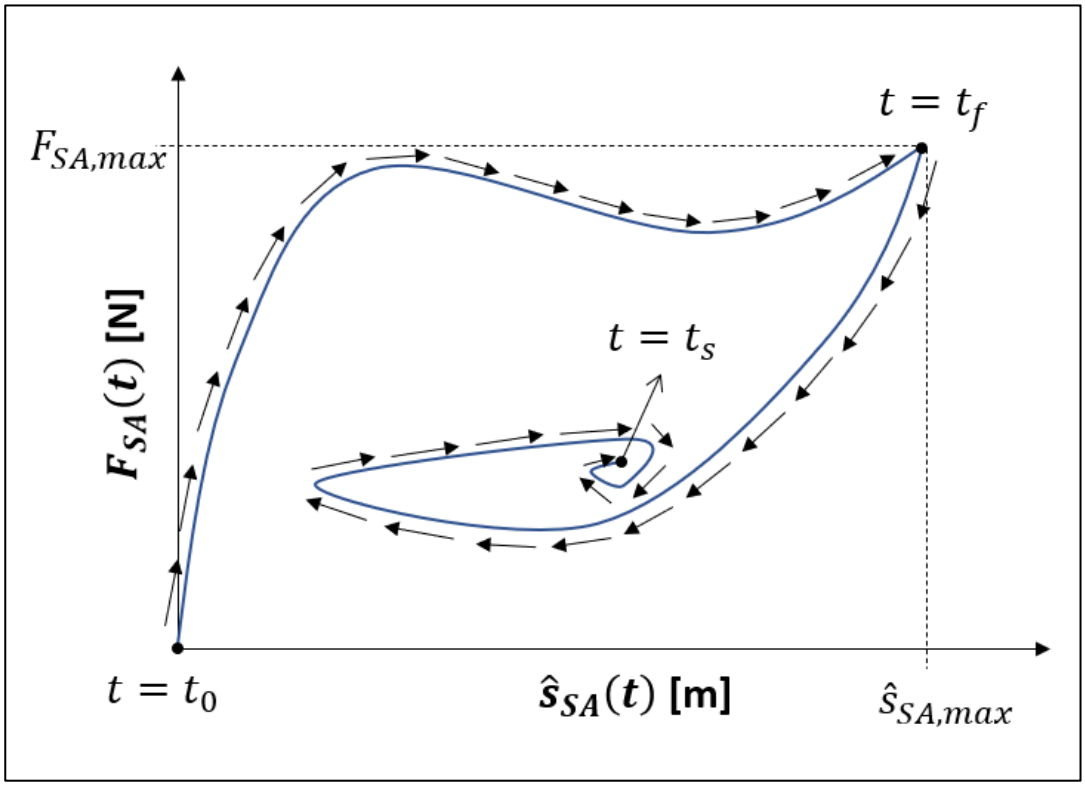

Figure 1.9. A typical drop test result

1.4 Scope and Organization of the Thesis

The objective of the thesis is to design a shock absorber for aircraft landing gear using MFGs.

To achieve this objective, a design methodology for MFG is introduced in Chapter 3. The use of MFG as a non-linear spring and non-linear damper is investigated. General methods to determine the slot shape of MFG for given dimensions and desired force characteristics are introduced. Construction of a special spring that may be used both in compression and tension is introduced during the derivation of the method for non-linear spring. Additionally, special spring cases with quadratic stiffness are investigated to bring out the possible opportunities of the use of MFG in other applications. Illustrative examples of MFG design as spring and damper are performed to explain the method and prove the validity of calculations.

A spring mass damper model with two degrees of freedom is introduced and validated with available test results. Using the reference parameters and conditions in test results, an optimization on landing gear shock absorber is performed. The objective of this optimization is to find the optimum non-linear spring and damper characteristics that result in the optimum shock absorber design.

In the last chapter, the design of landing gear with MFGs, which is designed against optimum spring and damper characteristics, is evaluated. The outcome of the design is compared with the shock absorber used in the test. With respect to this comparison, the applicability, and feasibility of the use of MFG on landing gear shock absorbers are discussed.

CHAPTER 2

LITERATURE REVIEW

In this chapter, a literature review regarding shock absorbers and their efficiency optimization is presented.

2.1 Oleo-Pneumatic Shock Absorbers

The properties of an oleo-pneumatic shock absorber have been previously explained in Section 1.2. There are many design alternatives for an oleo-pneumatic shock absorber. Some of these alternatives are investigated and presented in the preceding paragraphs.

Single-Stage Shock Absorber with Fixed Orifice

Single-stage shock absorbers are the simplest oleo-pneumatic shock absorbers with non-linear spring and damper characteristics.

A single-stage oleo-pneumatic shock absorber with a fixed orifice consists of an air chamber that acts as a non-linear spring (according to the gas compression law) and a fixed orifice that acts as a non-linear damper (according to the law of fluid discharge through an orifice). Typical spring and damper characteristics of the air spring and oil damper are depicted in Figure 2.1.

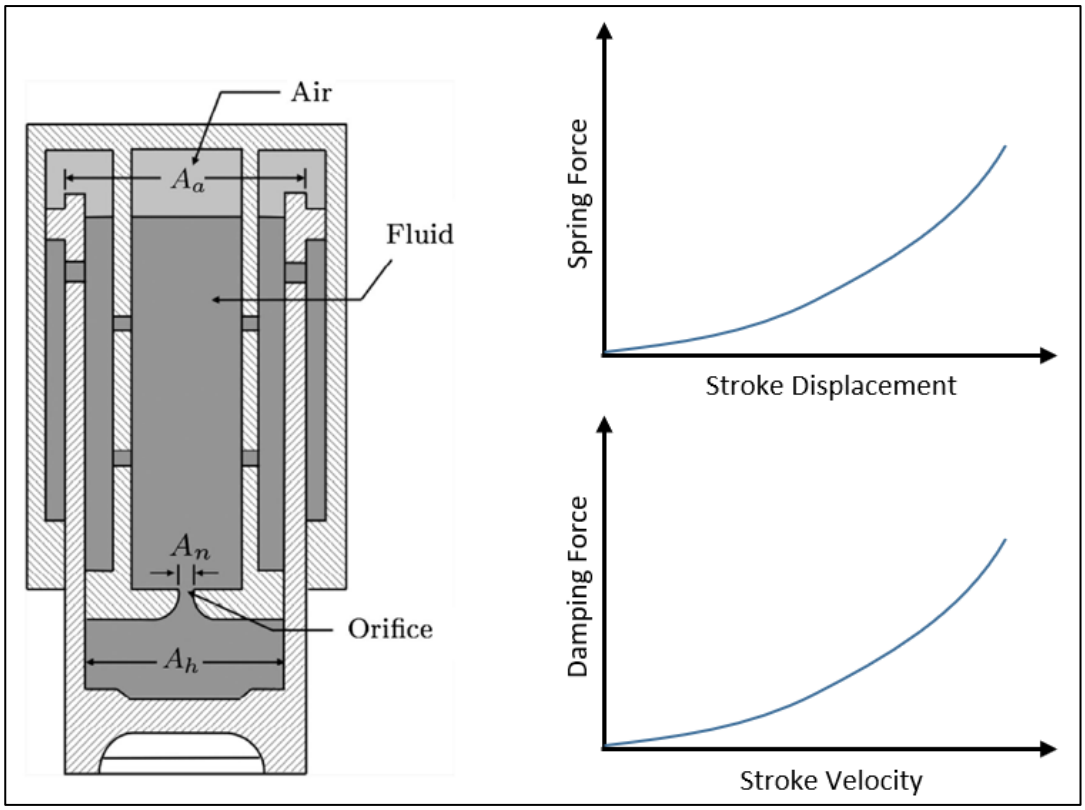

Figure 2.1. Single-stage SA with fixed orifice; cross-sectional view (left), example spring characteristic (upper-right), damper characteristics (lower-right) [14]

Dual-Stage Shock Absorber with Fixed Orifice

A dual-stage shock absorber is obtained by adding a second air chamber to a single-stage shock absorber.

A dual-stage shock absorber with a fixed orifice consists of two air chambers that act as a non-linear spring according to the gas compression law. The first air chamber works until the chamber comes to an end and compresses the second chamber's air. The damper characteristics are the same with a fixed orifice. Typical spring and damper characteristics of the air spring and oil damper are depicted in Figure 2.2.

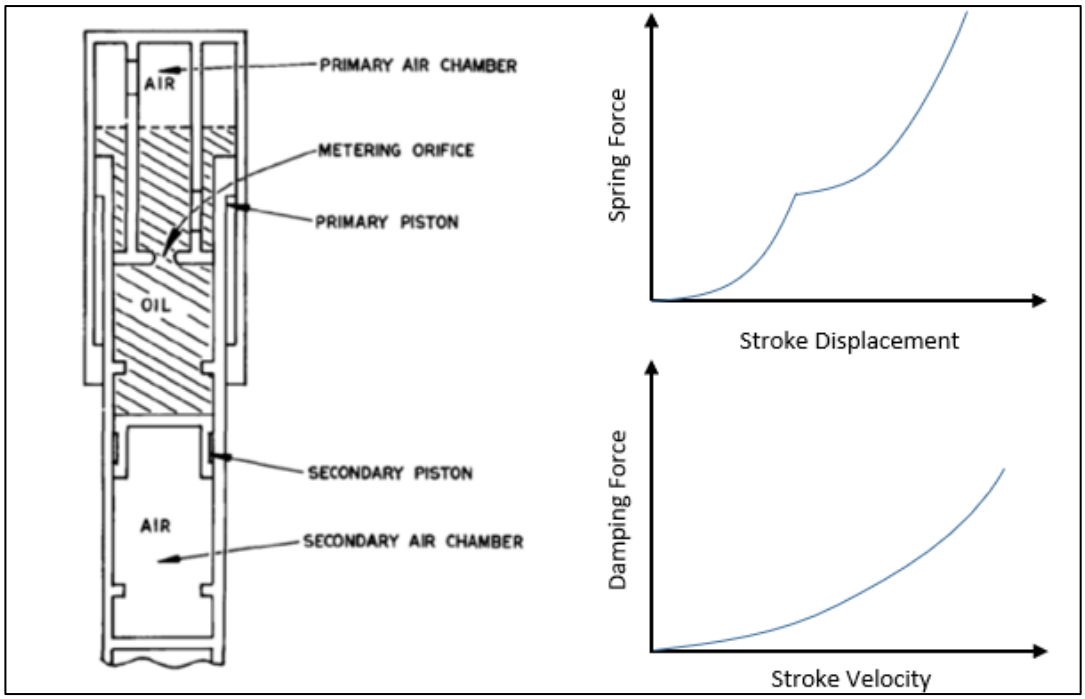

Figure 2.2. Dual-stage SA with fixed orifice; cross-sectional view (left), example spring characteristic (upper-right), damper characteristics (lower-right) [10]

Single-Stage Shock Absorber with Poppet Valve Orifice

Shock absorbers with a poppet valve design are the most practical shock absorbers because of their ease of design and adjustability.

A single-stage shock absorber with a poppet valve orifice is similar to a single-stage fixed orifice shock absorber as far as the air spring characteristics are concerned. The damper characteristic is designed such that it changes with the force inside the shock absorber. Typical spring and damper characteristics of the air spring and oil damper are depicted in Figure 2.3.

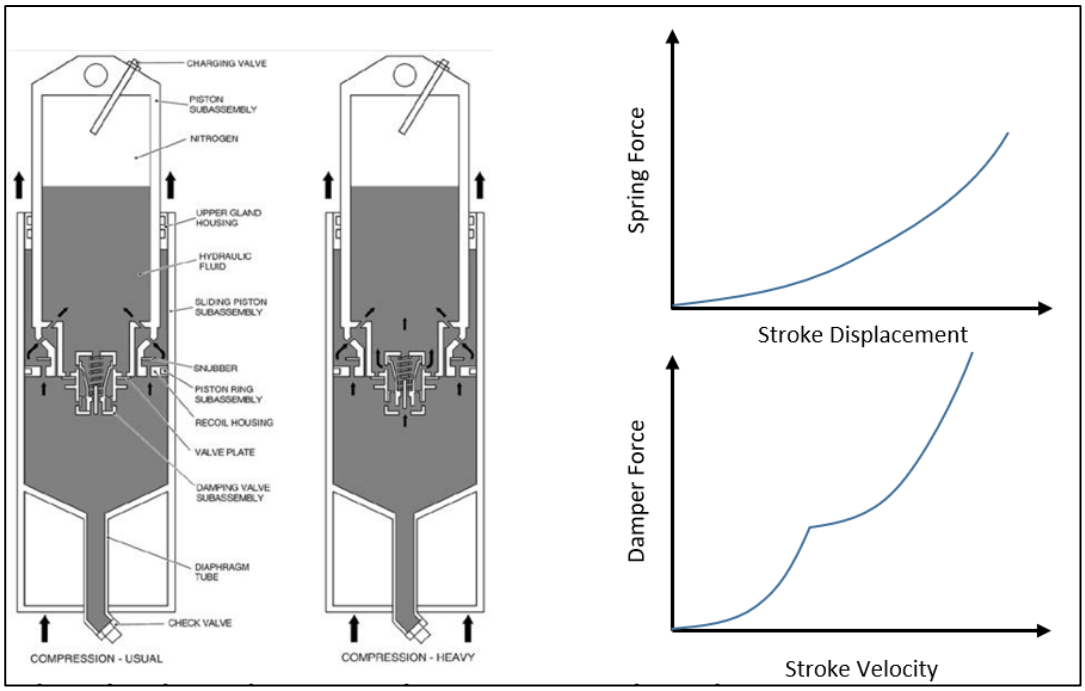

Figure 2.3. Single-Stage SA with poppet valve orifice; cross-sectional view (left), spring characteristic (upper-right), damper characteristics (lower-right) [10]

Single-Stage Shock Absorber with Metering Pin

Shock absorbers with metering pin are the most suitable and optimized shock absorbers for obtaining highly non-linear damping characteristics. They are known for being reliable and for having low maintenance cost [9]. Efficiency (which will be explained later in 4.2.1) of 90% can be achieved with metering pins with several drop tests for development of the design [10].

The damper characteristic is designed to change with the displacement, as presented in Figure 2.4 left, and the velocity of the shock absorber. Typical spring and damper characteristics of the air spring and oil damper are depicted in Figure 2.4 [15].

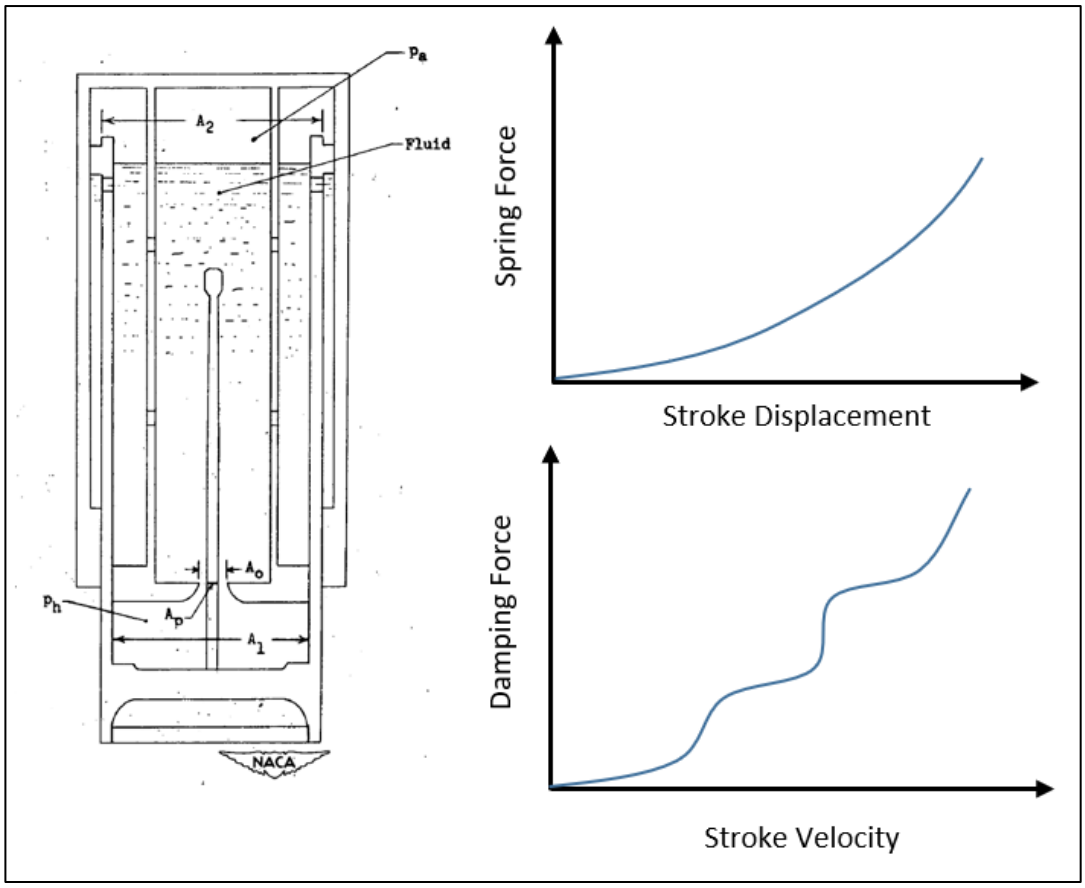

Figure 2.4. Single-stage SA with metering pin; cross-sectional view (left), example spring characteristic (upper-right), damper characteristics (lower-right) [15]

2.2 Shock Absorber Design Optimization

The design of a shock absorber is focused, mainly, on the damper characteristics; because, the spring characteristic of oleo-pneumatic shock absorbers (air spring) allow the dampers to absorb most of the energy during compression at landing [9]. Dampers, on the other hand, can be classified into two groups; namely, active/adaptive dampers and passive dampers.

2.2.1 Active/Adaptive Damper Design

Oleo-pneumatic shock absorbers are the most popular type of shock absorbers today. Since 1970s, many studies have focused on implementing closed loop control to shock absorbers; leading to various active/adaptive damper designs [16], [17]. One of the initial studies was performed by Ghiringhelli [18], who aimed to use semi-active control for the orifice size (see Figure 2.5). The benefit of using semi-active control is that it is simple, lightweight, and safe (compared to fully active control). In the simulations, increased landing gear efficiency has been obtained. The test results also showed an increase in the performance. However, they are not at the same level as the simulation results. The reason for this, probably, is that the control equipment utilized in the tests was insufficient for the intended purpose.

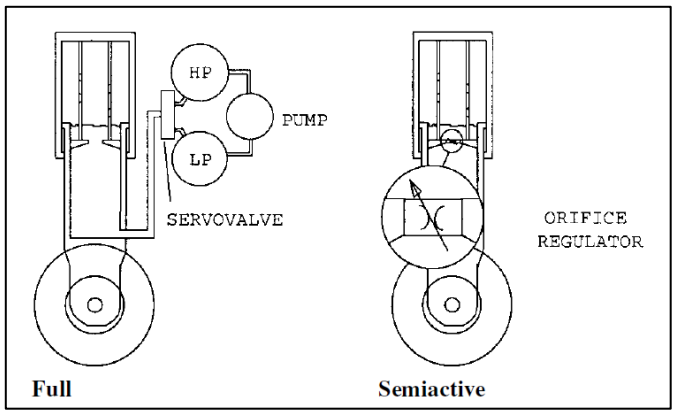

Figure 2.5. Active and semi-active control concepts [18]

In 2003, Mikulowski aimed for an increase in performance using a magnetorheological (MR) fluid in the shock absorber [19]. MR fluids have viscosity properties that change with the magnetic field. The control strategy was employing fully active control by providing feedback to the system (see Figure 2.6). However, an increase in the performance was not achieved because of the system's response time during the landing impact. In his study, Mikulowski stated that [19] MR fluid was able to change its properties in 25 ms, whereas the landing impact typically lasts only for 100 ms.

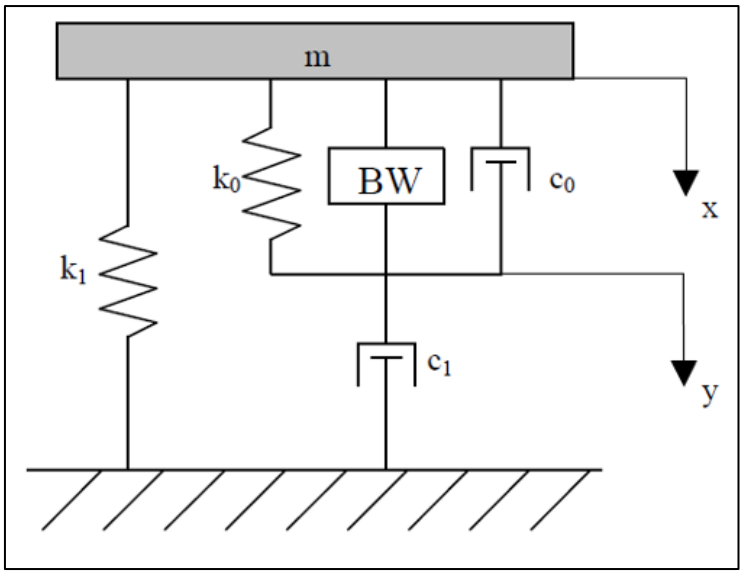

Figure 2.6. Mass-spring-damper model with MR damper [19]

Han has recently revisited the available active shock absorption methods using an MR fluid in 2019 [20]. In his study, an optimization is performed by using an MR fluid in the shock absorber with the Skyhook damper concept (see Figure 2.7, left) for the fully active control. Increased landing gear efficiency has been obtained with the use of this active suspension (see Figure 2.7, right). However, experimental validation of the study has not been realized. Previously, in his study, Mikulowski [19] stated that realization of this application was not possible due to response time of the controller. Thus an experimental study is required in order to validate Han's study.

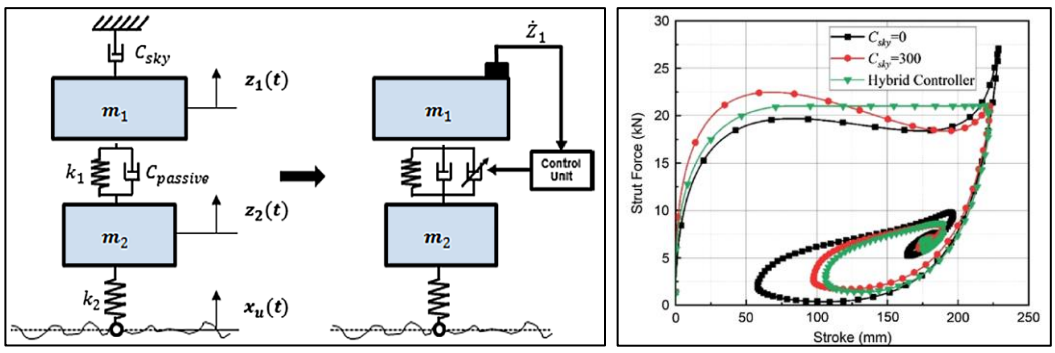

Figure 2.7. Skyhook controller concept (left), comparison of efficiency curves (right) [20]

2.2.2 Passive Damper Design

Most oleo-pneumatic shock absorbers utilize passive dampers. The system works in the open-loop philosophy; thus, it is optimized for a specific condition or condition spectrum. Since aircraft landings occur within a predictable range of conditions, passive shock absorbers are suitable for such applications.

In 2017, Li approached the shock absorber design from a new perspective by utilizing an inerter. Inerter is a mechanical element similar to a spring or a damper (see Figure 2.8). It has also been referred to be the "missing mechanical element of the dynamic systems" [21]. In his study, Li focused on the optimization of the shock absorber by adding an inerter to the system [14]. The inerter, however, poses some challenges since the elongation of the strut will be limited during landing. This limitation may lead to a rebound in the shock strut, which will pose a significant risk of unexpected loads on the landing gear and the aircraft.

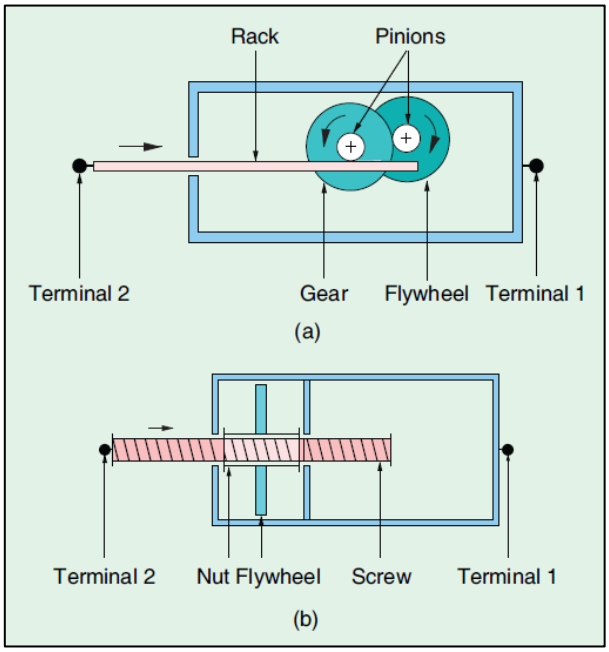

Figure 2.8. Schematics of two types of inerter; rack and pinion (a), ball screw (b) [21]

Shi has focused on the optimization of the metering pin design with different profiles (see Figure 2.9) in 2019 [22]. The results have shown that optimum solutions can be achieved for specific landing conditions (regarding the mass of the aircraft, vertical speed during landing etc.). This may be a good approach because, usually, an aircraft performs its landing operation within specific mass range [12]. However, the production of these complex metering pin configurations needs to be further investigated.

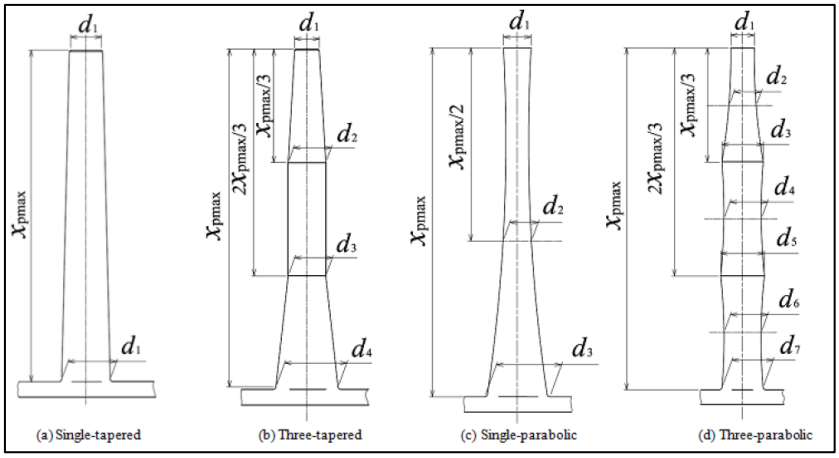

Figure 2.9. Metering pin profiles investigated in Shi's study [22]

CHAPTER 3

MECHANICAL FORCE GENERATOR

In the beginning of this chapter, the position, velocity, and acceleration of the MFG are mathematically defined. Then, two different uses of the MFG are investigated: one is using a spring inside the MFG to create a non-linear spring, Mechanical Force Generator Spring (MFGS), the other is using a damper inside the MFG to create a non-linear damper, Mechanical Force Generator Damper (MFGD). Mathematical derivations are performed for the MFGS and the MFGD separately to find a general solution for MFGS or MFGD for a given force characteristic. The general properties of the MFG are explained in Section 3.1. The notation of the MFG defined in Figure 3.1 is kept as a general notation and is applicable for both MFGS and MFGD. After derivation of the slot shape solution, realizability checks are defined to evaluate the feasibility of the solution against the design constraints. During derivation of methodology for MFGS, the design of an equivalent spring which can create compression and tension force is defined. Since MFGS is a mechanism that can be designed for non-linear force characteristics, special cases for springs with quadratic stiffness are investigated to observe the possible use area of MFGS. Illustrative examples for the design of MFGS and MFGD are performed at the end of the chapter to explain the design steps clearly and evaluate the validity of the mathematical derivations performed at the beginning of the chapter.

3.1 General MFG Properties

Overconstrained mechanisms [23] are mechanisms where the actual degree of freedom (DoF) is strictly greater than the DoF predicted by the Kutzbach Criterion. Mechanical Force Generator is an overconstrained mechanism with 1 DoF [1]. If the MFG is designed properly and if the weights of the links are neglected, the reaction

forces and reaction moments, acting on the four prismatic joints, that connect the MFG to the ground are identically zero (at all times and for all possible motions of the MFG) (see Figure 3.1). Therefore, frictional losses and wear at these four joints are minimized. Furthermore, the shaking forces and shaking moments transmitted to the ground are identically zero (at all times and for all possible motions).

MFG consists of 9 links. The names and the descriptions of the links are listed below (see Figure 3.1).

1 – Ground: This link is the case that encloses the whole MFG mechanism and is treated to be the fixed link. It is connected to Link 2, Link 4, Link 3 and Link 5 with four prismatic joints.

Links 2 and 4 – Input Links: These links translate along the $\vec{z}^{(1)}$ direction. There is a prismatic joint between each input link and the ground link. There are four revolute joints between the two input links and the four rollers (Links 6-9).

Links 3 and 5 – Chamber Links: These links translate along the $\vec{x}^{(1)}$ direction. Each chamber link is connected to the ground with a prismatic joint. The two chamber links are connected to the four rollers with four cam joints (single point contact).

Links 6, 7, 8, and 9 – Roller Links: There is a revolute joint between each roller link and an input link. The rollers are connected to the chamber links with four cam joints.

Every link in the MFG has its own body-fixed reference frame denoted by $\mathcal{F}_i$ with an origin at O_i. $\mathcal{F}_i$ is a right-handed reference frame the axes of which are labeled as $\vec{x}^{(i)}$, $y^{(i)}$ and $\vec{z}^{(i)}$. All reference frames are oriented such that they are parallel to $\mathcal{F}_1$ which is the earth fixed reference frame. $\vec{\imath}$, $\vec{\jmath}$ and $\vec{k}$ denote unit vectors parallel to $\vec{x}^{(1)}$, $y^{(1)}$ and $\vec{z}^{(1)}$, respectively.

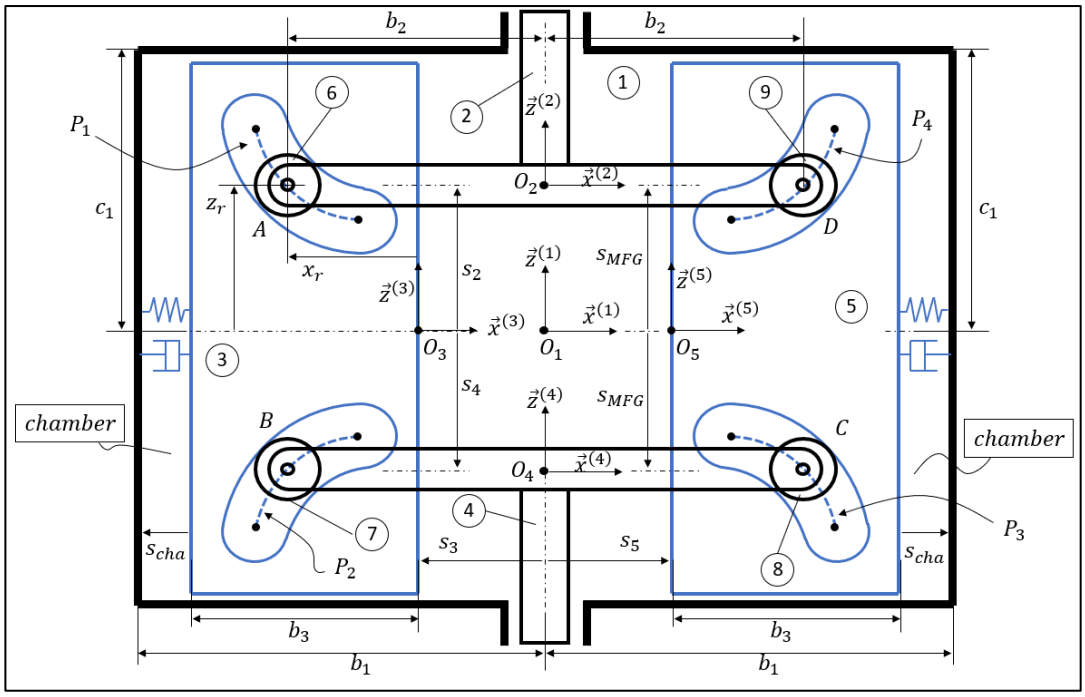

Figure 3.1. Mechanical Force Generator

Referring to Figure 3.1, b_1, b_2 and b_3 denote strictly positive scalar dimensions measured parallel to the $\vec{x}^{(1)}$ axis. c_1, on the other hand, is a strictly positive scalar dimension measured parallel to the $\vec{z}^{(1)}$ axis. Referring to Figure 3.1 again, s_2, s_3, s_4 and s_5 are signed scalars which yield the position of Links 2, 3, 4 and 5 (relative to Link 1), respectively. s_{cha} and s_{MFG} are also signed scalars which are presented in Figure 3.1.

s_2, s_3, s_4 and s_5 may be rigorously defined via the following equations.

$$s_2 = \overrightarrow{O_1O_2} \cdot \vec{k} \tag{3.1}$$

$$s_3 = -\overrightarrow{O_1O_3} \cdot \vec{\imath} \tag{3.2}$$

$$s_4 = -\overrightarrow{O_1O_4} \cdot \vec{k} \tag{3.3}$$

$$s_5 = \overrightarrow{O_1O_5} \cdot \vec{\imath} \tag{3.4}$$

The x and z coordinates, in $\mathcal{F}_3$, of the center of roller 6, i.e., A, are denoted by x_r and z_r, respectively, where

$$x_r = -\overrightarrow{O_3O_6} \cdot \vec{\imath} \tag{3.5}$$

$$z_r = \overrightarrow{O_3O_6} \cdot \vec{k} \tag{3.6}$$

The path of point A on Link 3 is the curve P_1 (see Figure 3.1), the defining equation of which is given by

$$x_r = f(z_r) \tag{3.7}$$

where f is a known function.

It should be noted that MFG is symmetrical with respect to the $\vec{x}^{(1)}$ and $\vec{z}^{(1)}$ axes. Hence, the equations of the paths P_2, P_3 and P_4 (on which roller centers B, C and D are restricted to move) may be obtained by using equation (3.7) and the symmetricity of the mechanism.

In this study, the volume between Link 3 and Link 1 (in which a spring and/or a damper may exist) is called to be "chamber" (see Figure 3.1). Similarly, the volume between Link 5 and Link 1 is also called to be "chamber". The stroke of the chamber, s_{cha}, is defined with the following equation.

$$s_{cha} = b_1 - b_3 - s_3 \tag{3.8}$$

There may be physical realizability constraints on s_{cha} which can be represented in the form

$$l_{cha,min} \leq s_{cha} \leq l_{cha,max} \tag{3.9}$$

where $l_{cha,min}$ and $l_{cha,max}$ are specified numbers.

The minimum and maximum allowable dimensions of the chamber (i.e., $l_{cha,min}$ and $l_{cha,max}$) change according to the design case. If a spring is used inside the chamber, then $l_{cha,min}$ and $l_{cha,max}$ will be the minimum and maximum allowable lengths of the spring, respectively. If a damper is employed inside the chamber, then $l_{cha,min}$ and $l_{cha,max}$ will be the minimum and maximum allowable lengths of the damper, respectively.

The stroke of the MFG, s_{MFG}, is defined via the equation

$$s_{MFG} = s_2 = s_4 \tag{3.10}$$

There may be physical realizability constraints on s_{MFG} which can be represented in the following form

$$l_{MFG,min} \leq s_{MFG} \leq l_{MFG,max} \tag{3.11}$$

where $l_{MFG,min}$ and $l_{MFG,max}$ are specified numbers (see Figure 3.2)

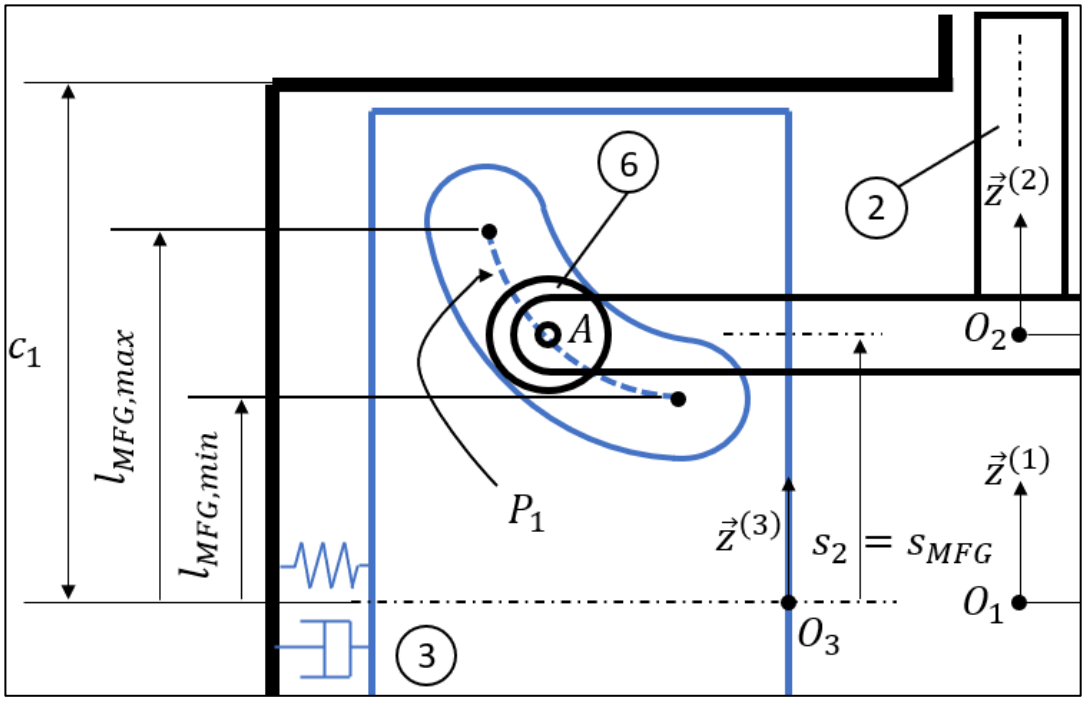

Figure 3.2. The minimum and maximum allowable MFG stroke lengths

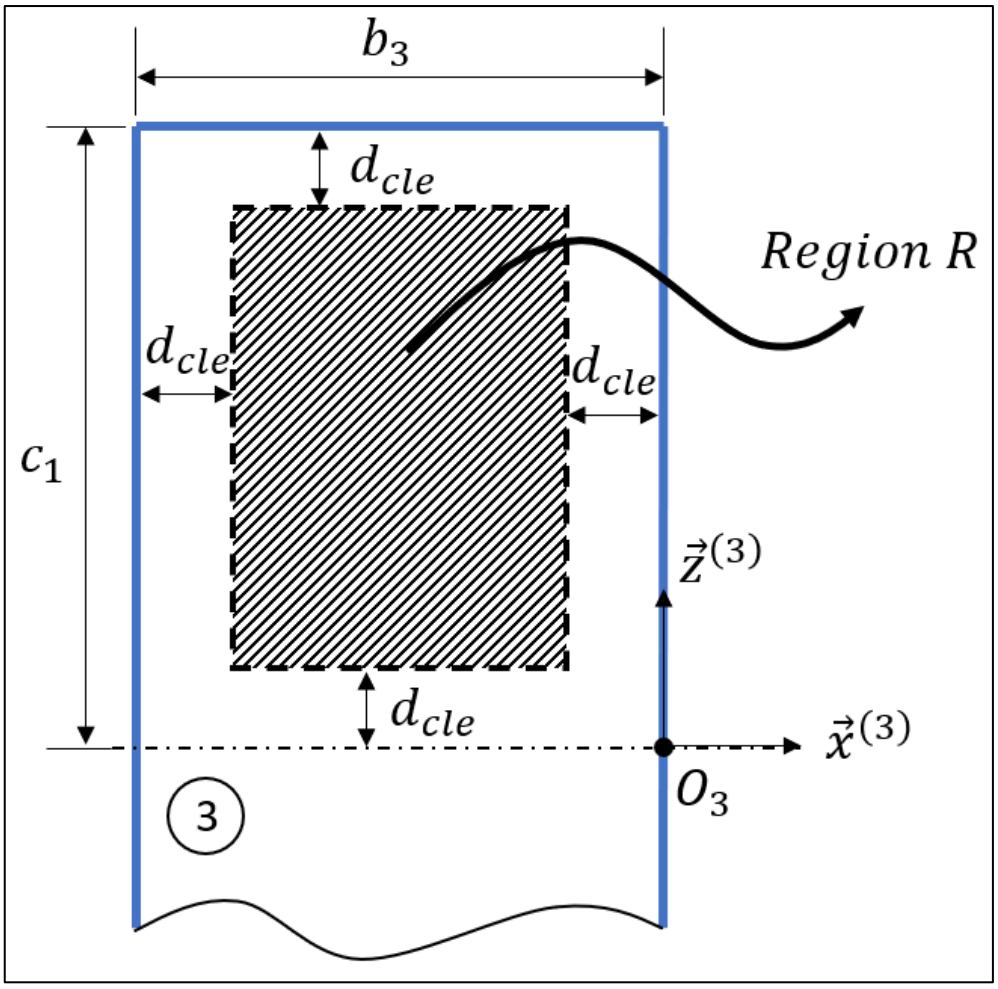

Figure 3.3. Definition of the clearance parameter d_{cle}

Referring to Figure 3.3, let the allowable region in which the path P_1 may lie be the region R (the hatched region). As can be observed from Figure 3.3, the region R is defined via the clearance parameter d_{cle}, which, later in this study, will be treated as a user specified input. Clearly, one can express $l_{MFG,min}$ and $l_{MFG,max}$ in terms of d_{cle}, yielding

$$l_{MFG,min} = d_{cle} \tag{3.12}$$

$$l_{MFG,max} = c_1 - d_{cle} \tag{3.13}$$

Hence, equation (3.11) yields

$$d_{cle} \leq s_{MFG} \leq c_1 - d_{cle} \tag{3.14}$$

It should be noted that concept of the allowable region R is introduced so that the mechanical construction of the MFG is simpler (in the sense that Links 3 and 5, as well as Links 2 and 4 can, physically, lie in the same $\vec{x}^{(1)}$ - $\vec{z}^{(1)}$ plane). If such a simplification regarding the mechanical construction of the MFG is not sought for, then the constraints introduced due to the allowable region R will not exist (i.e., the allowable region R can be as large as required).

Another user specified input that will be used in this study is Δs_{MFG}, which is defined via the equation

$$\Delta s_{MFG} = l_{MFG,max} - l_{MFG,min} \tag{3.15}$$

3.1.1 Loop Closure Equations

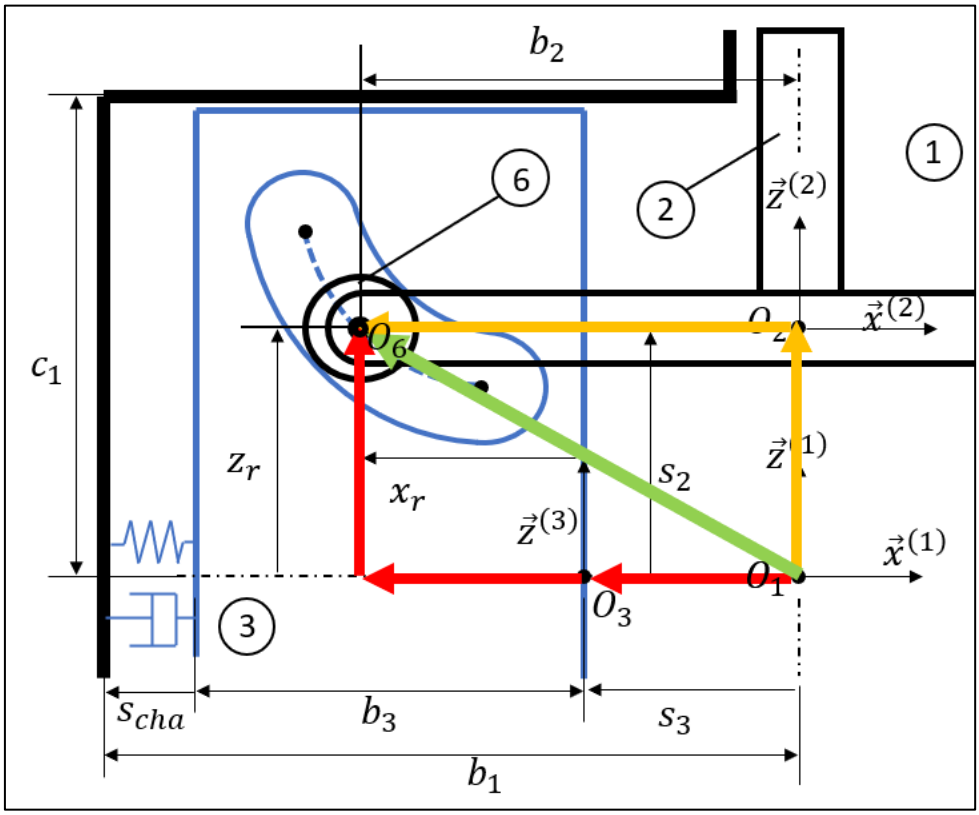

Figure 3.4. Sketch for writing down the loop closure equations

As can be observed from Figure 3.1, the mechanism is symmetrical with respect to $\vec{x}^{(1)}$ axis and $\vec{z}^{(1)}$ axis. Hence, the Loop Closure Equation obtained by considering $\overrightarrow{O_1O_6}$ will be identical with the remaining three loop closure equations that will be obtained considering $\overrightarrow{O_1O_7}$, $\overrightarrow{O_1O_8}$ and $\overrightarrow{O_1O_9}$.

Loop Closure Equation (LCE) obtained via $\overrightarrow{O_1O_6}$:

Referring to Figure 3.4,

$$\overrightarrow{O_1O_6} = s_2\vec{k} - b_2\vec{\imath} = -s_3\vec{\imath} + z_r\vec{k} - x_r\vec{\imath} \tag{3.16}$$

By equating the $\vec{k}$ and $\vec{\imath}$ components in equation (3.16), one obtains

$$s_2 = z_r \tag{3.17}$$

$$s_3 = b_2 - x_r \tag{3.18}$$

Here, it should be recalled that x_r and z_r are related to each other via the equation

$$x_r = f(z_r) \tag{3.7}$$

where f is a known function. Since b_2 is a known constant (i.e., a dimension of the mechanism), there are three unknowns (namely s_2, s_3, z_r) in equations (3.17) and (3.18) (when one considers equation (3.7) as well). Hence, when one of the three unknowns is specified, the remaining two unknowns can be solved from equations (3.17), (3.18) and (3.7). Therefore, if there is no slippage between Roller 6 and the slot, the mechanism consisting of Links 1, 2, 6, and 3 in Figure 3.4 is a 1 degree of freedom mechanism.

Solving s_3, in terms of s_{cha}, from (3.8), and solving s_2, in terms of s_{MFG}, from (3.10) and substituting the results into (3.18) and (3.17), one obtains

$$s_{cha} = x_r + b_1 - b_3 - b_2 \tag{3.19}$$

$$s_{MFG} = z_r \tag{3.20}$$

which involve the 3 unknowns s_{cha}, s_{MFG} and z_r (when one considers equation (3.7) as well).

Velocity Loop Equation (VLE) obtained via $\overrightarrow{O_1O_6}$:

By taking derivative of equation (3.16) with respect to time, the VLE can be obtained as follows

$$\dot{s}_2\vec{k} = -\dot{s}_3\vec{\imath} + \dot{z}_r\vec{k} - \dot{x}_r\vec{\imath} \tag{3.21}$$

where

$$\dot{s}_2 = \frac{ds_2}{dt}, \dot{s}_3 = \frac{ds_3}{dt}, \dot{x}_r = \frac{dx_r}{dt}, \dot{z}_r = \frac{dz_r}{dt}$$

Since x_r is a function of z_r, using the chain rule, $\dot{x}_r$ can be written as a function of z_r and $\dot{z}_r$ as follows.

$$\dot{x}_r = \frac{dx_r}{dz_r}\dot{z}_r = f'(z_r)\dot{z}_r \tag{3.22}$$

where the prime denotes derivative with respect to z_r. Using the $\vec{k}$ and $\vec{\imath}$ components of the VLE given by equation (3.21) and utilizing equation (3.22), the following equations are obtained.

$$\dot{s}_2 = \dot{z}_r \tag{3.23}$$

$$\dot{s}_3 = -\dot{x}_r = -\frac{dx_r}{dz_r}\dot{z}_r \tag{3.24}$$

It should be noted that, when the position of the mechanism is known, there will be three generalized velocities ($\dot{s}_2, \dot{s}_3, \dot{z}_r$) in the two equations (3.23) and (3.24). Hence, when one of the generalized velocities is specified, the remaining two generalized velocities may be solved, linearly, from equations (3.23) and (3.24).

Note that, by taking time derivatives of equations (3.19) and (3.20), the following relations may also be obtained.

$$\dot{s}_{cha} = \dot{x}_r = \frac{dx_r}{dz_r}\dot{z}_r \tag{3.25}$$

$$\dot{s}_{MFG} = \dot{z}_r \tag{3.26}$$

Acceleration Loop Equation (ALE) obtained via $\overrightarrow{O_1O_6}$:

By taking derivative of equation (3.21) with respect to time, the ALE may be obtained as follows.

$$\ddot{s}_2\vec{k} = -\ddot{s}_3\vec{\imath} + \ddot{z}_r\vec{k} - \ddot{x}_r\vec{\imath} \tag{3.27}$$

The time derivative of equation (3.22), on the other hand, yields

$$\ddot{x}_r = \frac{d^2x_r}{dz_r^2}\dot{z}_r^2 + \frac{dx_r}{dz_r}\ddot{z}_r \tag{3.28}$$

Thus, equations (3.27) and (3.28) yield the following two scalar equations

$$\ddot{s}_2 = \ddot{z}_r \tag{3.29}$$

$$\ddot{s}_3 = -\ddot{x}_r = -\frac{d^2x_r}{dz_r^2}\dot{z}_r^2 - \frac{dx_r}{dz_r}\ddot{z}_r \tag{3.30}$$

which involve the generalized accelerations, $\ddot{s}_2$, $\ddot{s}_3$ and $\ddot{z}_r$.

Note that time derivatives of equations (3.25) and (3.26) yield the following two equations.

$$\ddot{s}_{cha} = \ddot{x}_r = \frac{d^2x_r}{dz_r^2}\dot{z}_r^2 + \frac{dx_r}{dz_r}\ddot{z}_r \tag{3.31}$$

$$\ddot{s}_{MFG} = \ddot{z}_r \tag{3.32}$$

Normally, LCE and VLE are sufficient for the purposes of determining the slot shape (which is the objective in this study). However, ALE (which would be needed for a dynamic force analysis) is also derived in this study for the sake of completion.

3.2 MFG Spring (MFGS)

In this study, MFG Spring (MFGS) denotes the mechanism that is obtained from MFG, such that it converts two real, linear, identical springs (with a constant

stiffness) into two equivalent, virtual non-linear springs. The two linear springs are attached between Links 1 and 3; and Links 1 and 5 (see Figure 3.1). The forces applied on Links 3 and 5, by the two linear springs, are designated by $\vec{F}_{cha,spr,3}$ and $\vec{F}_{cha,spr,5}$ respectively (see Figure 3.5), where

$$\vec{F}_{cha,spr,3} = -F_{cha,spr}\vec{\imath} \tag{3.33}$$

$$\vec{F}_{cha,spr,5} = F_{cha,spr}\vec{\imath} \tag{3.34}$$

In equations (3.33) and (3.34):

$$F_{cha,spr} = k_{cha}\left(s_{cha} - l_{f,cha}\right) \tag{3.35}$$

where

$l_{f,cha}$: Free length of the two linear, identical springs

k_{cha} : Spring constant of the two linear, identical springs

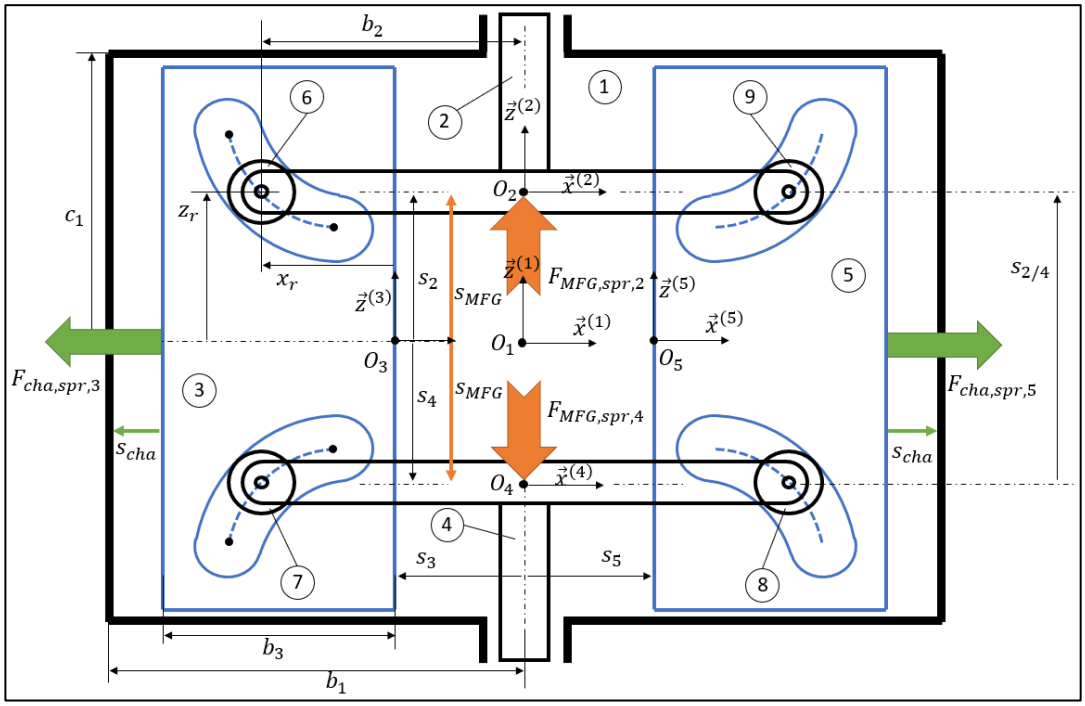

Figure 3.5. Spring forces acting on MFGS

The real spring inside the chamber works as a

- Compression spring if $l_{f,cha} \geq s_{cha}$
- Tension spring if $l_{f,cha} \leq s_{cha}$

Practically, it is necessary to keep the spring always in compression or tension due to differences in the nature of the compression and tension springs. Physically, it is not possible to use a tension spring as a compression spring due to the hook-like attachment at the end of the tension spring (see Figure 3.6).

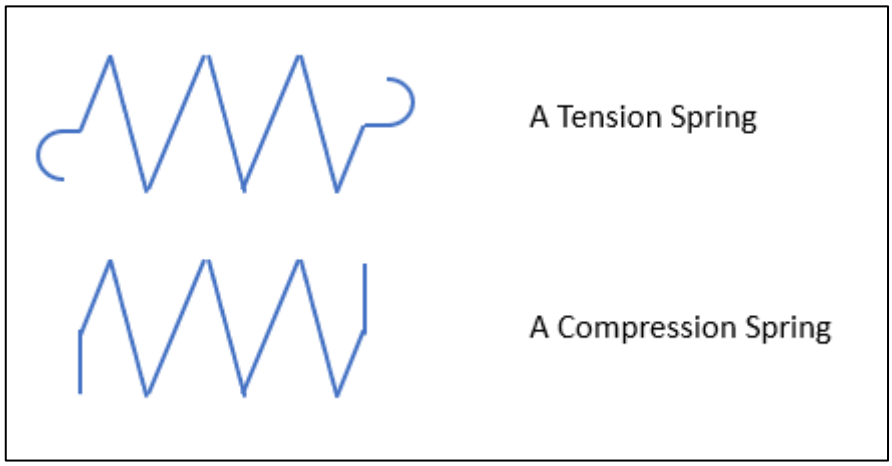

Figure 3.6. Physical differences between tension and compression springs

Using the definition of s_{cha} given by equation (3.19), the spring force inside the chamber, given by equation (3.35), can be written as follows.

$$F_{cha,spr} = k_{cha}\left((x_r + b_1 - b_3 - b_2) - l_{f,\,cha}\right) \tag{3.36}$$

Alternatively, $F_{cha,spr}$ can be expressed as

$$F_{cha,spr} = k_{cha}(x_r - l^*_{cha}) \tag{3.37}$$

where

$$l^*_{cha} = b_2 + b_3 - b_1 + l_{f,cha}$$

Referring to Figure 3.5, let the force $\vec{F}_{MFG,spr,2}$, applied on Link 2, be the force which is equivalent to the spring force $\vec{F}_{cha,spr,3}$. In other words, for rigid body mechanics

purposes, one can replace the spring force $\vec{F}_{cha,spr,3}$ with the equivalent force $\vec{F}_{MFG,spr,2}$. Here it should be noted that although the spring force $\vec{F}_{cha,spr,3}$ is an actual force, equivalent force $\vec{F}_{MFG,spr,2}$ is fictitious. Similarly, let the force $\vec{F}_{MFG,spr,4}$ be a fictitious force which is equivalent to the actual spring force $\vec{F}_{cha,spr,5}$. In this study, the equivalent fictitious forces $\vec{F}_{MFG,spr,2}$ and $\vec{F}_{MFG,spr,4}$ will be represented as follows.

$$\vec{F}_{MFG,spr,2} = F_{MFG,spr}\vec{k} \tag{3.38}$$

$$\vec{F}_{MFG,spr,4} = -F_{MFG,spr}\vec{k} \tag{3.39}$$

In equations (3.38) and (3.39), let $F_{MFG,spr}$ be defined via the equation

$$F_{MFG,spr} = k_{MFG}[s_{MFG}]\left(s_{MFG} - l_{0,MFG}\right) \tag{3.40}$$

where

$l_{0,MFG}$: Fictitious free length (a constant parameter) of the two fictitious, identical equivalent springs, which are assumed to be attached between the $\vec{x}^{(1)}$ axis and Link 2; and the $\vec{x}^{(1)}$ axis and Link 4 (see Figure 3.5)

$k_{MFG}[s_{MFG}]$: Spring coefficient of the two fictitious, identical equivalent springs (which is a function of the variable s_{MFG}) which are assumed to be attached between the $\vec{x}^{(1)}$ axis and Link 2; and the $\vec{x}^{(1)}$ axis and Link 4 (see Figure 3.5)

Here, it should be noted that, $k_{MFG}\,[s_{MFG}]$ is a user-defined function and $l_{0,MFG}$ is a user-defined parameter which are utilized to define the desired variation of $F_{MFG,spr}$ given by equation (3.40). It should also be noted that from equation (3.40), the value of $F_{MFG,spr}$ at s_{MFG} = 0, $F_{MFG,spr}[0]$, is given by

$$F_{MFG,spr}[0] = -\,k_{MFG}\,[0]\;\; l_{0,MFG} \tag{3.41}$$

Hence, after selecting the user-defined function $k_{MFG}\,[s_{MFG}]$, the value $F_{MFG,spr}[0]$ can be set to any desired value by selecting the user-defined parameter $l_{0,MFG}$ in accordance with equation (3.41) (see Figure 3.7).

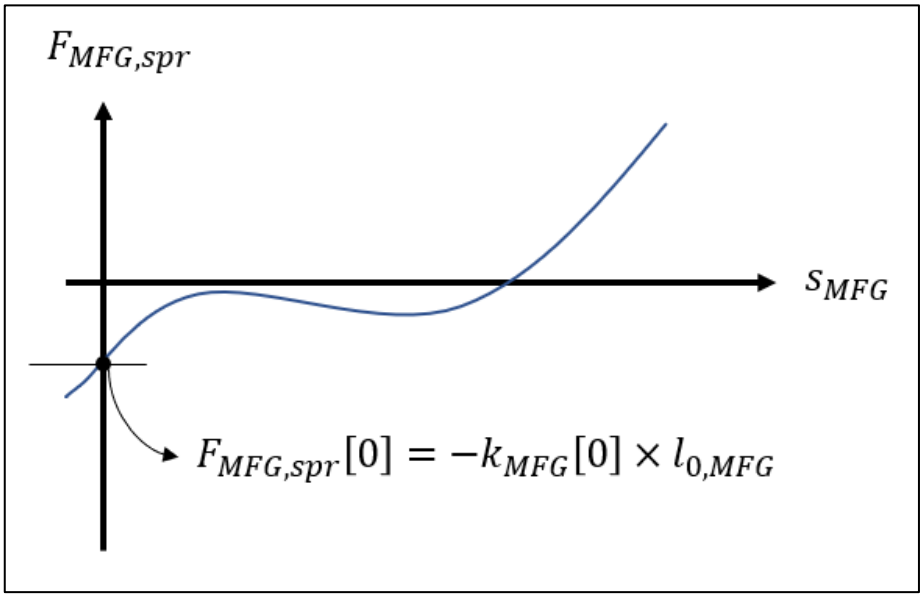

Figure 3.7. Graphical representation of $F_{MFG,spr}[0]$

Since the MFG spring is a fictitious non-linear spring, its compression and tension characteristics do not resemble to a real spring. While the real spring inside the chamber is in compression or tension only, the MFG spring may have the ability to work in both "compression" and "tension".

Note that, since $s_{MFG} = z_r$ from equation (3.20), equation (3.40) yields

$$F_{MFG,spr} = k_{MFG}[z_r]\big(z_r - l_{0,MFG}\big) \tag{3.42}$$

It should be noted that the equivalent spring coefficient of the fictitious spring, k_{MFG} (see equation (3.40)), and the force developed in the fictitious spring, $F_{MFG,spr}$ (see equation (3.40)), have been specified in terms of s_{MFG}. On the other hand, s_{MFG} can be expressed in terms of $s_{2/4}$ (see Figure 3.5) via the equation

$$s_{MFG} = s_{2/4}/2 \tag{3.43}$$

In equation (3.43), $s_{2/4}$ is defined, rigorously, via the equation

$$s_{2/4} = \overrightarrow{O_1O_2} \cdot \vec{k} \tag{3.44}$$

where $\vec{k}$ is a unit vector parallel to the $\vec{z}^{(1)}$ axis. It should be noted that $s_{2/4}$ yields the relative position (parallel to the $\vec{z}^{(1)}$ direction) of Link 2 with respect to Link 4. Hence, $s_{2/4}$ may be considered to be the fictitious "length" of a fictitious, nonlinear spring that is connected between Links 2 and 4. Hence, by replacing s_{MFG} that appears in equation (3.40) with the right hand side of equation (3.43), one may conveniently obtain expressions that yield k_{MFG} and $F_{MFG,spr}$ in terms of $s_{2/4}$.

3.2.1 MFG Spring Slot Shape Determination

Suppose that, it is desired to design an MFGS such that the desired variation of the equivalent forces $\vec{F}_{MFG,spr,2}$ and $\vec{F}_{MFG,spr,4}$ (with respect to s_{MFG}) are specified via the user-defined function $k_{MFG}[s_{MFG}]$ and the user-defined parameter $l_{0,MFG}$. Furthermore, suppose that the two identical linear springs to be used in the MFGS have also been selected. Hence, the spring constant and the free length of these springs (i.e., k_{cha} and $l_{f,cha}$) are also known. Now, by designing the shapes of the four symmetrical slots suitably; and by selecting the remaining kinematic dimensions of the MFGS appropriately, it is possible to design an MFGS which will generate the desired equivalent forces $\vec{F}_{MFG,spr,2}$ and $\vec{F}_{MFG,spr,4}$. In this section, an algorithm that yields the shapes of slots and kinematic dimensions of the MFGS is presented.

While designing an MFGS, gravitational, inertial and frictional effects are neglected in this study. Similarly, gravitational, inertial and frictional effects are also neglected while designing an MFGD (see Section 3.3). In the preceding two paragraphs, for a specific MFG (with a specific motion and loading), the effects of inertial and frictional loads on the power losses are discussed. For the specific cases under consideration, it is shown that the inertial and frictional effects are negligible (as assumed in this study). In cases where gravitational, inertial and frictional effects are

not negligible, they should also be taken into account while designing an MFGS, or MFGD.

Effect of Inertial Loads for an MFG

One of the comprehensive studies, performed by Mencek in 2015 [4], investigated the effect of inertial loads on the power consumption of the actuators that drive an MFG. For a specific MFG (with a specific motion and loading), the input and output powers are compared for Case A, where the inertial and frictional effects are neglected, and Case B, where the inertial effects are taken into account, but the frictional effects are neglected (see Figure 3.8). The efficiency of the system is evaluated, via simulation, for these cases. The comparison shows that, by taking power consumption of Case A as reference (100%), the efficiency of the system is obtained as 98.98%. It is proved that, for this specific case, neglecting the inertial loads is an acceptable assumption.

Effect of Frictional Losses for an MFG

The effect of frictional losses has been investigated by Mencek [4] and Erdinç [3] separately. Similar to inertial loads, Mencek performed a comparison between Case A, where the inertial and frictional effects are neglected, and Case C, where the frictional losses are considered, but the inertial effects are neglected (see Figure 3.8). The comparison shows that, by taking power consumption of Case A as reference (100%), the efficiency of the system is obtained as 88.4%. Besides, in his study, Erdinç stated that the friction losses in different case studies were 6.2% and 8.9% of the total power consumption.

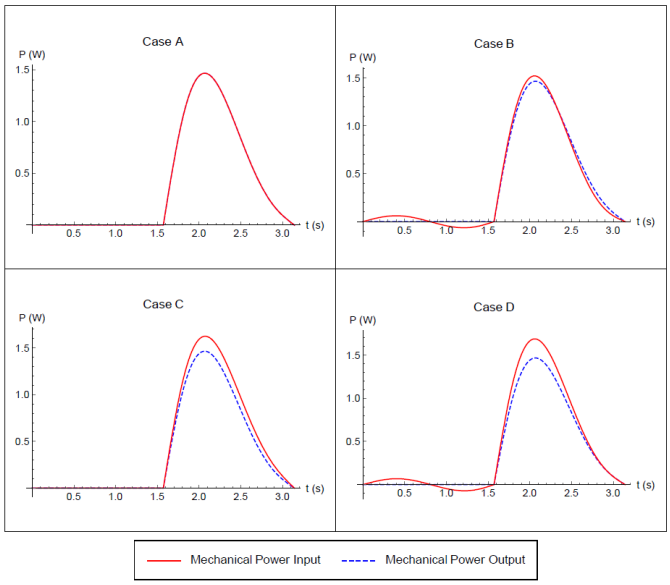

Figure 3.8. Results for different cases in Mencek's study [4]

Referring to Figure 3.5, neglecting gravitational, frictional and inertial effects, in order for the fictitious force $\vec{F}_{MFG,spr,2}$ to be equivalent to the spring force $\vec{F}_{cha,spr,3}$, the instantaneous powers due to these two forces must be equal to each other at all times, i.e.,

$$\vec{F}_{cha,spr,3} \cdot \vec{v}_3 = \vec{F}_{MFG,spr,2} \cdot \vec{v}_2 \tag{3.45}$$

where $\vec{v}_3$ and $\vec{v}_2$ are the velocities of Links 3 and 2, respectively, given by

$$\vec{v}_3 = \dot{s}_{cha}\vec{\imath} \tag{3.46}$$

$$\vec{v}_2 = \dot{s}_{MFG}\vec{k} \tag{3.47}$$

Substituting equations (3.33), (3.46), (3.38), and (3.47) into equation (3.45), one obtains

$$-F_{cha,spr}\dot{s}_{cha} = F_{MFG,spr}\dot{s}_{MFG} \tag{3.48}$$

where $F_{cha,spr}$ and $F_{MFG,spr}$ are given by equations (3.35) and (3.40), respectively.

Similarly, in order for the fictitious force $\vec{F}_{MFG,spr,4}$ to be equivalent to the spring force $\vec{F}_{cha,spr,5}$, the instantaneous powers due to these two forces must be equal to each other at all times, i.e.

$$\vec{F}_{cha,spr,5} \cdot \vec{v}_5 = \vec{F}_{MFG,spr,4} \cdot \vec{v}_4 \tag{3.49}$$

where $\vec{v}_5$ and $\vec{v}_4$ are the velocities of Links 5 and 4, given by

$$\vec{v}_5 = -\dot{s}_{cha}\vec{\imath} \tag{3.50}$$

$$\vec{v}_4 = -\dot{s}_{MFG}\vec{k} \tag{3.51}$$

Substituting equations (3.34), (3.50), (3.39), and (3.51) into equation (3.49), one obtains, once more, equation (3.48). Hence, equation (3.48) is, simultaneously, the condition for the fictitious force $\vec{F}_{MFG,spr,2}$ to be equivalent to the spring force $\vec{F}_{cha,spr,3}$; and the condition for the fictitious force $\vec{F}_{MFG,spr,4}$ to be equivalent to the spring force $\vec{F}_{cha,spr,5}$.

Using equations (3.37) and (3.42) with equations (3.25) and (3.26), equation (3.48) becomes

$$-k_{cha}(x_r - l^*_{cha})\ \frac{dx_r}{dz_r}\dot{z}_r = k_{MFG}[z_r]\big(z_r - l_{0,MFG}\big)\dot{z}_r$$

which yields

$$-k_{cha}(x_r - l^*_{cha})\ dx_r = k_{MFG}[z_r]\big(z_r - l_{0,MFG}\big)dz_r \tag{3.52}$$

The differential equation above is already in separate form and, thus, can be solved with direct integration using separation of variables ($\int f[x]dx = \int g[y]dy$) yielding

$$\int_{(x_r)_i}^{x_r}(x_r - l^*_{cha})dx_r = \int_{(z_r)_i}^{z_r} h[z_r]dz_r \tag{3.53}$$

where

$$h[z_r] = -\frac{k_{MFG}[z_r]}{k_{cha}}\big(z_r - l_{0,MFG}\big) \tag{3.54}$$

In equation (3.53), $(x_r)_i$ and $(z_r)_i$ are the x and z coordinates (in $\mathcal{F}_3$) of a user selected point Q_i that is required to lie on the path P_1 (see Figure 3.2). Recall that P_1 is the path, on Link 3, on which the center of Roller 6 is restricted to move.

Clearly, the lower limits of the integrals, $(x_r)_i$ and $(z_r)_i$, affect the solution for the slot shape center line. So, selecting the limits is important in finding a feasible solution for a particular problem. The realizability checks (see Section 3.2.2) are always performed after the solution is obtained. However, a convenient selection of the lower limits reduces the amount of work spent on these realizability checks. For example, it is convenient to select the lower corners of the region R in Figure 3.3 (i.e. $(x_r)_i = d_{cle}$ and $(z_r)_i = d_{cle}$ or $(x_r)_i = b_3 - d_{cle}$ and $(z_r)_i = c_1 - d_{cle}$). With this selection, satisfaction of the criterion in given Section 3.2.2 may become easier.

Integrating equation (3.53), one obtains

$$\frac{x_r^2}{2} - x_r l_{cha}^* \Big|_{(x_r)_i}^{x_r} = p[z_r] \Big|_{(z_r)_i}^{z_r}$$

which yields

$$\frac{x_r^2}{2} - \frac{(x_r)_i^2}{2} - [x_r - (x_r)_i] l_{cha}^* = p[z_r] - p[(z_r)_i] \tag{3.55}$$

where

$$p[z_r] = \int h[z_r] dz_r \tag{3.56}$$

Now, for simplicity, define the constants K_1, K_2 and K_3 via the following equations

$$K_1 = (x_r)_i^2$$

$$K_2 = (x_r)_i l_{cha}^*$$

$$K_3 = p[(z_r)_i]$$

Hence, equation (3.55) yields

$$x_r^2 - 2x_r l_{cha}^* - 2p[z_r] - K_1 + 2K_2 + 2K_3 = 0 \tag{3.57}$$

Now, introduce a new function $q[z_r]$, via the equation

$$q[z_r] = -2p[z_r] - K_1 + 2K_2 + 2K_3$$

Now, using the definition of $q[z_r]$, equation (3.57) can be written in the following form

$$x_r^2 - 2x_r l_{cha}^* + q[z_r] = 0 \tag{3.58}$$

Equation (3.58) is a quadratic equation in x_r. Using this equation, one may obtain two solutions for x_r (in terms of z_r). These two solutions yield two different P_1 curves (see Figure 3.2), on which the center of Roller 6 is restricted to lie. The two solutions of equation (3.58) for x_r, i.e., $(x_r)_p$ and $(x_r)_n$, are given below.

$$(x_r)_{p,n} = l_{cha}^* \pm \sqrt{\Delta[z_r]} \tag{3.59}$$

where

$$\Delta[z_r] = {l_{cha}^*}^2 - q[z_r]$$

and $(x_r)_p$ and $(x_r)_n$ are the solutions obtained by using the $(+)$ and $(-)$ signs in equation (3.59), respectively. Note that, $(x_r)_p$ and $(x_r)_n$ need to be real numbers, which would be true if

$$\Delta[z_r] = {l_{cha}^*}^2 - q[z_r] \geq 0$$

for all z_r in the working range of MFGS. Recalling that $z_r = s_{MFG}$ (see equation (3.20)), note that the working range of MFGS is given by $l_{MFG,min} \leq s_{MFG} \leq l_{MFG,max}$ (see equation (3.11)).

$(x_r)_p$ and $(x_r)_n$ given by equation (3.59) yield two different P_1 paths (see Figure 3.2) on which the center of Roller 6 is restricted to lie. As can be observed from equation (3.59), these two paths are symmetrical with respect to the line $x_r = l_{cha}^*$. In order to determine whether these P_1 paths lie in the allowable region R presented in Figure 3.3, it is necessary to determine the minimum and maximum values of x_r which are denoted as $(x_r)_{min}$ and $(x_r)_{max}$, respectively. In order to determine

$(x_r)_{min}$ and $(x_r)_{max}$, on the other hand, one needs to determine the critical points of $(x_r)_p$ and $(x_r)_n$. These critical points are obtained from the equation

$$\frac{dx_r}{dz_r} = 0$$

which is equivalent to

$$h[z_r] = 0 \tag{3.60}$$

where $h[z_r]$ is given by equation (3.54).

Now, let the roots of equation (3.60) be denoted by $(z_r)_1$, $(z_r)_2$, … , $(z_r)_n$. Clearly, $(x_r)_{min}$ and $(x_r)_{max}$ can be obtained by evaluating $(x_r)_p$ (or, $(x_r)_n$) at the critical points obtained from equation (3.60) and at the lower and upper bounds of z_r (which are $l_{MFG,min}$ and $l_{MFG,max}$).

It should be noted that the number of P_1 paths that lie in the allowable region R may be zero, or infinitely many.

Note that the design procedure presented in this section is applicable to the case where Link 4 (rather than Link 1) is the ground (see Appendix A). The design procedure is also applicable when none of the links in the MFGS, including Link 1, is grounded (see Appendix B).

3.2.2 MFG Spring Slot Shape Realizability Checks

The MFGS is a non-linear spring that can be designed with respect to user needs and design constraints. The solution found in equation (3.59) is only a mathematical solution. This mathematical solution shall be checked against the physical dimensions and design constraints of the MFGS. Thus, the following checks shall be made on the MFGS dimensions.

Spring working range check

The working range defined here is applicable for the use of a compression spring only or a tension spring only. The working range for the use of an equivalent special spring (which can work as a tension and compression spring simultaneously) is defined in Section 3.2.3.

The working range of a spring is limited by its shape or mechanical properties. For a compression spring, the operating range is limited by the spring shape. Let the minimum allowable length of a compression spring be defined as $l_{spr,min}$ and the maximum allowable length of a compression spring be defined as $l_{f,spr}$, which is the free length of the spring, then the following criterion shall be satisfied.

- $s_{cha,max} \geq s_{cha} \geq s_{cha,min}$ which yields

$$l_{f,spr} \geq s_{cha} \geq l_{spr,min} \tag{3.61}$$

For a tension spring, the operating range is limited by the strength properties of the spring. If the maximum allowable length of the tension spring is defined as $l_{spr,max}$ and the minimum allowable length of a tension spring is defined as $l_{f,spr}$, which is the free length of the spring, then the following criterion shall be satisfied.

- $s_{cha,min} \leq s_{cha} \leq s_{cha,max}$ which yields

$$l_{f,spr} \leq s_{cha} \leq l_{spr,max} \tag{3.62}$$

3.2.3 Design of an Equivalent Spring, the Generated Spring Force of which can Change Direction

The force generated by a tension spring, F_{ten}, is given by

$$F_{ten} = k_{ten}\left(x_{ten} - l_{f,ten}\right) \tag{3.63}$$

where

k_{ten} : Spring constant of linear tension spring

x_{ten} : Length of the tension spring

$l_{f,ten}$: Free length of the tension spring

Equation (3.63) is only valid if

$$x_{ten} \geq l_{f,ten} \tag{3.64}$$

yielding

$$F_{ten} > 0$$

which implies that the direction of the force provided by a tension spring cannot change.

The force generated by a compression spring is given by

$$F_{com} = k_{com}(x_{com} - l_{f,com}) \tag{3.65}$$

where

k_{com} : Spring constant of linear compression spring

x_{com} : Length of the compression spring

$l_{f,com}$: Free length of the compression spring

Equation (3.65) is only valid if

$$x_{com} \leq l_{f,com} \tag{3.66}$$

yielding

$$F_{com} < 0$$

which implies that the direction of the force provided by a compression spring cannot change.

Now, suppose that it is necessary to design a linear spring that generates a spring force, the direction of which can change. This can be realized by using a tension

spring and compression spring in parallel (see Figure 3.9), such that the lengths of the two springs, which are equal, are given by

$$x_{tc} = x_{ten} = x_{com} \tag{3.67}$$

and the free lengths of the two springs satisfy the following two constraints

$$l_{f,ten} < l_{f,com} \tag{3.68}$$

$$l_{f,ten} \leq x_{tc} \leq l_{f,com} \tag{3.69}$$

In Figure 3.9, the dashed lines represent the relaxed positions of the springs, while the solid lines represent the extended/compressed positions of the springs.

The net force developed by the two springs in Figure 3.9, F_{tc}, is clearly given by

$$F_{tc} = F_{ten} + F_{com} \tag{3.70}$$

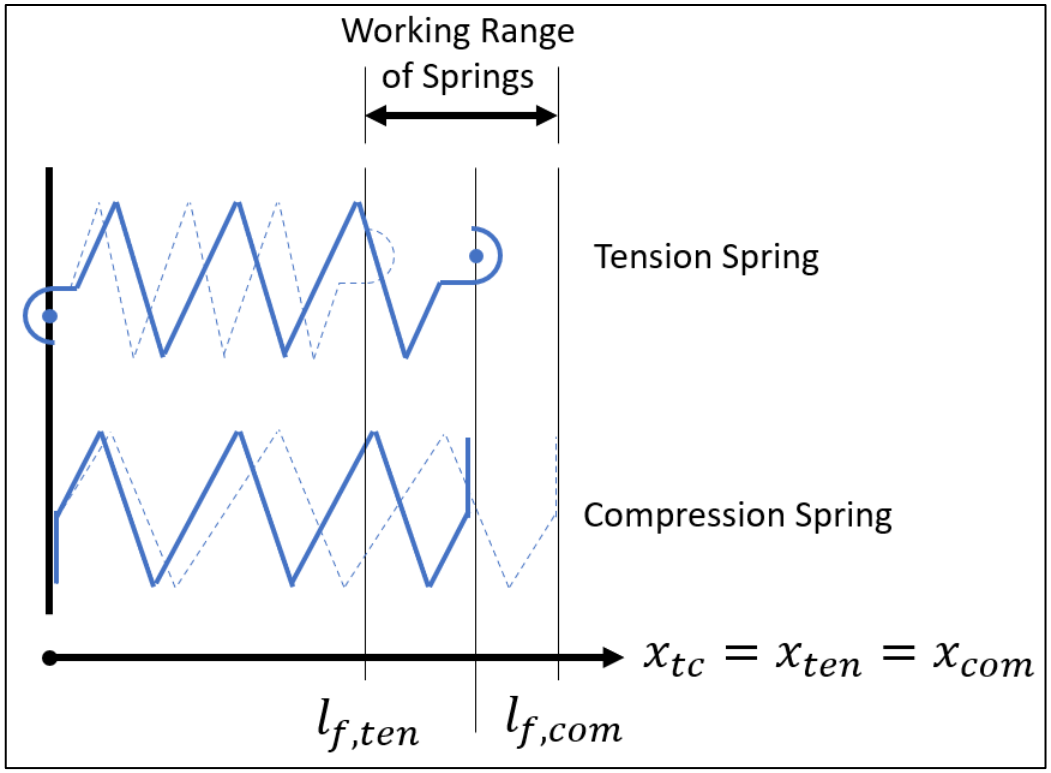

Figure 3.9. Combined use of a tension spring and a compression spring connected parallel to each other

If equations (3.63), (3.65) and (3.67) are inserted into equation (3.70), the following equation is obtained.

$$F_{tc} = k_{ten}\left(x_{tc} - l_{f,ten}\right) + k_{com}\left(x_{tc} - l_{f,com}\right) \tag{3.71}$$

which can be arranged in the form

$$F_{tc} = (k_{ten} + k_{com})\left[x_{tc} - \frac{k_{ten}l_{f,ten} + k_{com}l_{f,com}}{k_{ten} + k_{com}}\right] \tag{3.72}$$

which can be expressed as

$$F_{tc} = k_{tc}\left(x_{tc} - l_{f,tc}\right) \tag{3.73}$$

where

$$k_{tc} = k_{ten} + k_{com} \tag{3.74}$$

$$l_{f,tc} = \frac{k_{ten}l_{f,ten} + k_{com}l_{f,com}}{k_{tc}} \tag{3.75}$$

and

k_{tc} : Spring constant of the equivalent tension/compression spring

$l_{f,tc}$: Fictitious free length of the equivalent tension/compression spring

Assuming that k_{tc} and $l_{f,tc}$ are specified in the desired manner, equations (3.74) and (3.75) constitute two equations with four unknowns (namely k_{ten}, $l_{f,ten}$, k_{com}, $l_{f,com}$). Hence, it should always be possible to select these four unknowns, from the spring catalogs, such that equations (3.74) and (3.75) yield the desired k_{tc} and $l_{f,tc}$ values (exactly, or very closely).

As an illustrative numerical example, the force developed in tension, compression and tension/compression spring (i.e., F_{ten}, F_{com} and F_{tc}, respectively) are presented in Figure 3.10.

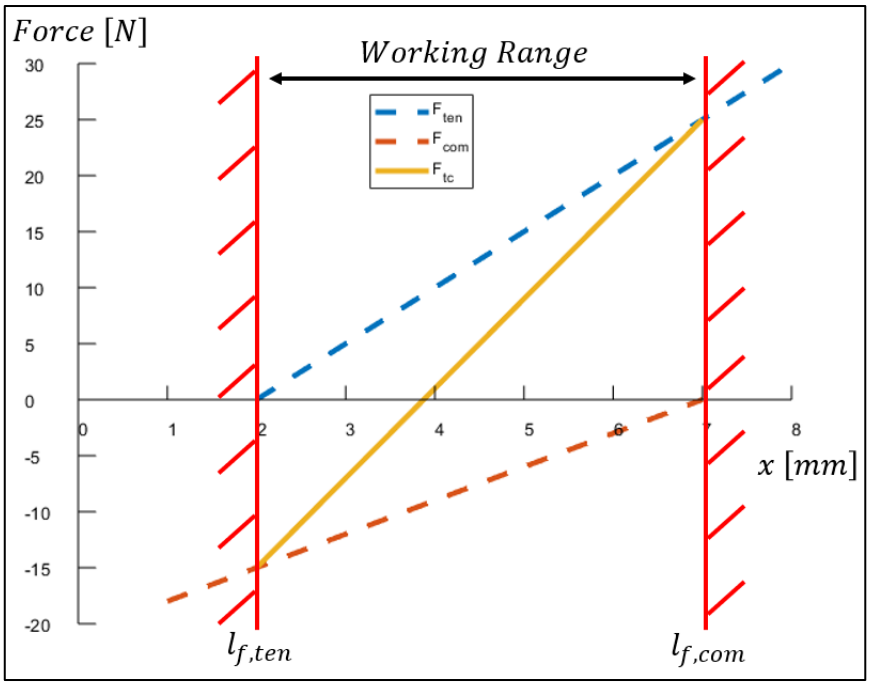

Figure 3.10. Comparison of the force characteristics between tension, compression, and tension/compression springs

The properties of the tension and compression springs used in Figure 3.10 are listed in Table 3.1.

Table 3.1. Spring parameters used in the numerical example

Spring Parameter	*Value*
k_{ten} $[N/mm]$	5
$l_{f,ten}$ $[mm]$	2
k_{com} $[N/mm]$	3
$l_{f,com}$ $[mm]$	7

3.3 MFG Damper (MFGD)

In this study, MFG Damper (MFGD) denotes the mechanism that is obtained from MFG, such that it converts two linear, identical dampers (with constant damping coefficients) into two equivalent, virtual non-linear dampers. The two linear dampers

are attached between Links 1 and 3; and Links 1 and 5 (see Figure 3.1). The forces applied on Links 3 and 5, by the 2 linear dampers, are designated by $\vec{F}_{cha,dmp,3}$ and $\vec{F}_{cha,dmp,5}$ respectively (see Figure 3.11), where;

$$\vec{F}_{cha,dmp,3} = -F_{cha,dmp}\vec{\imath} \tag{3.76}$$

$$\vec{F}_{cha,dmp,5} = F_{cha,dmp}\vec{\imath} \tag{3.77}$$

In equations (3.76) and (3.77)

$$F_{cha,dmp} = b_{cha}\dot{s}_{cha} \tag{3.78}$$

where

b_{cha} : Damping coefficient of the two linear, identical dampers

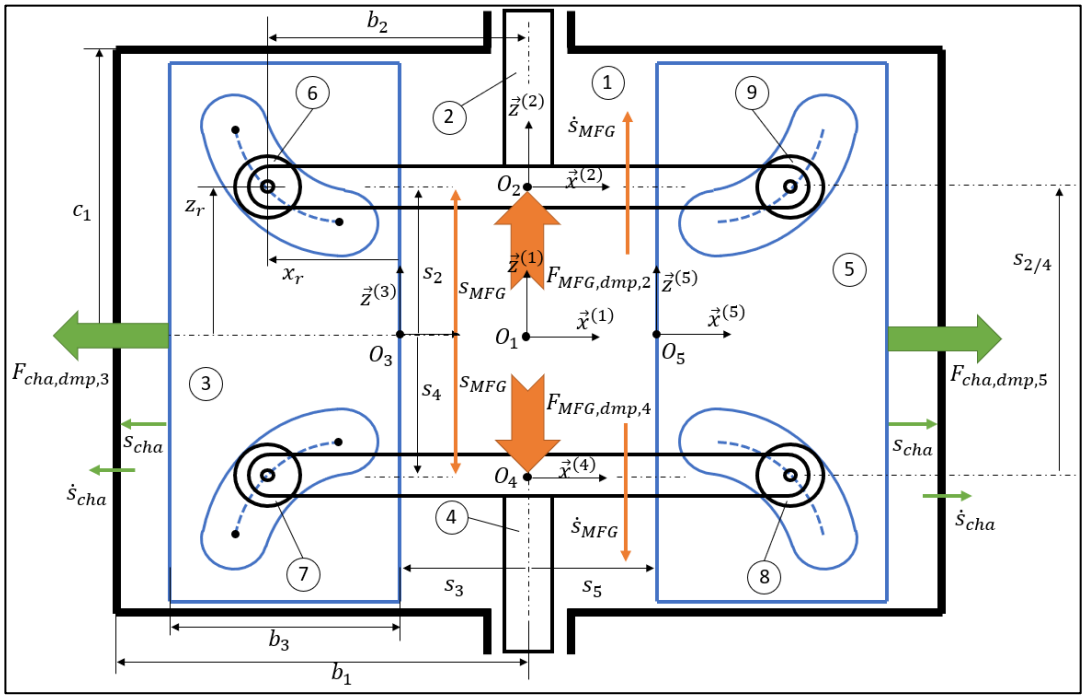

Figure 3.11. Damper forces acting on MFG

It should be noted that due to the physical nature of a damper, the damping coefficient cannot be smaller than zero, i.e.,

$$b_{cha} > 0$$

Using the definition of $\dot{s}_{cha}$ given by equation (3.25) and equation (3.78), the damper force inside the chamber can be written as follows.

$$F_{cha,dmp} = b_{cha}\dot{x}_r \tag{3.79}$$

Referring to Figure 3.11, let the force $\vec{F}_{MFG,dmp,2}$, applied on Link 2, be the force which is equivalent to the damper force $\vec{F}_{cha,dmp,3}$. In other words, for rigid body mechanics purposes, one can replace the damper force $\vec{F}_{cha,dmp,3}$ with the equivalent force $\vec{F}_{MFG,dmp,2}$. Here, it should be noted that although the damper force $\vec{F}_{cha,dmp,3}$ is an actual force, the equivalent force $\vec{F}_{MFG,dmp,2}$ is fictitious. Similarly, let the force $\vec{F}_{MFG,dmp,4}$, applied on Link 4, be a fictitious force which is equivalent to the actual damper force $\vec{F}_{cha,dmp,5}$. In this study, the equivalent fictitious forces $\vec{F}_{MFG,dmp,2}$ and $\vec{F}_{MFG,dmp,4}$ will be represented as follows.

$$\vec{F}_{MFG,dmp,2} = F_{MFG,dmp}\vec{k} \tag{3.80}$$

$$\vec{F}_{MFG,dmp,4} = -F_{MFG,dmp}\vec{k} \tag{3.81}$$

In equations (3.80) and (3.81):

$$F_{MFG,dmp} = -b_{MFG}[s_{MFG}]\dot{s}_{MFG} \tag{3.82}$$

where

$b_{MFG}[s_{MFG}]$: The damping coefficient of the two fictitious, identical equivalent dampers (which is a function of the variable s_{MFG}) which are assumed to be attached between the $\vec{x}^{(1)}$ axis and Link 2; and the $\vec{x}^{(1)}$ axis and Link 4 (see Figure 3.11)

Note that $b[s_{MFG}] > 0$ for all possible values of s_{MFG} in the domain of its definition.

Substituting equations (3.20) and (3.26) into equation (3.82), the fictitious non-linear damper force can be written as follows.

$$F_{MFG,dmp} = -b_{MFG}[z_r]\dot{z}_r \tag{3.83}$$

where

$$b_{MFG}[z_r] > 0$$

Here, it should be noted that the damping coefficient of the MFGD is defined as a function of position.

It should also be noted that the equivalent damping coefficient of the fictitious damper, b_{MFG}, and the force developed in the fictitious damper, $F_{MFG,dmp}$ (see equation (3.82)) have been specified in terms of s_{MFG} and $\dot{s}_{MFG}$. Using equation (3.43) ($s_{MFG} = s_{2/4}/2$), on the other hand, $\dot{s}_{MFG}$ is given by

$$\dot{s}_{MFG} = \dot{s}_{2/4}/2 \tag{3.84}$$

where $\dot{s}_{2/4}/2$ is the relative velocity (parallel to the $\vec{z}^{(1)}$ direction) of Link 2 with respect to Link 4 (see Figure 3.11). Now, by replacing s_{MFG} and $\dot{s}_{MFG}$ that appear in equation (3.82) with the right hand sides of equation (3.43) and equation (3.84), one may conveniently obtain expressions that yield b_{MFG} and $F_{MFG,dmp}$ in terms of $s_{2/4}/2$ and $\dot{s}_{2/4}/2$.

3.3.1 MFG Damper Slot Shape Determination

Suppose that it is desired to design an MFGD such that the desired variation of the equivalent forces $\vec{F}_{MFG,dmp,2}$ and $\vec{F}_{MFG,dmp,4}$ (with respect to s_{MFG} and $\dot{s}_{MFG}$) are specified via the user-defined function $b_{MFG}[s_{MFG}]$. Furthermore, suppose that the two identical linear dampers that are to be used in the MFGD have also been selected. Hence, the damping coefficient of these dampers (i.e., b_{cha}) are also known. Now, by designing the shapes of the four symmetrical slots suitably; and by selecting the remaining kinematic dimensions of the MFGD appropriately, it is possible to design an MFGD which will generate the desired equivalent damping forces $\vec{F}_{MFG,dmp,2}$ and $\vec{F}_{MFG,dmp,4}$. An algorithm that yields the shapes of slots and kinematic dimensions of the MFGD is presented in this section.

Neglecting gravitational, frictional and inertial effects, in order for the fictitious force $\vec{F}_{MFG,dmp,2}$ to be equivalent to the damper force $\vec{F}_{cha,dmp,3}$, the instantaneous powers due to these two forces must be equal to each other at all times, i.e.

$$\vec{F}_{cha,dmp,3} \cdot \vec{v}_3 = \vec{F}_{MFG,dmp,2} \cdot \vec{v}_2 \tag{3.85}$$

where $\vec{v}_3$ and $\vec{v}_2$ are the velocities of Links 3 and 2, respectively, which have been given previously as follows.

$$\vec{v}_3 = \dot{s}_{cha}\vec{\imath} \tag{3.46}$$

$$\vec{v}_2 = \dot{s}_{MFG}\vec{k} \tag{3.47}$$

Substituting equations (3.76), (3.46), (3.80), and (3.47) into equation (3.85), one obtains

$$-F_{cha,dmp}\dot{s}_{cha} = F_{MFG,dmp}\dot{s}_{MFG} \tag{3.86}$$

where $F_{cha,dmp}$ and $F_{MFG,dmp}$ are given by equations (3.78) and (3.82), respectively.

Similarly, in order for the fictitious force $\vec{F}_{MFG,dmp,4}$ to be equivalent to the damper force $\vec{F}_{cha,dmp,5}$, the instantaneous powers due to these two forces must be equal to each other at all times, i.e.

$$\vec{F}_{cha,dmp,5} \cdot \vec{v}_5 = \vec{F}_{MFG,dmp,4} \cdot \vec{v}_4 \tag{3.87}$$

where $\vec{v}_5$ and $\vec{v}_4$ are the velocities of Links 5 and 4, respectively, which have been given previously as follows.

$$\vec{v}_5 = -\dot{s}_{cha}\vec{\imath} \tag{3.50}$$

$$\vec{v}_4 = -\dot{s}_{MFG}\vec{k} \tag{3.51}$$

Substituting equations (3.77), (3.50), (3.81), and (3.51) into equation (3.87), one obtains, once more, equation (3.86). Hence, equation (3.86) is, simultaneously, the condition for the fictitious force $\vec{F}_{MFG,dmp,2}$ to be equivalent to the damper force

$\vec{F}_{cha,dmp,3}$; and the condition for the fictitious force $\vec{F}_{MFG,dmp,4}$ to be equivalent to the damper force $\vec{F}_{cha,dmp,5}$.

Using equations (3.79), (3.83), (3.25), (3.26) and (3.22), equation (3.86) becomes

$$b_{cha}\left(\frac{dx_r}{dz_r}\right)^2 \dot{z}_r^2 = b_{MFG}[z_r]\dot{z}_r^2$$

which, upon simplification, yields

$$\left(\frac{dx_r}{dz_r}\right)^2 = \frac{b_{MFG}[z_r]}{b_{cha}} \tag{3.88}$$

Taking the square root of both sides, one obtains

$$\frac{dx_r}{dz_r} = \pm\sqrt{\frac{b_{MFG}[z_r]}{b_{cha}}} \tag{3.89}$$

Recall that $b_{MFG} > 0$ for all possible values of z_r in the domain of its definition. Furthermore, $b_{cha} > 0$ as well. Hence, it follows that equation (3.89) always yields two distinct and real solutions for $\frac{dx_r}{dz_r}$.

Now, let

$$\sigma = \pm 1$$

and define $g[z_r]$ via the equation

$$g[z_r] = \sqrt{\frac{b_{MFG}[z_r]}{b_{cha}}} \tag{3.90}$$

Using the above two definitions and solving dx_r from equation (3.89), one obtains

$$dx_r = \sigma g[z_r]dz_r \tag{3.91}$$

The differential equation above is already in separated form and can be solved with direct integration using separation of variables ($\int f[x]dx = \int g[y]dy$) yielding

$$\int_{(x_r)_i}^{x_r} dx_r = \int_{(z_r)_i}^{z_r} \sigma g[z_r]dz_r \tag{3.92}$$

In equation (3.92), $(x_r)_i$ and $(z_r)_i$ are the x and z coordinates (in $\mathcal{F}_3$) of a user selected point Q_i that it is required to lie on the path P_1 (see Figure 3.2). Recall that P_1 is the path, on Link 3, on which the center of Roller 6 is restricted to move.

Clearly, the lower limits of the integrals, $(x_r)_i$ and $(z_r)_i$, affect the solution for the slot shape centerline. So, selecting the limits accurately is essential in finding a feasible solution for a particular problem. The realizability checks (see Section 3.3.2) are always performed after the solution is obtained; however, a convenient selection of this point may reduce the amount of work spent on these realizability checks. For example, it is convenient to select the lower corners of the region R in Figure 3.3 (i.e. $(x_r)_i = d_{cle}$ and $(z_r)_i = d_{cle}$ or $(x_r)_i = b_3 - d_{cle}$ and $(z_r)_i = c_1 - d_{cle}$) which leads to a 3-step algorithm presented at the end of this section.

Integrating equation (3.92), one obtains

$$x_r \Big|_{(x_r)_i}^{x_r} = \sigma p[z_r] \Big|_{(z_r)_i}^{z_r}$$

which yields

$$x_r = \sigma(p[z_r] - p[(z_r)_i]) + (x_r)_i \tag{3.93}$$

where

$$p[z_r] = \int g[z_r] dz_r$$

Since $\sigma = \pm 1$, equation (3.93) can be rewritten as follows.

$$(x_r)_{p,n} = (x_r)_i \pm (p[z_r] - p[(z_r)_i]) \tag{3.94}$$

where $(x_r)_p$ and $(x_r)_n$ denote the two solutions (in terms of z_r) of the differential equation given by equation (3.89). Note that $(x_r)_p$ denotes the solution with the $(+)$ sign in equation (3.94). $(x_r)_n$, on the other hand, denotes the solution with the $(-)$ sign. These two solutions for x_r yield two different P_1 paths (see Figure 3.2), on which the center of Roller 6 is restricted to lie.

From equation (3.94), it follows that the two P_1 paths thus obtained are symmetrical with respect to the line $x_r = (x_r)_i$. Furthermore, since $g[z_r] > 0$ for all z_r, the P_1 curve corresponding to $(x_r)_p$ will always lie "above" the line $x_r = (x_r)_i$ for $z_r > (z_r)_i$. The P_1 curve corresponding to $(x_r)_n$, on the other hand, will always lie "below" the line $x_r = (x_r)_i$. These observations lead to a 3-step algorithm which may be used to determine P_1 paths that lie in the allowable region R (see Figure 3.3).

(1) Let

$$(x_r)_i = d_{cle} \tag{3.95}$$

$$(z_r)_i = l_{MFG,min} \tag{3.96}$$

If

$$(x_r)_p \Big|_{z_r = l_{MFG,max}} < (b_3 - d_{cle}) \tag{3.97}$$

then the path corresponding to $(x_r)_p$ lies in the region R. Note that there may also be other P_1 paths that lie in R corresponding to the selection

$$(x_r)_i > d_{cle} \tag{3.98}$$

$$(z_r)_i = l_{MFG,min} \tag{3.99}$$

(2) Let

$$(x_r)_i = b_3 - d_{cle} \tag{3.100}$$

$$(z_r)_i = l_{MFG,min} \tag{3.101}$$

If

$$(x_r)_n \Big|_{z_r = s_{MFG,max}} > d_{cle} \tag{3.102}$$

then the path corresponding $(x_r)_n$ lies in the region R. Note that there may also be other P_1 paths that lie in R corresponding to the selection

$$(x_r)_i < b_3 - d_{cle} \tag{3.103}$$

$$(z_r)_i = l_{MFG,min} \tag{3.104}$$

(3) If steps (1) and (2) of the algorithm yield no allowable paths that lie fully in R, then there exists no allowable paths, P_1, that lie in R.

3.3.2 MFG Damper Slot Shape Realizability Check

The working range of a damper is limited by its shape in terms of displacement. In this study, the allowable minimum and maximum working strokes of a damper are defined as $l_{dmp,min}$ and $l_{dmp,max}$, respectively. Hence, in order to prevent a clash/contact at the damper, the following criterion should be satisfied.

$$l_{dmp,max} \geq s_{cha} \geq l_{dmp,min} \tag{3.105}$$

Since s_{cha} is defined as $s_{cha} = b_1 - b_3 - s_3$ in equation (3.8) and s_3 is defined as $s_3 = b_2 - x_r$ in equation (3.18), equation (3.105) can be written as follows.

$$l_{dmp,max} - b_1 + b_2 + b_3 \geq x_r \geq l_{dmp,min} - b_1 + b_2 + b_3 \tag{3.106}$$

3.4 Quadratic Equivalent Springs

The solutions obtained in Section 3.2 are general solutions and applicable for any spring case. An example of slot shape determination and spring properties evaluation is performed for a quadratic spring characteristic of MFGS in Section 3.4.1. Examples of different spring characteristics are investigated in this section to evaluate the possible benefits of using MFGS for different purposes.

Let the MFGS have a quadratic fictitious spring coefficient given by

$$k_{MFG}[s_{MFG}] = k_2 s_{MFG}^2 + k_1 s_{MFG} + k_0 \tag{3.107}$$

and let the fictitious free length of the MFGS be $l_{0,MFG}$.

Referring to Figure 3.5, recall that $\vec{F}_{MFG,spr,2} = F_{MFG,spr}\vec{k}$ and $\vec{F}_{MFG,spr,4} = -F_{MFG,spr}\vec{k}$ are the forces applied by the fictitious spring on Links 2 and 4,

respectively. Hence, the forces applied by Links 2 and 4 on the fictitious spring will have the same magnitude (i.e., $F_{MFG,spr}$) in the opposite direction. Hence, the energy stored in the MFGS is defined with the following equation.

$$E_{MFG,spr} = 2\int_{l_{0,MFG}}^{s_{MFG}} -F_{MFG,spr}\,ds_{MFG} \tag{3.108}$$

In equation (3.108), the coefficient 2 is due to the fact that both of the forces $\vec{F}_{MFG,spr,2}$ and $\vec{F}_{MFG,spr,4}$ do contribute to the work done. The minus sign in equation (3.108), on the other hand, is because of the fact that the directions of the two forces applied on the spring and the directions of the displacements (i.e., ds_{MFG} and $-ds_{MFG}$) are opposite.

Referring to equations (3.40) and (3.108), note that

$$-2\big(F_{MFG,spr}\big) = \frac{dE_{MFG,spr}}{ds_{MFG}} \tag{3.109}$$

Now, let $s_{MFG} = (s_{MFG})_{cr}$ denote a critical point of $E_{MFG,spr}$ which is obtained by solving the equation

$$-2\big(F_{MFG,spr}\big) = \frac{dE_{MFG,spr}}{ds_{MFG}} = 0 \tag{3.110}$$

for s_{MFG}. Note that $s_{MFG} = (s_{MFG})_{cr}$ will correspond to an equilibrium point. Furthermore, let $\hat{k}_{MFG}[s_{MFG}]$ (namely, the equivalent stiffness corresponding to $k_{MFG}[s_{MFG}]$) be defined via the equation below.

$$\hat{k}_{MFG}[s_{MFG}] = 0.5\frac{d^2E_{MFG,spr}}{ds_{MFG}^2} = \frac{d\big(-F_{MFG,spr}\big)}{ds_{MFG}} \tag{3.111}$$

Note that by differentiating $-F_{MFG,spr}$ (given by equation (3.40)) with respect to s_{MFG}, one obtains

$$\hat{k}_{MFG}[s_{MFG}] = -\frac{dk_{MFG,spr}}{ds_{MFG}}\big(s_{MFG} - l_{0,MFG}\big) - k_{MFG} \tag{3.112}$$

which yields $\hat{k}_{MFG}[s_{MFG}]$ when $k_{MFG}[s_{MFG}]$ and $l_{0,MFG}$ are given.

Whether the equilibrium point given by equation (3.110) is stable or not, on the other hand, will depend upon whether $E_{MFG,spr}$ has a minimum, a maximum, or an inflection point at $s_{MFG} = (s_{MFG})_{cr}$. In order to determine the nature of the critical point $s_{MFG} = (s_{MFG})_{cr}$, one may use the higher order derivative test, which yields the following results.

(i) If $\hat{k}_{MFG}[(s_{MFG})_{cr}] < 0$, then $(s_{MFG})_{cr}$ corresponds to a maximum of $E_{MFG,spr}$. Therefore, the equilibrium point corresponding to $(s_{MFG})_{cr}$ is unstable.

(ii) If $\hat{k}_{MFG}[(s_{MFG})_{cr}] > 0$, then $(s_{MFG})_{cr}$ corresponds to a minimum of $E_{MFG,spr}$. Therefore, the equilibrium point corresponding to $(s_{MFG})_{cr}$ is stable.

(iii) If $\hat{k}_{MFG}[(s_{MFG})_{cr}] = 0$ and $\frac{d\hat{k}_{MFG}}{ds_{MFG}}[(s_{MFG})_{cr}] \neq 0$, then $(s_{MFG})_{cr}$ corresponds to an inflection point of $E_{MFG,spr}$. Therefore, the equilibrium point corresponding to $(s_{MFG})_{cr}$ is marginally-stable (which is considered to be unstable).

3.4.1 Special Cases of a Quadratic, Non-Linear Spring

The MFGS was previously introduced as a fictitious non-linear spring. If one defines the force characteristic required from a spring, then the MFGS can be designed to satisfy that requirement. The flexibility of this definition may enable further ideas about the use of MFGS. Thus, some special spring characteristics are investigated in this section. The force created at MFGS was previously defined in equation (3.40) as follows.

$$F_{MFG,spr} = k_{MFG}[s_{MFG}]\left(s_{MFG} - l_{0,MFG}\right) \tag{3.40}$$

Again, it shall be noted that, k_{MFG} is fictitious spring coefficient of that fictitious spring. However, some important properties of a spring are solely defined with the stiffness of that spring which is defined as

$$\hat{k}_{MFG} = \frac{d(F_{MFG,spr})}{ds_{MFG}} \tag{3.113}$$

Thus, five special spring cases are defined and investigated for their special properties.

The following set of parameters have been used to find a solution.

Table 3.2. Coefficients of the spring coefficient given by equation (3.107)

Spring Case	$k_2\ [N/mm^3]$	$k_1\ [N/mm^2]$	$k_0\ [N/mm]$	$l_{0,MFG}\ [mm]$
1	1	1	200	10
2	1	20	-100	10
3	0	2	-50	10

3.4.1.1 Spring Case 1

The spring coefficient corresponding to the first spring is

$$k_{MFG,1} = s_{MFG}^2 + s_{MFG} + 200\ N/mm \tag{3.114}$$

Accordingly, the spring force in Case 1 is

$$F_{MFG,spr,1} = (s_{MFG}^2 + s_{MFG} + 200)(s_{MFG} - 10)\ N \tag{3.115}$$

Taking derivative of $-F_{MFG,spr,1}$ w.r.t. s_{MFG} (as explained in equation (3.111)), equation (3.115) yields

$$\hat{k}_{MFG,1} = -3s_{MFG}^2 + 18s_{MFG} - 190\ N/mm \tag{3.116}$$

As presented in Figure 3.12, spring stiffness is less than zero for all s_{MFG}, i.e.,

$$\hat{k}_{MFG,1}[s_{MFG}] < 0 \quad \text{for any } s_{MFG} \tag{3.117}$$

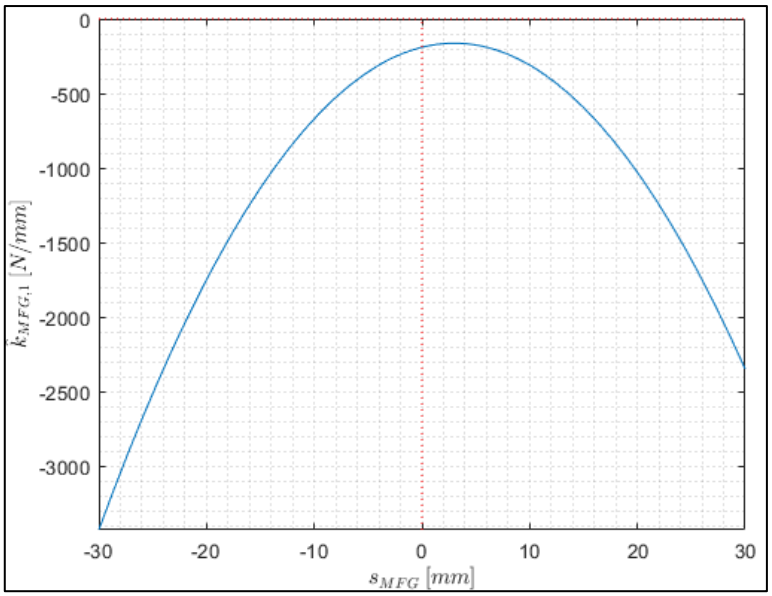

Figure 3.12. Spring stiffness for Spring Case 1

Taking the integral of $-F_{MFG,spr,1}$, one can obtain the energy stored in the spring such that $E_{MFG,spr} = 2\int_{l_{0,MFG}}^{s_{MFG}} -F_{MFG,spr} ds_{MFG}$, defined in equation (3.108), as

$$E_{MFG,spr,1} = -\frac{(s_{MFG}-10)^2\left(s_{MFG}^2+8s_{MFG}+440\right)}{2000}\ Joule \tag{3.118}$$

Now, solving $\frac{dE_{MFG,spr}}{ds_{MFG}} = 0$ given by equation (3.110), one obtains only one critical point for case 1 as

$$\left(s_{MFG,1}\right)_{cr} = 10\ mm \tag{3.119}$$

Using the higher order derivative test, one can determine

$$\hat{k}_{MFG,1}\left[\left(s_{MFG,1}\right)_{cr}\right] = -310\ N/mm < 0 \tag{3.120}$$

Thus, $\left(s_{MFG,1}\right)_{cr} = 10\ mm$ is an unstable equilibrium point which can be observed from $E_{MFG,spr,1}$ plot in Figure 3.18.

3.4.1.2 Spring Case 2

The spring coefficient corresponding to the second spring is

$$k_{MFG,2} = s_{MFG}^2 + 20s_{MFG} - 100\ N/mm \tag{3.121}$$

Accordingly, the spring force in Case 2 is

$$F_{MFG,spr,2} = (s_{MFG}^2 + 20s_{MFG} - 100)(s_{MFG} - 10)\ N \tag{3.122}$$

Taking the derivative w.r.t. s_{MFG}, equation (3.122) yields

$$\hat{k}_{MFG,2} = -3s_{MFG}^2 - 20s_{MFG} + 300\ N/mm \tag{3.123}$$

As presented in Figure 3.13, spring stiffness may acquire negative or positive values.

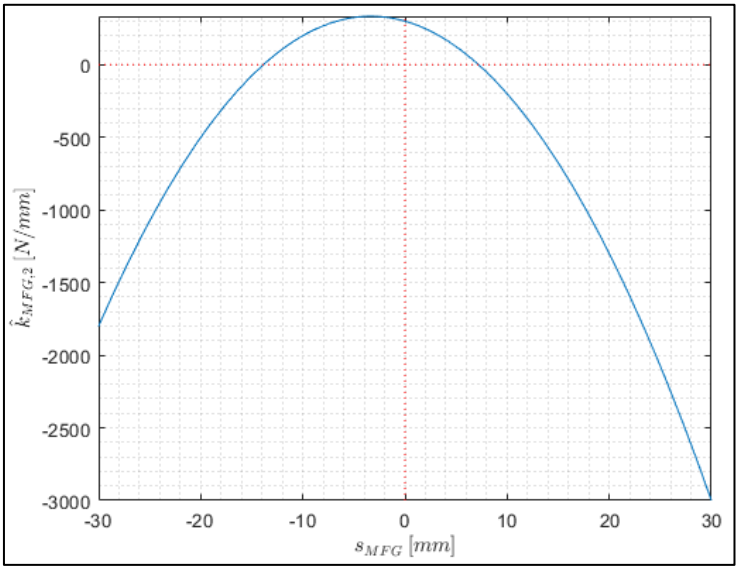

Figure 3.13. Spring stiffness for Spring Case 2

Taking the integral of $-F_{MFG,spr,2}$, one can obtain the energy stored in the spring such that $E_{MFG,spr} = 2\int_{l_{0,MFG}}^{s_{MFG}} -F_{MFG,spr} ds_{MFG}$, defined in equation (3.108), as

$$E_{MFG,spr,2} = -\frac{(s_{MFG}-10)^2(3s_{MFG}^2+100s_{MFG}-100)}{6000}\ Joule \tag{3.124}$$

Now, solving $\frac{dE_{MFG,spr}}{ds_{MFG}} = 0$ given by equation (3.110), one obtains three critical points for case 2 as

$$\left(s_{MFG,2}\right)_{cr,1,2,3} = -24.14,\ 4.14,\ 10\ mm \tag{3.125}$$

Using the higher order derivative test, one can determine

$$\hat{k}_{MFG,2}\left[\left(s_{MFG,2}\right)_{cr,1}\right] = -965.4\ N/mm < 0 \tag{3.126}$$

$$\hat{k}_{MFG,2}\left[\left(s_{MFG,2}\right)_{cr,2}\right] = 165.8\ N/mm > 0 \tag{3.127}$$

$$\hat{k}_{MFG,2}\left[\left(s_{MFG,2}\right)_{cr,3}\right] = -200\ N/mm < 0 \tag{3.128}$$

Thus, $\left(s_{MFG,2}\right)_{cr,1} = -24.14\ mm$ and $\left(s_{MFG,2}\right)_{cr,3} = 10\ mm$ are unstable equilibrium points which can be observed from $E_{MFG,spr,2}$ plot in Figure 3.18, where $\left(s_{MFG,2}\right)_{cr,2} = 4.14\ mm$ is a stable equilibrium point.

3.4.1.3 Spring Case 3

The third case represents linear spring characteristics, since k_2 is zero. Hence, the spring coefficient corresponding to the third spring is

$$k_{MFG,3} = 2s_{MFG} - 50\ N/mm \tag{3.129}$$

Accordingly, the spring force in Case 3 is

$$F_{MFG,spr,3} = (2s_{MFG} - 50)(s_{MFG} - 10)\ N \tag{3.130}$$

Taking derivative w.r.t. s_{MFG}, equation (3.130) yields

$$\hat{k}_{MFG,3} = -4s_{MFG} + 70\ N/mm \tag{3.131}$$

As presented in Figure 3.14, spring stiffness is a linear curve that may acquire negative or positive values.

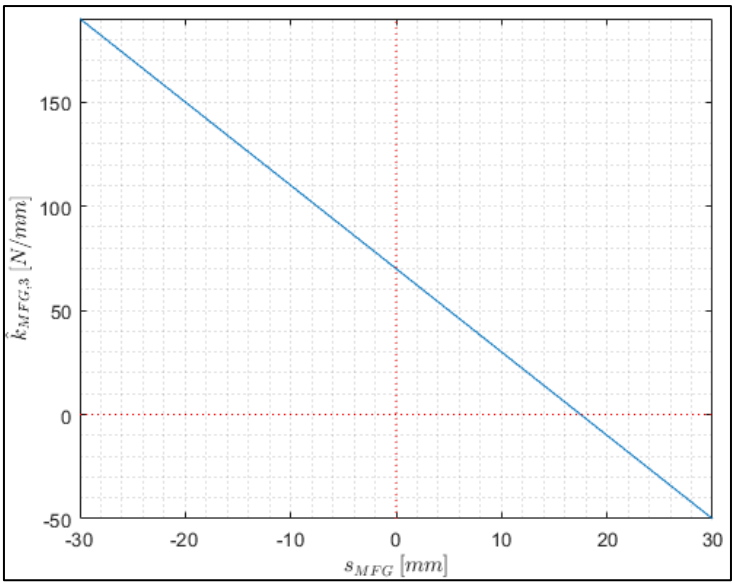

Figure 3.14. Spring stiffness for Spring Case 3

Taking the integral of $-F_{MFG,spr,3}$, one can obtain the energy stored in the spring such that $E_{MFG,spr} = 2\int_{l_{0,MFG}}^{s_{MFG}} -F_{MFG,spr} ds_{MFG}$, defined in equation (3.108), as

$$E_{MFG,spr,3} = -\frac{(s_{MFG}-10)^2(2s_{MFG}-65)}{1500}\ Joule \tag{3.132}$$

Now, solving $\frac{dE_{MFG,spr}}{ds_{MFG}} = 0$ given by equation (3.110), one obtains two critical points for case 3 as

$$\left(s_{MFG,3}\right)_{cr,1,2} = 10,\ 25\ mm \tag{3.133}$$

Using the higher order derivative test, one can determine

$$\hat{k}_{MFG,3}\left[\left(s_{MFG,3}\right)_{cr,1}\right] = 30\ N/mm > 0 \tag{3.134}$$

$$\hat{k}_{MFG,3}\left[\left(s_{MFG,3}\right)_{cr,2}\right] = -30\ N/mm < 0 \tag{3.135}$$

Thus, $\left(s_{MFG,3}\right)_{cr,1} = 10\ mm$ is a stable and $\left(s_{MFG,3}\right)_{cr,2} = 25\ mm$ is an unstable equilibrium point which can be observed from $E_{MFG,spr,3}$ plot in Figure 3.18.

3.4.1.4 Spring Case 4

In this case study, an MFGS-4-gr (see Figure A.1 in Appendix A) which can act as a high-static-low-dynamic-stiffness (HSLDS) spring [24], [25] will be designed. Referring to Figure A.1, m_L denotes the mass of a load that is placed on Link 2 (which is assumed to be a vibration isolation table), and g denotes the gravitational acceleration. L is the vertical distance between O_2 and m_L; and $s_{MFG,eq}$ is the value of s_{MFG} such that Link 2 in Figure A.1 is in static equilibrium. H, on the other hand, denotes horizontal line, attached rigidly to the ground, which is the reference line for gravitational potential energy (due to the mass m_L).

In the previous 3 cases, $F_{MFG,spr}$ has been defined via equation (3.40) by specifying the user defined function $k_{MFG}[s_{MFG}]$ and the user defined parameter $l_{0,MFG}$. Note that, in order to define $F_{MFG,spr}$ it is not necessary to use equation (3.40). In other words, one could define $F_{MFG,spr}$ directly as a function of s_{MFG} which is the method that will be adapted in this case study. Now, considering equations (A.1) and (A.11) in Appendix A, let the desired $F_{MFG,spr}$ be given via the equation

$$F_{MFG,spr,2,4-gr} = F_{MFG,spr} = c\left(s_{MFG} - s_{MFG,eq}\right)^n + m_L g \tag{3.136}$$

In equation (3.136), c is a constant such that

$$c < 0 \tag{3.137}$$

and n is an odd, positive integer such that

$$n \geq 3 \tag{3.138}$$

i.e., $n = 3, 5, 7,$ ... etc. Recall that $F_{MFG,spr,2,4-gr} = F_{MFG,spr}$ is the force applied on Link 2 by the fictitious spring. Hence, the force applied on the fictitious spring by Link 2 is $-F_{MFG,spr,2,4-gr} = -F_{MFG,spr}$. Hence, the energy stored in the spring is given by

$$E_{MFG,spr} = 2\int_{s_{MFG,eq}}^{s_{MFG}} \left(-F_{MFG,spr}\right) ds_{MFG} \tag{3.139}$$

which, upon substituting equation (3.136), yields

$$E_{MFG,spr} = 2\left[-\frac{c}{n+1}\left(s_{MFG} - s_{MFG,eq}\right)^{n+1} - m_L g\left(s_{MFG} - s_{MFG,eq}\right)\right] \quad (3.140)$$

The multiplier 2 in front of the integral on the right hand side of equation (3.139) is due to the fact that when s_{MFG} increases by an amount of ds_{MFG}, the displacement (in the $\vec{k}$ direction) of the application point of $F_{MFG,spr}$ (i.e., point O_2) will be $2ds_{MFG}.\,\hat{k}_{MFG}[s_{MFG}]$, on the other hand, is given by

$$\hat{k}_{MFG}[s_{MFG}] = \frac{d\left(-F_{MFG,spr}\right)}{ds_{MFG}} \quad (3.141)$$

which, upon substituting equation (3.136), yields

$$\hat{k}_{MFG}[s_{MFG}] = -cn\left(s_{MFG} - s_{MFG,eq}\right)^{n-1} \quad (3.142)$$

Note that, considering equations (3.139) and (3.141), one obtains

$$\hat{k}_{MFG}[s_{MFG}] = 0.5\,\frac{d^2 E_{MFG,spr}}{ds_{MFG}^2} \quad (3.143)$$

Now, differentiating equation (3.142) with respect to s_{MFG} twice, one obtains

$$\hat{k}'_{MFG}[s_{MFG}] = \frac{d\hat{k}_{MFG}}{ds_{MFG}} = -c(n-1)n\left(s_{MFG} - s_{MFG,eq}\right)^{n-2} \quad (3.144)$$

$$\hat{k}''_{MFG}[s_{MFG}] = \frac{d^2\hat{k}_{MFG}}{ds_{MFG}^2} = -c(n-2)(n-1)n\left(s_{MFG} - s_{MFG,eq}\right)^{n-3} \quad (3.145)$$

where, $\hat{k}'_{MFG}[s_{MFG}]$ denotes the first, $\hat{k}''_{MFG}[s_{MFG}]$ denotes the second derivative of $\hat{k}_{MFG}$ with respect to s_{MFG}.

Let, now, the horizontal, stationary line H (see Figure A.1) be the reference line for gravitational potential energy. Hence, the gravitational potential energy due to the mass m_L, E_g, will be given by

$$E_g = 2m_L g\left(s_{MFG} - s_{MFG,eq}\right) \quad (3.146)$$

Hence, the total potential energy of the system (due to fictitious spring and the gravitational potential energy due to the mass m_L), PE, will be

$$PE = E_{MFG,spr} + E_g \tag{3.147}$$

which, upon substituting equations (3.140) and (3.146), yields

$$PE = -2\frac{c}{n+1}\left(s_{MFG} - s_{MFG,eq}\right)^{n+1} \tag{3.148}$$

Now, consider the following numerical values for m_L, g, n, c and $s_{MFG,eq}$.

$$\begin{aligned} m_L &= 1\ kg \\ g &= 9.807\ m/s^2 \\ n &= 3 \\ c &= -3\ N/cm^3 \\ s_{MFG,eq} &= 8\ cm \end{aligned} \tag{3.149}$$

Using the above randomly selected numerical values, equations (3.136), (3.140), (3.142), (3.144), (3.145), (3.146) and (3.148) yield

$$F_{MFG,spr} = 10 - 3(s_{MFG} - 8)^3\ N \tag{3.150}$$

$$E_{MFG,spr} = -20(s_{MFG} - 8) + 1.5(s_{MFG} - 8)^4\ Ncm \tag{3.151}$$

$$\hat{k}_{MFG}[s_{MFG}] = 9(s_{MFG} - 8)^2\ N/cm \tag{3.152}$$

$$\hat{k}'_{MFG}[s_{MFG}] = 18(s_{MFG} - 8)\ N/cm^2 \tag{3.153}$$

$$\hat{k}''_{MFG}[s_{MFG}] = 18\ N/cm^3 \tag{3.154}$$

$$E_g = 20(s_{MFG} - 8)\ N/cm \tag{3.155}$$

$$PE = 1.5(s_{MFG} - 8)^4\ N/cm \tag{3.156}$$

respectively, where s_{MFG} is measured in centimeters.

In Figure 3.15, $E_{MFG,spr}$, PE, $F_{MFG,spr}$, $\hat{k}_{MFG}$, $\frac{d\hat{k}_{MFG}}{ds_{MFG}}$ and $\frac{d^2\hat{k}_{MFG}}{ds_{MFG}^2}$ are plotted as a function of s_{MFG} (for the data set given in equation (3.149)). As can be observed from the plot of PE in part b, potential energy is minimum at the equilibrium position given by $s_{MFG} = s_{MFG,eq} = 8\,cm$. Hence, $s_{MFG} = s_{MFG,eq} = 8\,cm$ is a stable equilibrium point. As can be observed from the plot of $\hat{k}_{MFG}$ in part d, $\hat{k}_{MFG} = 0$ at this stable equilibrium position. Furthermore, in the vicinity of the equilibrium position $\hat{k}_{MFG}$ is positive, but "close" to zero.

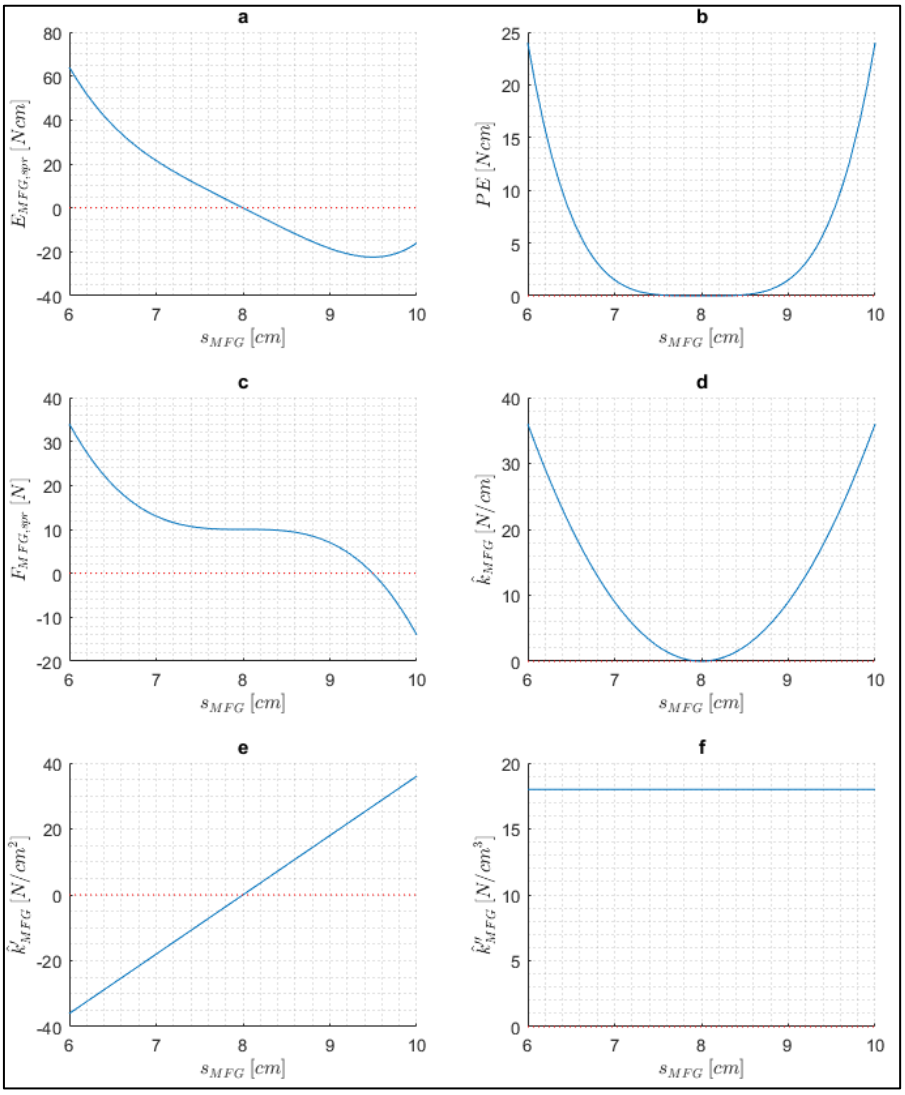

Figure 3.15. Plots of: a) $E_{MFG,spr}$, b) PE, c) $F_{MFG,spr}$, d) $\hat{k}_{MFG}$, e) $\hat{k}'_{MFG}$, f) $\hat{k}''_{MFG}$ as a function of s_{MFG}

Note that, the $\hat{k}_{MFG}$ curve will be more "flat" around the equilibrium position as n gets larger. In Figure 3.16, plots of $\hat{k}_{MFG}$ are compared for cases of $n = 3$ and $n = 5$. Other than n, the numerical data used to obtain these plots are identical with the numerical data given by equation (3.149), except the unit of c is "N/cm^5" for $n = 5$.

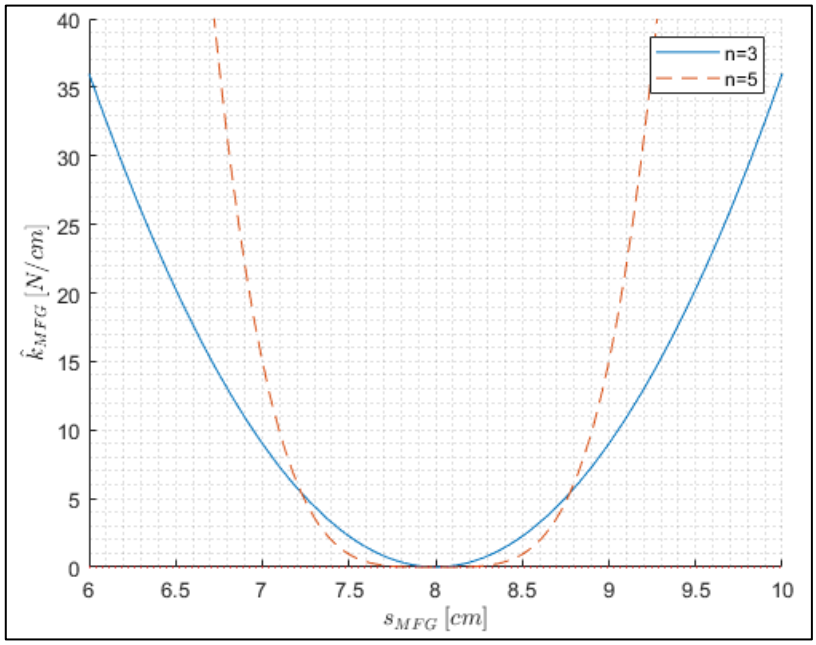

Figure 3.16. Comparison of $\hat{k}_{MFG}$ plots for $n = 3$ and $n = 5$

Figure 3.17, on the other hand, shows the effect of the parameter c on the $\hat{k}_{MFG}$ curve. In this figure, plots of $\hat{k}_{MFG}$ are compared for the cases of $c = -3\ N/cm^3$ and $c = -0.5\ N/cm^3$. Other than c, the numerical data used to obtain these plots are identical with the numerical data given by equation (3.149).

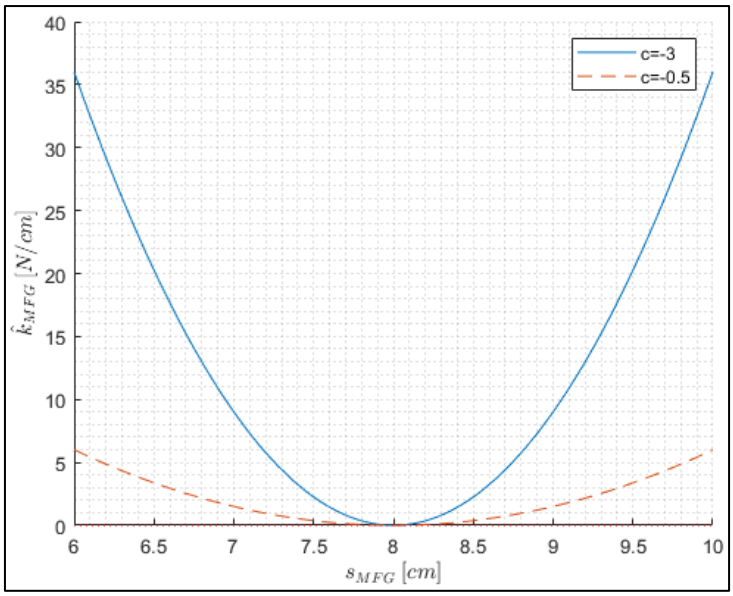

Figure 3.17. Comparison of $\hat{k}_{MFG}$ plots for $c = -3$ and $c = -0.5$

3.4.2 Comparison of Spring Cases

In Figure 3.18, the properties of different fictitious springs are plotted as a function of displacement, s_{MFG}. The first row of plots is the spring stiffness curves, $\hat{k}_{MFG}$. At the second row, the force characteristic of the corresponding MFGS is plotted. These force characteristics are obtained according to the equation (3.40) and are dependent on the fictitious free length of the MFGS. The energy stored in MFGS is calculated and plotted in the third row of Figure 3.18, which is defined in equation (3.108).

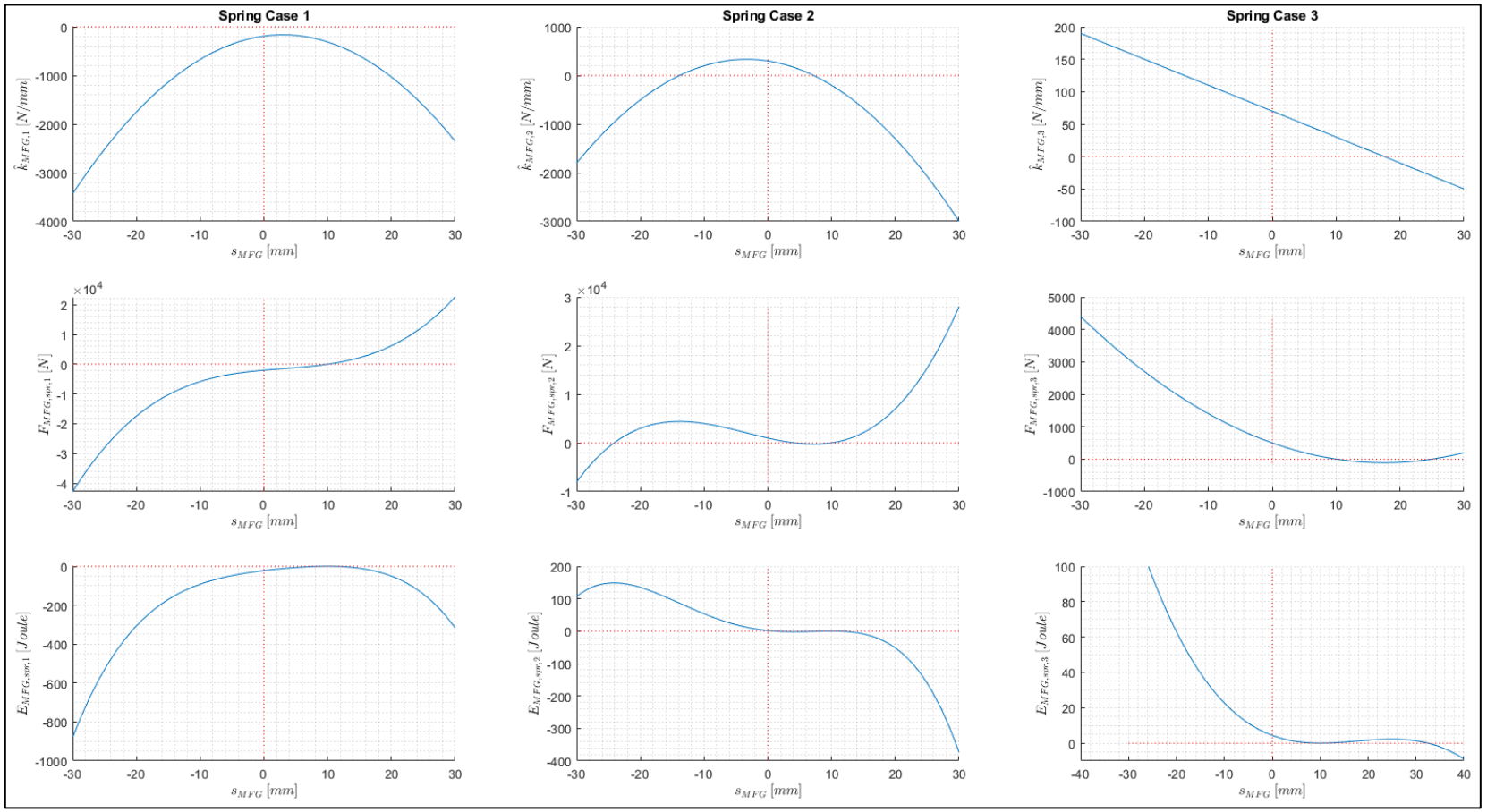

Figure 3.18. Properties of MFGS for Special Spring Cases

3.5 Design Examples of MFG

Theoretical solution for the design of an MFG for a spring and a damper is mathematically performed in Sections 3.2 and 3.3 previously. Examples of MFGS and MFGD design for given dimensions and properties of damper and spring are explained in this section.

3.5.1 Illustrative Example for MFGS

A step-by-step example of slot shape determination of MFGS for given parameters has been presented in this section. Note that all dimensions and spring properties in this section are arbitrarily selected. The units are used for the sake of convenience.

Assume that a spring with non-linear characteristics, so called an equivalent spring, is desired. Let that spring have the desired force characteristics, F_{des}, same with the Spring Case 2 defined in Section 3.4.1 as follows.

$$k_{des}[s_{des}] = s_{des}^2 + 20s_{des} - 100\ N/mm \tag{3.157}$$

$$l_{0,des} = 10\ mm \tag{3.158}$$

where

$l_{0,des}$: Fictitious free length of the desired equivalent spring

$k_{des}[s_{des}]$: Spring coefficient of the desired equivalent spring

s_{des} : Length of the desired spring

Referring to equation (3.40), force characteristic of such spring, F_{des}, can be defined as

$$F_{des}[s_{des}] = (s_{des}^2 + 20s_{des} - 100)(s_{des} - 10)\ N \tag{3.159}$$

which is presented in Figure 3.19.

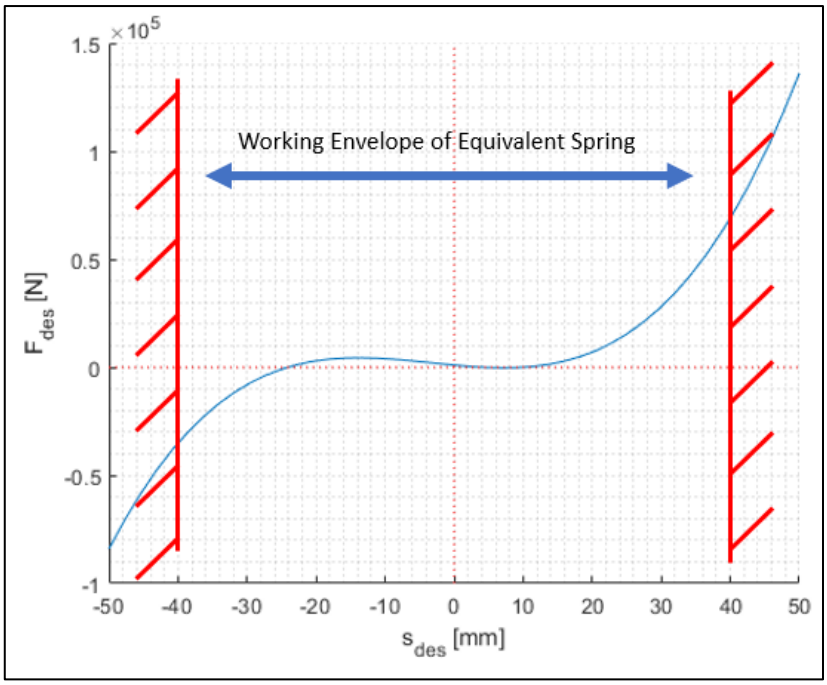

Figure 3.19. Desired force characteristics of equivalent spring (Spring Case 2)

It is assumed that the spring defined in equation (3.159), has a working envelope between $s_{des} = -40\ mm$ to $s_{des} = 40\ mm$.

Let this equivalent spring defined in equation (3.159), be designed using an MFG with the following dimensions,

$$b_1 = 100\ mm \tag{3.160}$$

$$b_2 = 65\ mm \tag{3.161}$$

$$b_3 = 50\ mm \tag{3.162}$$

$$c_1 = 100\ mm \tag{3.163}$$

$$d_{cle} = 10\ mm \tag{3.164}$$

and a spring with the following characteristics.

$$k_{cha} = 4000\ N/mm \tag{3.165}$$

$$l_{f,cha} = 25\ mm \tag{3.166}$$

Referring to Figure 3.3, an MFG with dimension defined in equations (3.160), (3.161), (3.162) and (3.163) would have the allowable region presented in Figure 3.20.

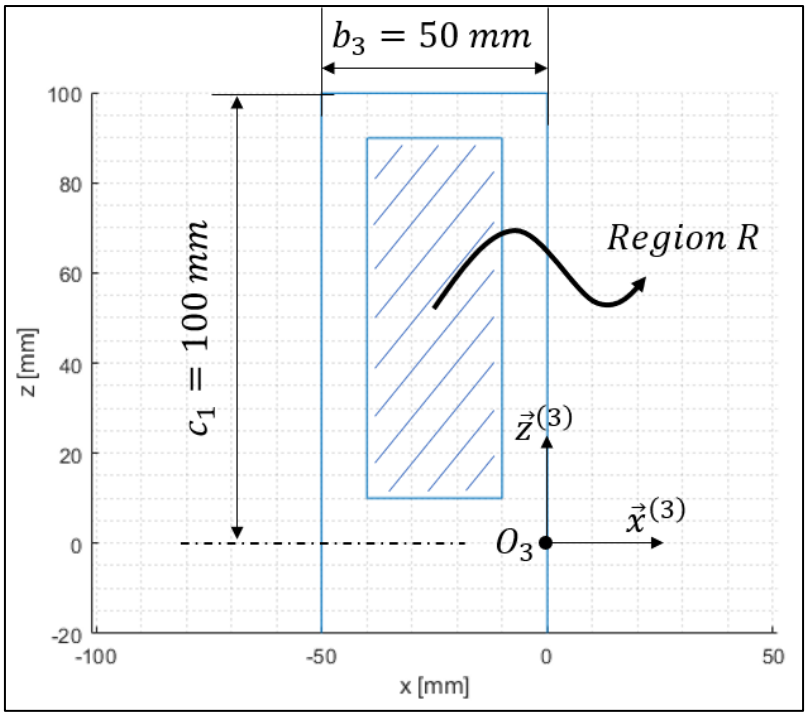

Figure 3.20. Allowable region R for MFGS

Referring to equation (3.14) ($d_{cle} \leq s_{MFG} \leq c_1 - d_{cle}$), the stroke of the MFG, s_{MFG}, shall be in accordance with the following equation.

$$10\ mm \leq s_{MFG} \leq 90\ mm \tag{3.167}$$

The force characteristics defined in Spring Case 2 is not suitable to design an MFGS directly because s_{MFG} has a working envelope starting from $10\ mm$ as defined in equation (3.167). However, the working envelope defined in the Spring Case 2 starts from $s_{des} = -40\ mm$ (see Figure 3.19). Thus, the working envelope defined in s_{des} domain needs to be shifted to be assumed as s_{MFG} to design the MFGS. Thus, the non-linear force characteristics of MFGS is defined by making the following change in F_{des} (see equation (3.159)).

$$s_{des} = s_{MFG} - 50\ mm \tag{3.168}$$

If equation (3.168) is plugged in equation (3.159), one obtains

$$F_{MFG,spr}[s_{MFG}] = (s_{MFG}^2 - 80s_{MFG} + 1400)(s_{MFG} - 60)\ N \qquad (3.169)$$

where the spring coefficient and fictitious free length of the spring would be as

$$k_{MFG}[s_{MFG}] = s_{MFG}^2 - 80s_{MFG} + 1400\ N/mm \qquad (3.170)$$

$$l_{0,MFG} = 60\ mm \qquad (3.171)$$

The spring coefficient of the MFGS, i.e., $k_{MFG}[s_{MFG}]$, is presented in Figure 3.21.

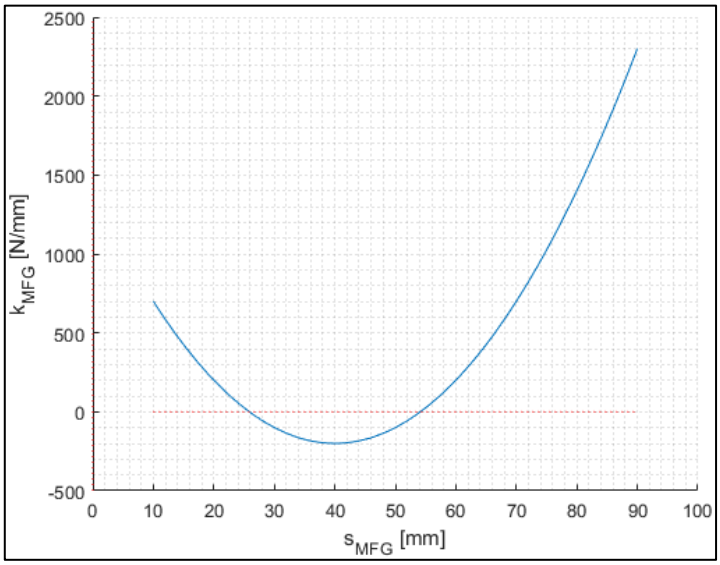

Figure 3.21. Spring coefficient of the MFGS

Thus, the MFGS that is wanted to be designed would have a force characteristic as presented in Figure 3.22.

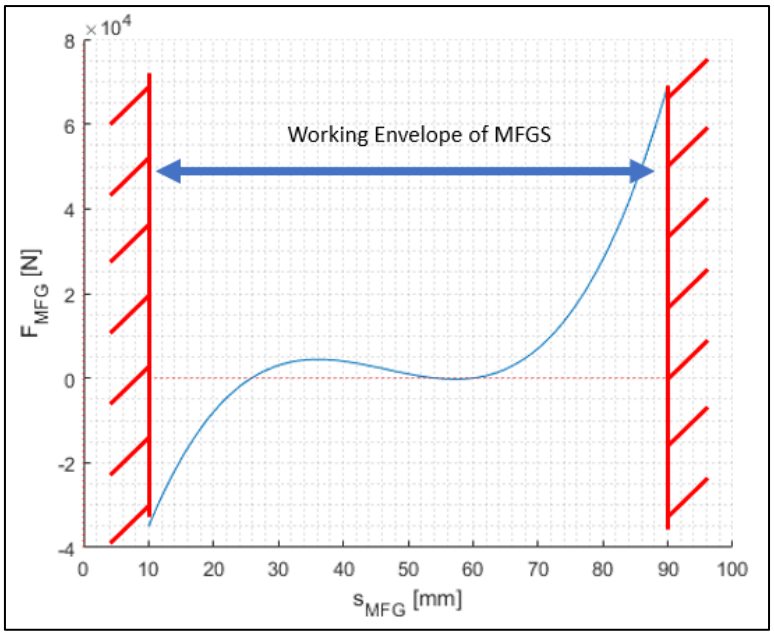

Figure 3.22. Force characteristics of MFGS

Referring to equation (3.111), one could determine the spring stiffness of the MFGS as

$$\hat{k}_{MFG}[s_{MFG}] = -3s_{MFG}^2 + 280s_{MFG} - 6200 \tag{3.172}$$

plotted in Figure 3.23.

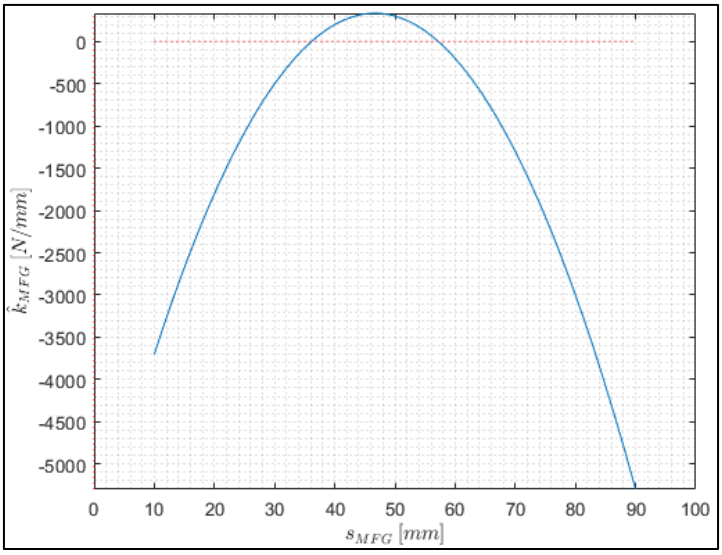

Figure 3.23. Spring stiffness of MFGS, $\hat{k}_{MFG}[s_{MFG}]$

The equilibrium points of this MFGS can be found using equation (3.110), in which $F_{MFG,spr} = 0$ at these points, can be found as follows.

$$(s_{MFG})_{cr,1} = 25.858\ mm$$
$$(s_{MFG})_{cr,2} = 54.142\ mm \quad (3.173)$$
$$(s_{MFG})_{cr,3} = 60\ mm$$

Using the spring stiffness found in equation (3.172), the equilibrium points found in equation (3.173) can be tested for stability by plugging the points defined by equation (3.173) into equation (3.172) as

$$\hat{k}_{MFG}\left[(s_{MFG})_{cr,1}\right] \cong -965.7\ N/mm < 0$$
$$\hat{k}_{MFG}\left[(s_{MFG})_{cr,2}\right] \cong 165.7\ N/mm > 0 \quad (3.174)$$
$$\hat{k}_{MFG}\left[(s_{MFG})_{cr,3}\right] = -200\ N/mm < 0$$

Thus, $(s_{MFG})_{cr,2}$ is a stable equilibrium point where $(s_{MFG})_{cr,1}$ and $(s_{MFG})_{cr,3}$ are unstable equilibrium points.

Furthermore, the energy stored in MFGS, $E_{MFG,spr}$, is found by using equation (3.108) and plotted with in Figure 3.24 with the equilibrium points indicated as follows.

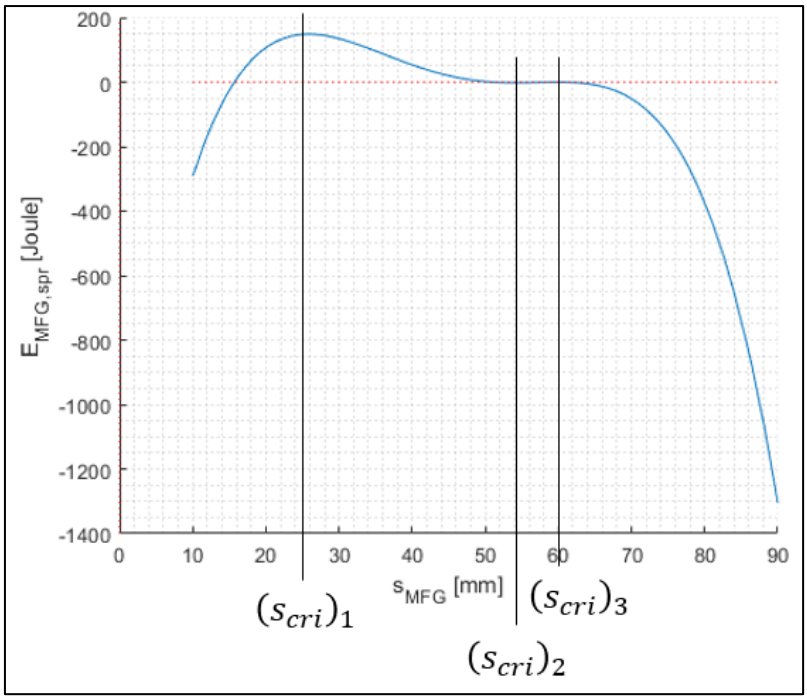

Figure 3.24. Energy stored in MFGS

So, as the dimensions of the MFGS and properties of the spring installed inside the chamber are given, slot shape can be determined for the equivalent spring in equation (3.169). Referring to equation (3.52), the equilibrium of instantaneous power is obtained as follows.

$$-4000(x_r - 40)\, dx_r = z_r^2 - 80z_r + 1400(z_r - 60)dz_r \qquad (3.175)$$

Rearranging the terms, the integral of equation (3.175) can be obtained as follows

$$\int_{20}^{x_r}(x_r - 40)dx_r = \int_{20}^{z_r} h[z_r]dz_r \qquad (3.176)$$

where

$$h[z_r] = -\frac{z_r^2 - 80z_r + 1400}{4000}(z_r - 60) \qquad (3.177)$$

The limits of the integrals in equation (3.176) are selected as $(x_r)_i = 20$ and $(z_r)_i = 20$ in a sensible manner with respect to the allowable region R defined in Figure 3.20.

With taking the integral, equation (3.176) yields

$$x_r^2 - 40x_r + q[z_r] = 0 \tag{3.178}$$

where

$$q[z_r] = -2p[z_r] - K_1 + 2K_2 + 2K_3$$

$$p[z_r] = -\frac{z_r^4}{16000} + \frac{7z_r^3}{600} - \frac{31z_r^2}{40} + 21z_r$$

$$K_1 = 400$$

$$K_2 = 800$$

$$K_3 = \frac{580}{3}$$

Referring to equation (3.59), two solutions are obtained as follows

$$(x_r)_{p,n} = 40 \pm \sqrt{\Delta[z_r]} \tag{3.179}$$

where

$$\Delta[z_r] = 1600 - q[z_r]$$

The two solutions for the slot shapes obtained in equation (3.179), are presented in Figure 3.25. Since the selected limits of the integral in equation (3.176), i.e., $(x_r)_i = 20$ and $(z_r)_i = 20$ are on $(x_r)_n$, $(x_r)_p$ is not the solution to this problem.

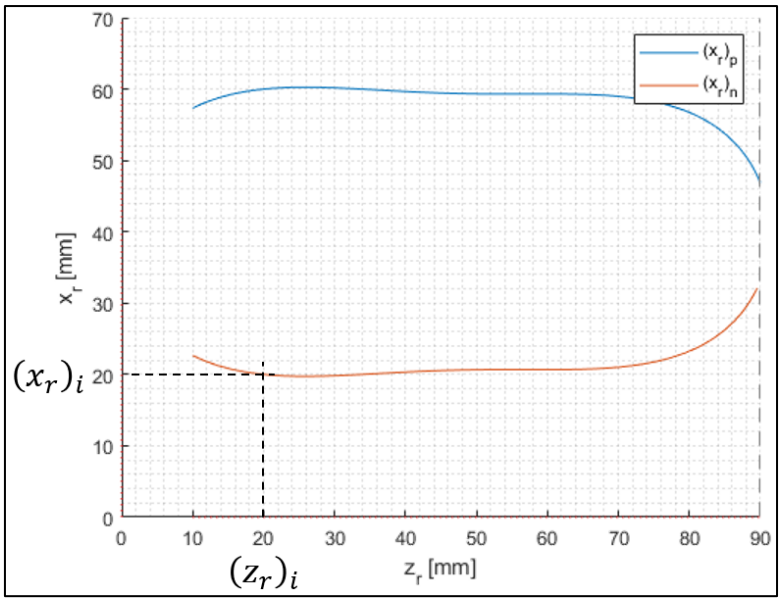

Figure 3.25. Solutions for $(x_r)_p$ and $(x_r)_n$ (for $(x_r)_i = 20$, $(z_r)_i = 20$)

If one applies the solutions found in equation (3.179), to the allowable region R of MFGS defined in Figure 3.20, one can observe that the slot shape center line sits inside the allowable region.

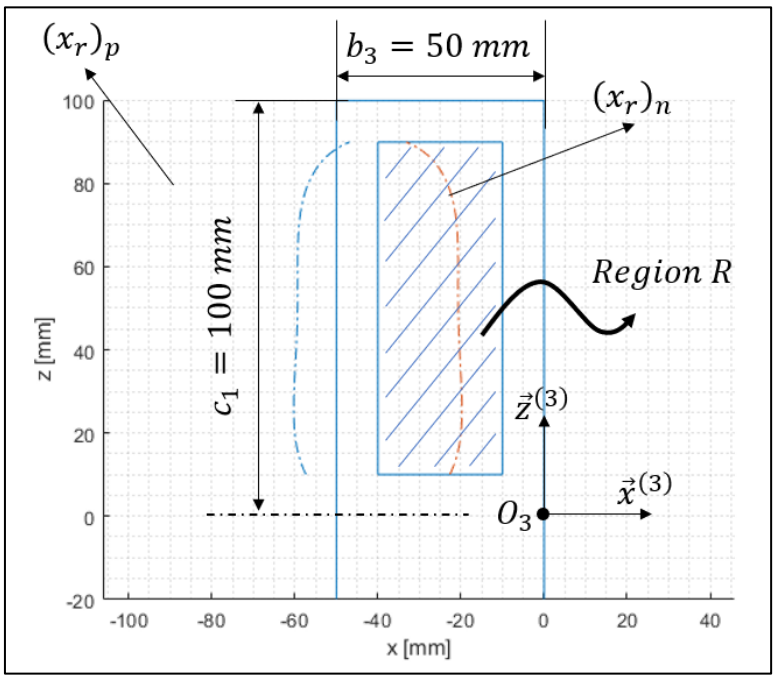

Figure 3.26. $(x_r)_p$ and $(x_r)_n$ on MFGS with selection of $(x_r)_i = 20$, $(z_r)_i = 20$

Since the solution for the slot shape is found in equation (3.179) as x_r as function of z_r, if one takes derivative of $(x_r)_p$ and $(x_r)_n$, one can obtain the velocity influence coefficient of the MFGS, i.e., $\frac{dx_r}{dz_r}$ which relates $\dot{z}_r$ with $\dot{x}_r$ as in equation (3.22), respectively as $\left(\frac{dx_r}{dz_r}\right)_n$ and $\left(\frac{dx_r}{dz_r}\right)_p$. The velocity influence coefficients for $(x_r)_p$ and $(x_r)_n$ are presented in Figure 3.27.

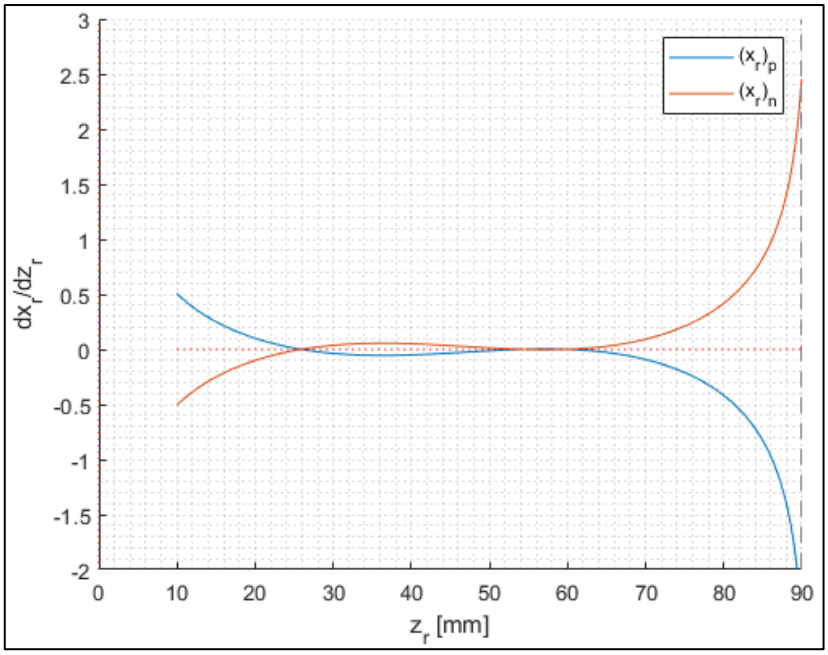

Figure 3.27. Velocity influence coefficient, $\frac{dx_r}{dz_r}$, for $(x_r)_p$ and $(x_r)_n$

Note that, $(x_r)_n$ is the feasible solution for an MFGS with the given dimensions. Thus, the position and velocity properties of the mechanism are investigated with respect to $(x_r)_n$.

Position and velocity analysis of the MFGS is performed referring to position LCEs and VLEs defined in (3.19), (3.20), (3.25) and (3.26). Using $(x_r)_n$ as the kinematic dimension of the system, solutions for those LCEs and VLEs are obtained as follows.

$$s_{cha} = (x_r)_n + b_1 - b_3 - b_2 \tag{3.180}$$

$$s_{MFG} = z_r \tag{3.181}$$

$$\dot{s}_{cha} = \dot{x}_r = \frac{dx_r}{dz_r}[z_r]\dot{z}_r \tag{3.182}$$

$$\dot{s}_{MFG} = \dot{z}_r \tag{3.183}$$

s_{cha} and s_{MFG} are determined with respect to z_r for $s_{MFG,min} < s_{MFG} < s_{MFG,max}$ in Figure 3.28. $\dot{s}_{cha}$ and $\dot{s}_{MFG}$ evaluated with respect to z_r with taking $\dot{s}_{MFG}$ as unit velocity ($\dot{s}_{MFG} = 1\ mm/s$) in Figure 3.29.

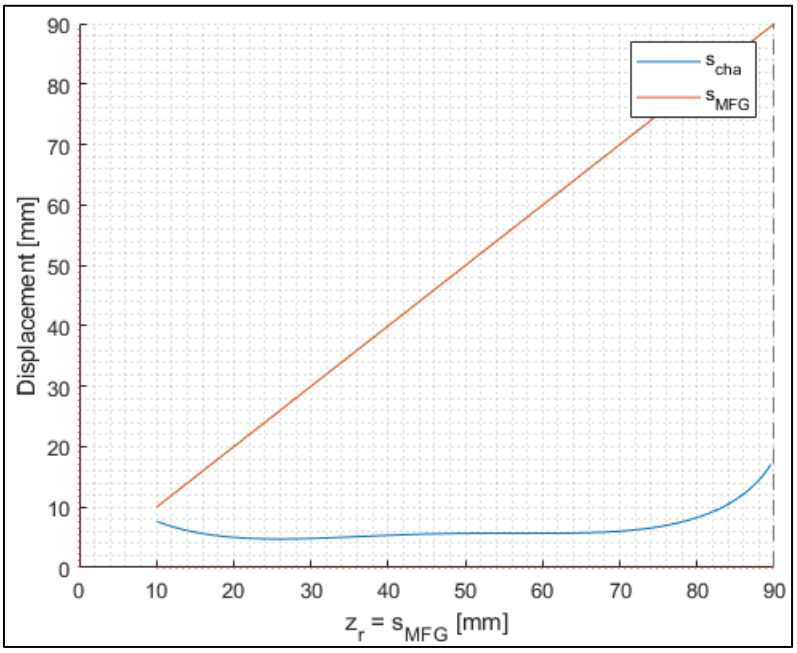

Figure 3.28. Position analysis of the example MFGS

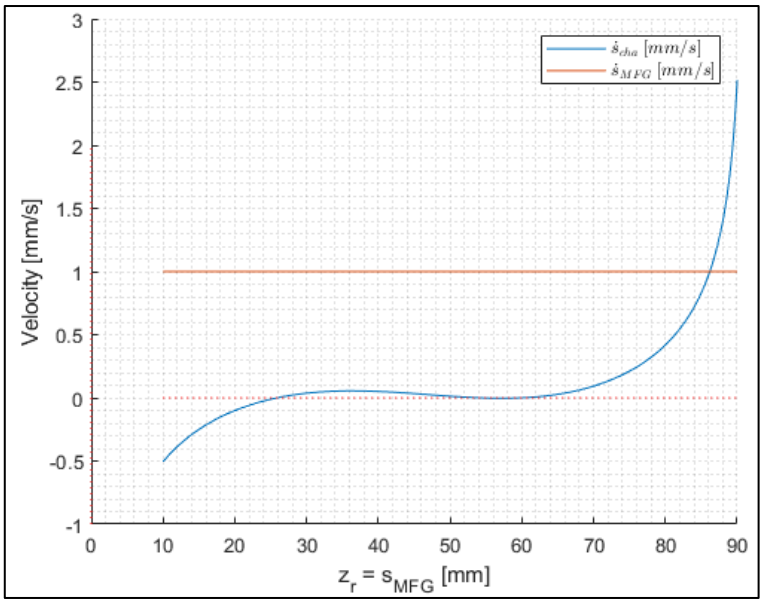

Figure 3.29. Velocity analysis of the example MFGS for $\dot{s}_{MFG} = 1\ mm/s$

The power input due to $F_{cha,spr}$ is defined as

$$P_{cha,spr} = -F_{cha,spr}\dot{s}_{cha} \tag{3.184}$$

while the power input due to $F_{MFG,spr}$ is defined as

$$P_{MFG,spr} = F_{MFG,spr}\dot{s}_{MFG} \tag{3.185}$$

As a final check, the power inputted due to spring inside the chamber, $P_{cha,spr}$, and power inputted due to MFGS, $P_{MFG,spr}$, are compared. $F_{MFG,spr}$ and $-F_{cha,spr}$ are presented in Figure 3.30 with respect to s_{MFG}. $\dot{s}_{cha}$ was also presented in Figure 3.29 with respect to s_{MFG} (note that $\dot{s}_{MFG} = 1\ mm/s$).

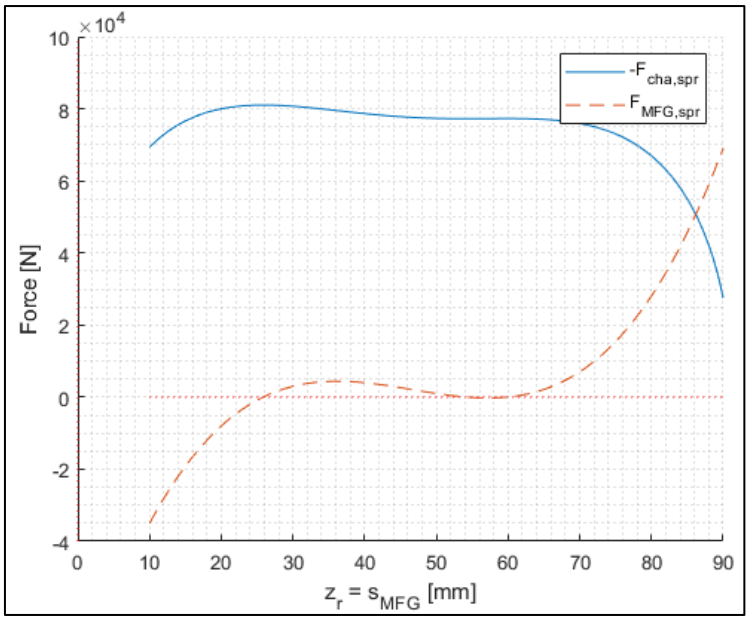

Figure 3.30. $F_{MFG,spr}$ and $-F_{cha,spr}$ w.r.t. s_{MFG}

Referring to equation (3.184) and equation (3.185), if "$-F_{cha,spr}$ in Figure 3.30" is multiplied with "$\dot{s}_{cha}$ in Figure 3.29", "$F_{MFG,spr}$ in Figure 3.30" will be obtained (remember that $\dot{s}_{MFG} = 1\ mm/s$).

3.5.2 Illustrative Example for MFGD

Note that all dimensions and damper properties in this section are arbitrarily selected. The units are used for the sake of convenience.

Assume that an equivalent damper with non-linear characteristics is desired. Let the damper have the force characteristics, F_{des}, defined as follows.

$$F_{des} = -b_{des}[s_{des}]\dot{s}_{des} \tag{3.186}$$

where

$b_{des}[s_{des}]$: Damping coefficient of the desired equivalent damper (function of variable s_{des})

s_{des} : Length of the desired damper

$\dot{s}_{des}$: Velocity of the desired damper

and

$$b_{des}[s_{des}] = s_{des}^2 - 120s_{des} + 4000\ N/mm/s \quad (3.187)$$

The damping coefficient of the desired damper, i.e., $b_{MFG}[s_{des}]$, is presented in Figure 3.31.

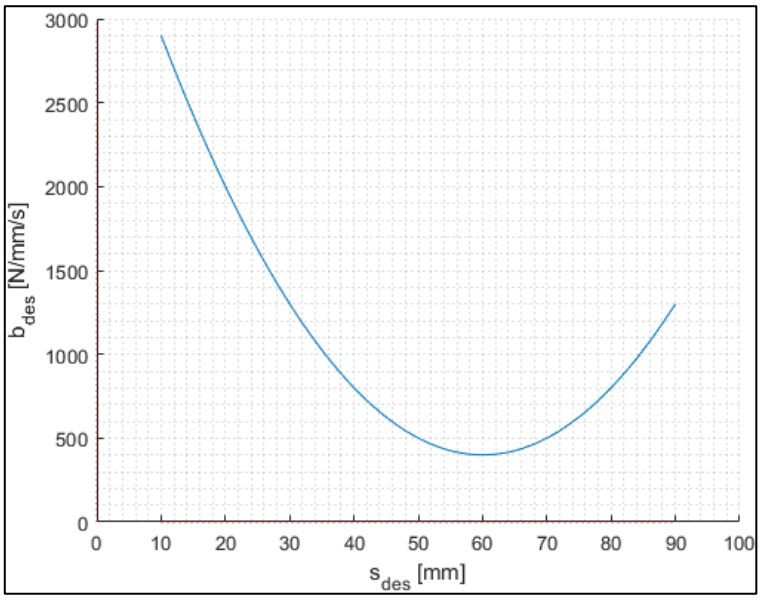

Figure 3.31. Damping coefficient of the desired equivalent damper

The force generated at this damper is a function of both the displacement and the velocity of the equivalent damper, as can be seen in Figure 3.32.

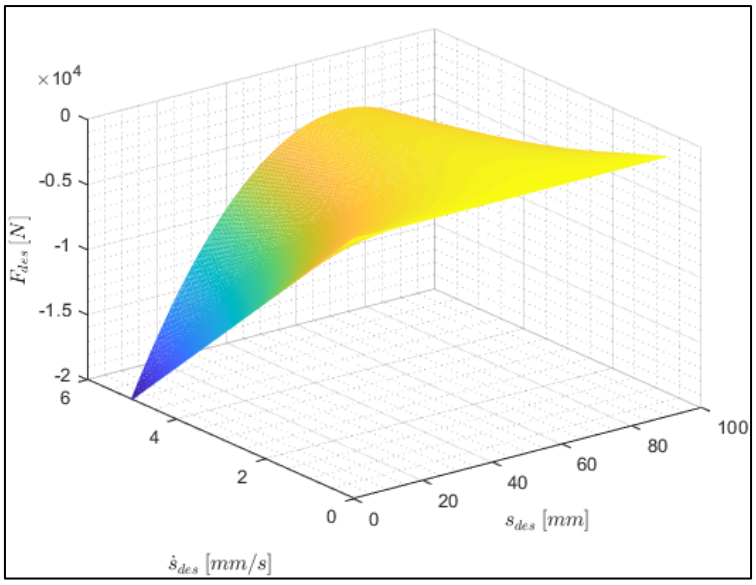

Figure 3.32. Desired force characteristics of the equivalent damper

Suppose that the equivalent damper with the force characteristics given by equation (3.186), is to be designed by using an MFG with the following dimensions.

$$b_1 = 100\ mm \tag{3.188}$$

$$b_2 = 55\ mm \tag{3.189}$$

$$b_3 = 50\ mm \tag{3.190}$$

$$c_1 = 100\ mm \tag{3.191}$$

$$d_{cle} = 10\ mm \tag{3.192}$$

Furthermore, let the damping coefficients of the "real" dampers be given by

$$b_{cha} = 8000\ N/mm/s \tag{3.193}$$

Referring to Figure 3.3, an MFG with the dimensions defined by equations (3.188), (3.189), (3.190) and (3.191) would have the allowable region presented in Figure 3.33.

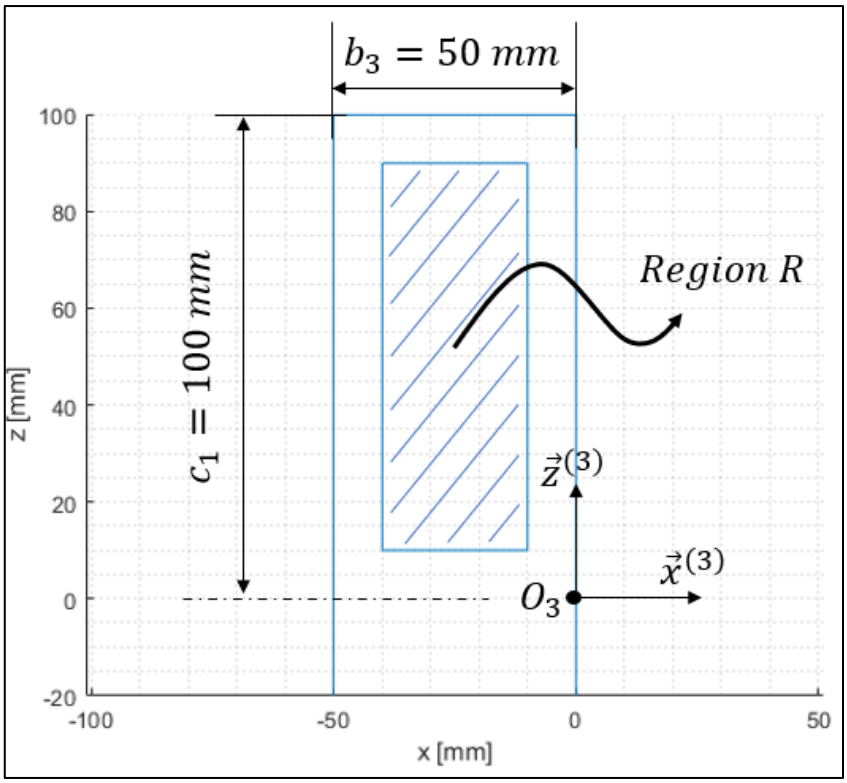

Figure 3.33. Allowable region R for MFGD

Clearly, the desired force characteristic, F_{des}, can be taken to be equal to $F_{MFG,dmp}$ without any modifications. In the MFGS example, the desired force characteristic is re-defined inside the MFGS working envelope. For the MFGD example, the desired force characteristics are defined as general and applicable for use in the design of MFGD directly. Thus, $F_{MFG,dmp}$ and s_{MFG} can be defined as follows.

$$s_{des} = s_{MFG} \tag{3.194}$$

where equations (3.186) and (3.187) yield

$$F_{MFG,dmp} = -(s_{MFG}^2 - 120 s_{MFG} + 4000\ )\dot{s}_{MFG} \tag{3.195}$$

The work done by the MFGD (from $s_{MFG} = 0$ to $s_{MFG} = s_{MFG}$) can be calculated via the following equation.

$$W_{MFG,dmp} = 2\int_0^{s_{MFG}} F_{MFG,dmp} ds_{MFG} \tag{3.196}$$

If one assumes $\dot{s}_{MFG}$ to be constant and using equation (3.195), equation (3.196) yields

$$W_{MFG,dmp}[s_{MFG}] = 2\dot{s}_{MFG}\int_0^{s_{MFG}} -(s_{MFG}^2 - 120s_{MFG} + 4000\,)ds_{MFG} \quad (3.197)$$

For instance, for $\dot{s}_{MFG} = 1\ mm/s = constant$, by using equation (3.197), the work done (energy absorbed) by the MFGD is obtained as presented in Figure 3.34.

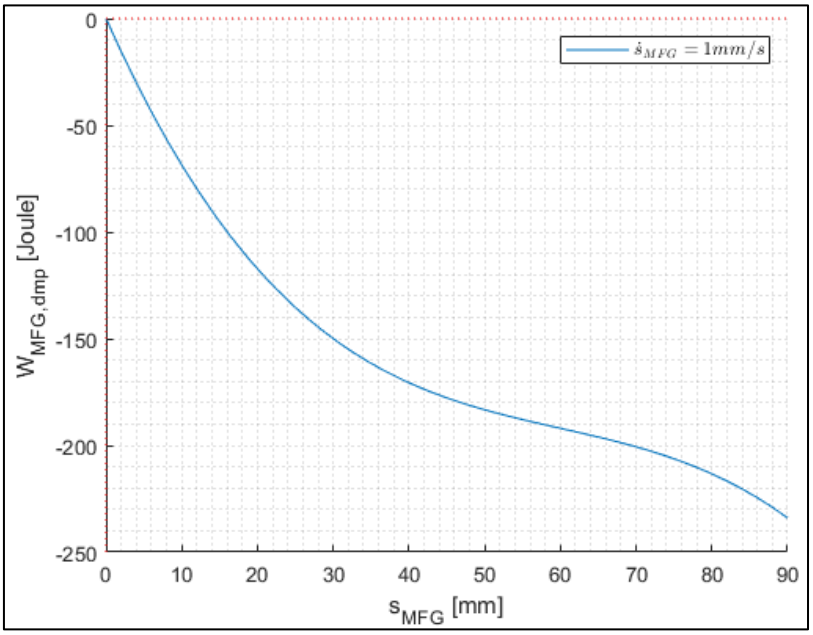

Figure 3.34. Energy absorbed by MFGD for $\dot{s}_{MFG} = 1\ mm/s$

When the dimensions of the MFGD and the properties of the damper installed inside the chamber are given, the slot shape of the equivalent damper generating the force defined by equation (3.195) may be obtained. Using equation (3.193) and (3.195), equation (3.86), yields

$$-8000\dot{s}_{cha}^2 = -(s_{MFG}^2 - 120s_{MFG} + 4000\,)\dot{s}_{MFG}^2 \quad (3.198)$$

which, upon substituting $s_{MFG} = z_r$ (see equation (3.20)), and using equations (3.25) and (3.26), yields

$$\left(\frac{dx_r}{dz_r}\right)^2 = \frac{(z_r^2 - 120z_r + 4000\,)}{8000} \quad (3.199)$$

Taking square root of both sides, equation (3.199) yields

$$\frac{dx_r}{dz_r} = \pm\sqrt{\frac{(z_r^2 - 120z_r + 4000)}{8000}} \tag{3.200}$$

Now, let

$$\sigma = \pm 1$$

and

$$g[z_r] = \sqrt{\frac{(z_r^2 - 120z_r + 4000)}{8000}} \tag{3.201}$$

Therefore, equation (3.200) yields

$$dx_r = \sigma g[z_r] dz_r \tag{3.202}$$

In accordance with equation (3.92), equation (3.202) yields

$$\int_{(x_r)_i}^{x_r} dx_r = \int_{(z_r)_i}^{z_r} \sigma g[z_r] dz_r \tag{3.203}$$

which, in accordance with equation (3.94) yields

$$(x_r)_{p,n} = (x_r)_i \pm (p[z_r] - p[(z_r)_i]) \tag{3.204}$$

where

$$p[z_r] = \int g[z_r] dz_r = \int \sqrt{\frac{(z_r^2 - 120z_r + 4000)}{8000}}\, dz_r$$

(1) Now, using equations (3.95) and (3.96), let

$$(x_r)_i = d_{cle} = 10\ mm \tag{3.205}$$

$$(z_r)_i = s_{MFG,min} = d_{cle} = 10\ mm \tag{3.206}$$

therefore, equation (3.204) gives the following two solutions.

$$(x_r)_p = 10 + (p[z_r] - p[10]) \tag{3.207}$$

$$(x_r)_n = 10 - (p[z_r] - p[10]) \tag{3.208}$$

The two solutions given by equations (3.207) and (3.208) are presented in Figure 3.35.

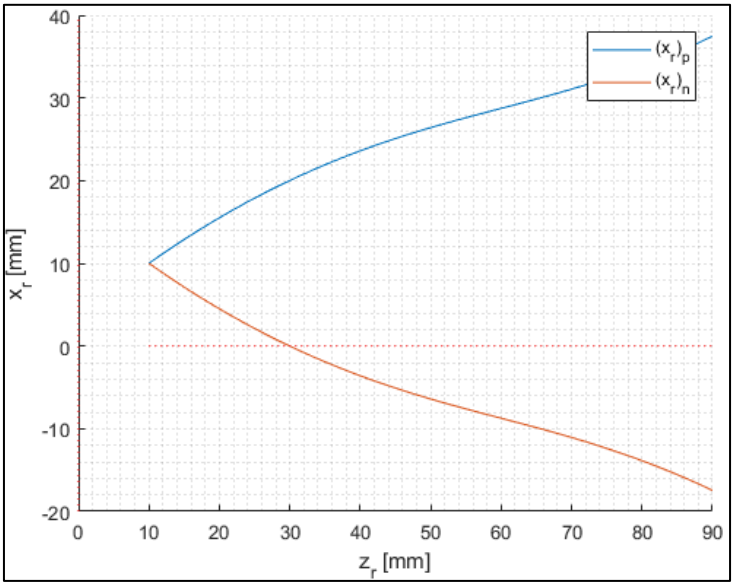

Figure 3.35. Solutions for $(x_r)_p$ and $(x_r)_n$ (for $(x_r)_i = 10$, $(z_r)_i = 10$)

Note that the condition defined by equation (3.97) yields

$$(x_r)_p \Big|_{z_r = 90} = 37.454 < 40 \tag{3.209}$$

and therefore, $(x_r)_p$ is a solution that lies in the allowable region R as presented in Figure 3.36.

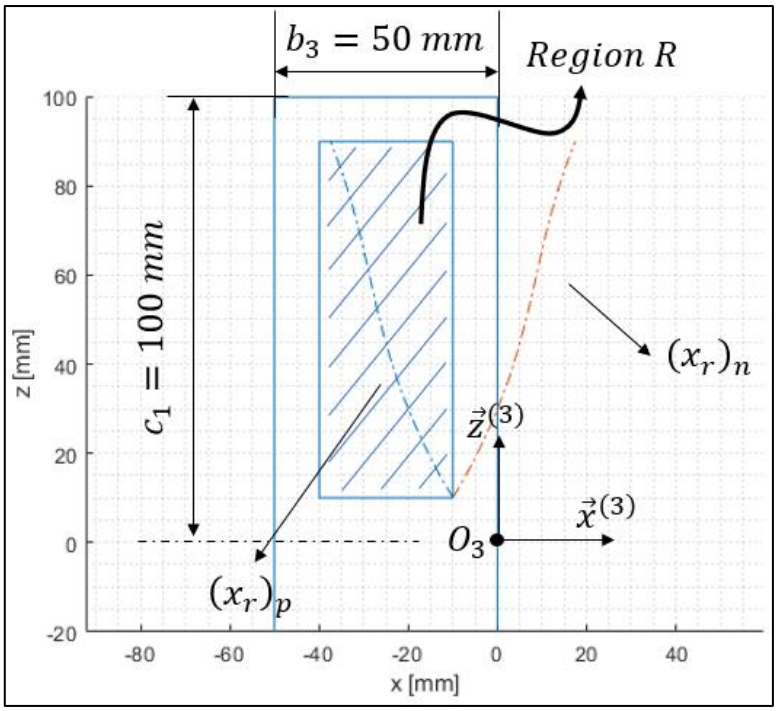

Figure 3.36. $(x_r)_p$ and $(x_r)_n$ on MFGD with selection of $(x_r)_i = 10$, $(z_r)_i = 10$

(2) Now, using equations (3.100) and (3.101) let

$$(x_r)_i = b_3 - d_{cle} = 40\ mm \tag{3.210}$$

$$(z_r)_i = s_{MFG,min} = d_{cle} = 10\ mm \tag{3.211}$$

Therefore, equation (3.204) gives the following two solutions.

$$(x_r)_p = 40 + (p[z_r] - p[10]) \tag{3.212}$$

$$(x_r)_n = 40 - (p[z_r] - p[10]) \tag{3.213}$$

The two solutions given by equations (3.212) and (3.213) are presented in Figure 3.37.

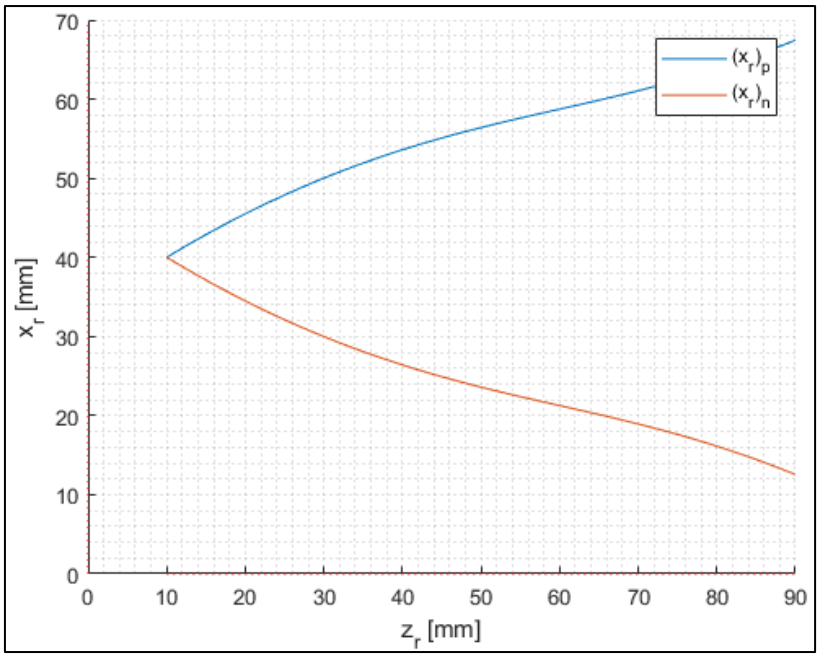

Figure 3.37. Solutions for $(x_r)_p$ and $(x_r)_n$ (for $(x_r)_i = 40$, $(z_r)_i = 10$)

Note that the condition defined by equation (3.102) yields

$$(x_r)_n \Big|_{z_r = 90} = 12.546 > 10 \tag{3.214}$$

and therefore, $(x_r)_n$ is a solution that lies in the allowable region R as presented in Figure 3.38.

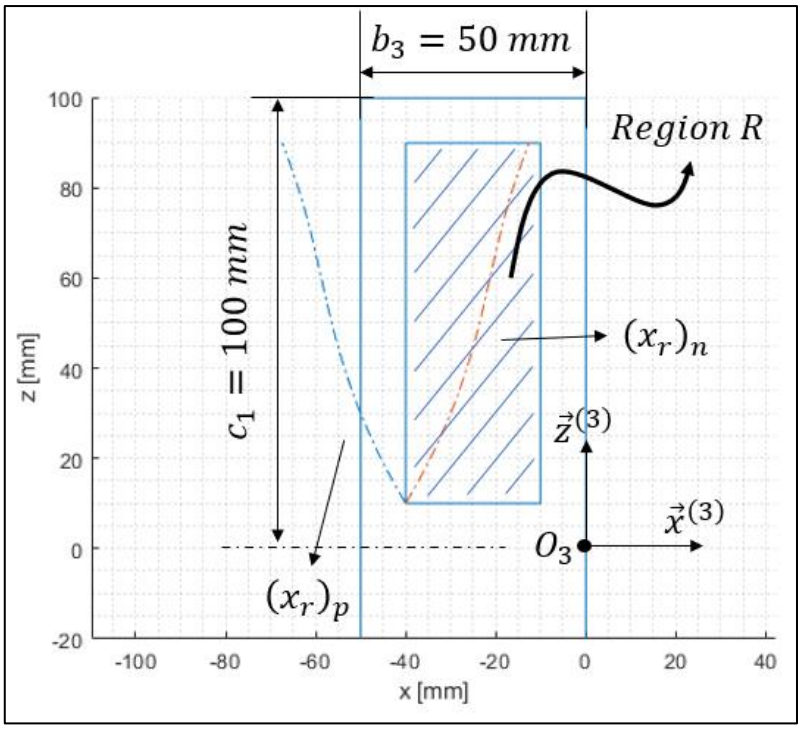

Figure 3.38. $(x_r)_p$ and $(x_r)_n$ on MFGD with selection of $(x_r)_i = 40$, $(z_r)_i = 10$

Note that two different solution sets have been found corresponding to two different selections for $(x_r)_i$ and $(z_r)_i$. The solution for $(x_r)_i = 10$, $(z_r)_i = 10$, given by equations (3.207) and (3.208), will be utilized in the rest of the calculations.

The velocity influence coefficient of the MFGD, $\frac{dx_r}{dz_r}$ (which relates $\dot{z}_r$ with $\dot{x}_r$ as in equation (3.22) ($\dot{x}_r = \frac{dx_r}{dz_r}\dot{z}_r$)), has been obtained in equation (3.200) and plotted for $(x_r)_p$ and $(x_r)_n$ in Figure 3.39.

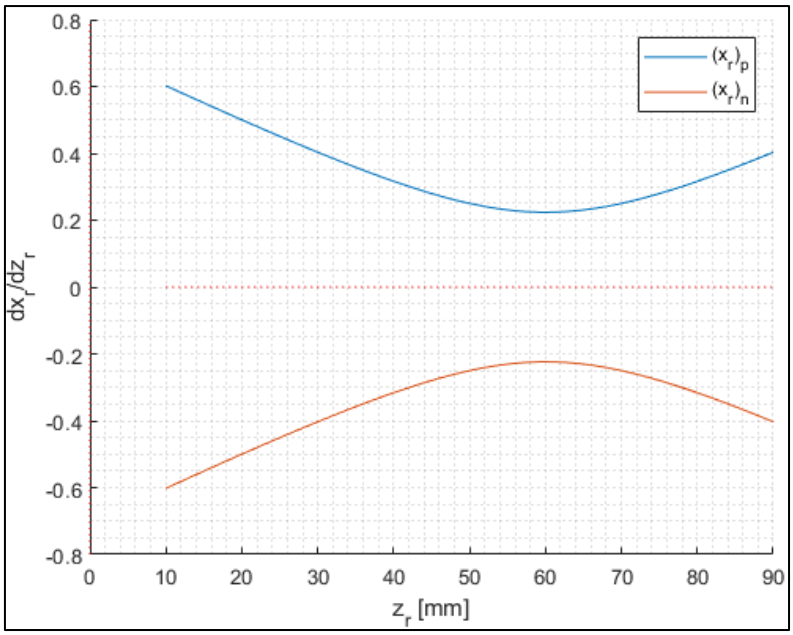

Figure 3.39. Velocity influence coefficient, $\frac{dx_r}{dz_r}$, for $(x_r)_p$ and $(x_r)_n$

Note that in the calculations the position and velocity analysis of the mechanism will be performed using $(x_r)_p$ in accordance with equations (3.19), (3.20), (3.25) and (3.26). Hence, using $(x_r)_p$ as the kinematic dimension of the system, one obtains

$$s_{cha} = (x_r)_p + b_1 - b_3 - b_2 \tag{3.215}$$

$$s_{MFG} = z_r \tag{3.216}$$

$$\dot{s}_{cha} = (\dot{x}_r)_p = \frac{d(x_r)_p}{dz_r}[z_r]\dot{z}_r \tag{3.217}$$

$$\dot{s}_{MFG} = \dot{z}_r \tag{3.218}$$

s_{cha} and s_{MFG} that have been thus obtained are plotted with respect to z_r for $s_{MFG,min} < s_{MFG} < s_{MFG,max}$ in Figure 3.40. Variations of $\dot{s}_{cha}$ and $\dot{s}_{MFG}$ with respect to z_r (by with taking $\dot{s}_{MFG}$ as unit velocity ($\dot{s}_{MFG} = 1\ mm/s$)) are plotted in Figure 3.41.

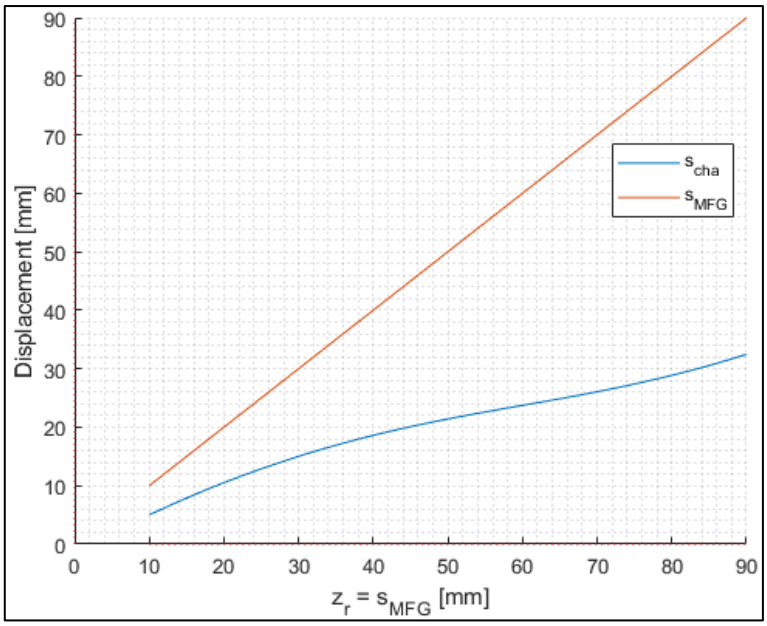

Figure 3.40. Position analysis of the example MFGD

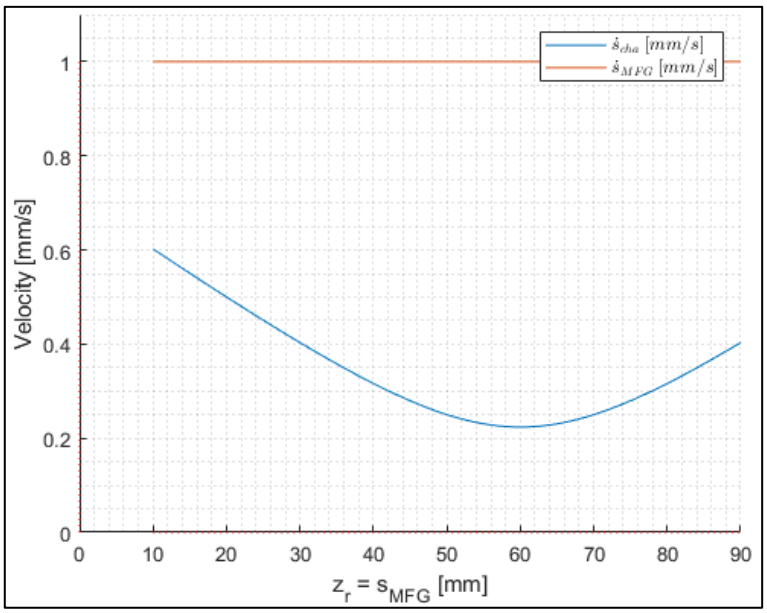

Figure 3.41. Velocity analysis of the example MFGD for $\dot{s}_{MFG} = 1\ mm/s$

The power input due to $F_{cha,dmp}$ is defined as

$$P_{cha,dmp} = -F_{cha,dmp}\dot{s}_{cha} \tag{3.219}$$

while the power input due to $F_{MFG,dmp}$ is defined as

$$P_{MFG,dmp} = F_{MFG,dmp}\dot{s}_{MFG} \tag{3.220}$$

$F_{MFG,dmp}$ and $-F_{cha,dmp}$ are presented in Figure 3.42 with respect to s_{MFG}.

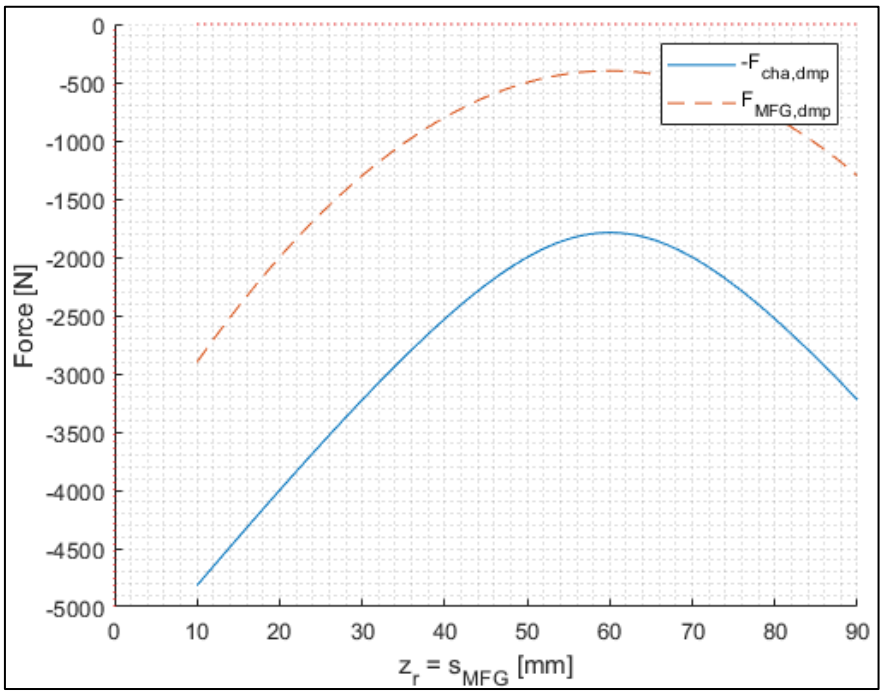

Figure 3.42. $F_{MFG,dmp}$ and $-F_{cha,dmp}$ w.r.t. s_{MFG}

As a final check, $P_{cha,dmp}$ and $P_{MFG,dmp}$ are compared. Referring to equation (3.219) and equation (3.220), if "$-F_{cha,dmp}$ in Figure 3.42" is multiplied with "$\dot{s}_{cha}$ in Figure 3.41", "$F_{MFG,dmp}$ in Figure 3.42" will be obtained (remember that $\dot{s}_{MFG} = 1\ mm/s$). The previous statement is true for all allowable s_{MFG} values.

CHAPTER 4

LANDING GEAR SHOCK ABSORBER MODELLING AND OPTIMIZATION

At the beginning of this chapter, a 2 DoF model of landing gear drop test is presented. Test results and model results available on the commercial research "NACA TN 2755 – Analysis of landing-gear behavior", which was released by the National Advisory Committee for Aeronautics (NACA), have been used as a reference to validate the model used in this thesis. The mathematical model in NACA TN 2755 is referred to as the "NACA Model". On the other hand, 2 DoF mathematical model, referred to as the "Thesis Model", is also prepared for use in the thesis. The model used in the thesis is compared to the NACA model, and the differences are discussed. The assumptions and simplifications of the drop test model are described.

In the second part of this chapter, using the Thesis Model, optimization of shock absorber characteristics has been presented. The optimization is performed for the same test parameters (i.e., mass properties, vertical speed during initial contact) used in NACA TN 2755 and compared to the results. Different optimization methods are evaluated in terms of their effectiveness in achieving the optimum solution and optimization time.

4.1 Modeling Landing Gear Drop Test

The landing gear drop test and its purpose were explained in Section 1.3. The landing gear drop test modeling is a primary means to analyze the achievability for the design goal of high efficiency and low force before manufacturing and testing an actual aircraft landing gear.

Firstly, the 2 DoF Thesis Model used in the optimization is introduced. Then, the validity of this model is presented with respect to test results in NACA TN 2755.

4.1.1 2 DoF Model

The drop test, by its name, is performed by dropping the landing gear from a height with a mass at the top of the gear, which represents the aircraft mass. The scope of the analysis and the optimization is limited from the initial touchdown to the settling of the dynamic system. In a normal drop test procedure, the tire is rotated to simulate the approach of the aircraft to the runway in a longitudinal direction [26]. However, for research purposes, the landing gear is installed vertically, and the tire rotation is not included to isolate the research on shock absorber characteristics [15].

Assumptions in the Thesis Model:

- The internal friction of the shock absorber is neglected because it was proven in NACA TN 2755 that a simplified model (friction is neglected) gives nearly the same result with a model with friction (see Figure 4.1).

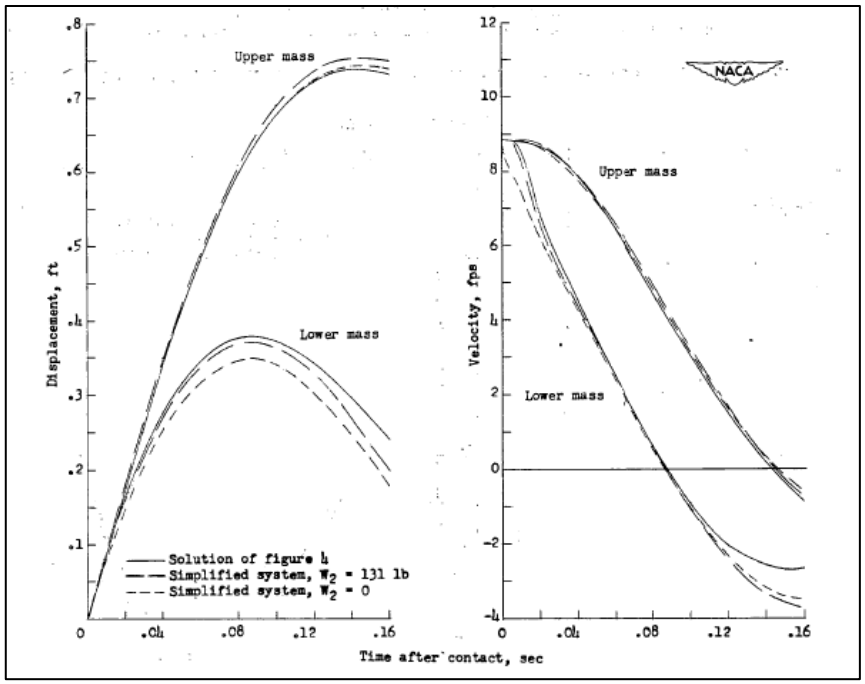

Figure 4.1. Response time history of simplified NACA model [15]

- There are two assumptions for the tire. First, the tire spring characteristic is assumed as linear, where the effect of the assumption is negligible [15]. Also,

the damping of the tire, so called hysteresis, is neglected because of its negligible effect on the results. The effects of both assumptions on the results are presented in Figure 4.2.

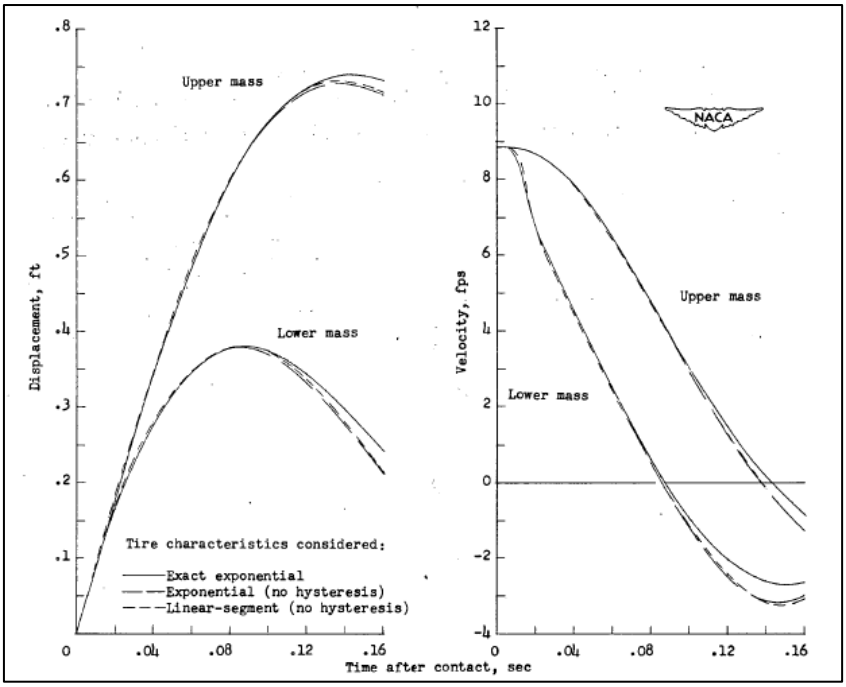

Figure 4.2. Time history of NACA Model for different tire assumptions [15]

- The flexibility of the landing gear is neglected. Since the landing gear is placed vertically in the test setup, the flexibility of the landing gear does not affect the load on the shock absorber spring and damper [15].
- The wing lift force acting on the aircraft body is assumed to be equal to aircraft weight [9], [15], because aircraft landings occur at a steady approach to the landing area. Thus, the aircraft descends at a constant velocity where the forces on the aircraft are balanced. This requires the wing lift during landing to be equal to aircraft weight.
- As it is practiced in other landing gears, there is not any shock loading on the landing gear during the initial contact of the tire to the ground.

With the assumptions above, a drop test can be modeled as a 2 DoF simplified spring-mass-damper system without impairing the validity of the shock absorber (see

Section 4.1.3. Validation of 2 DoF Model w.r.t Test Results), as presented in Figure 4.3.

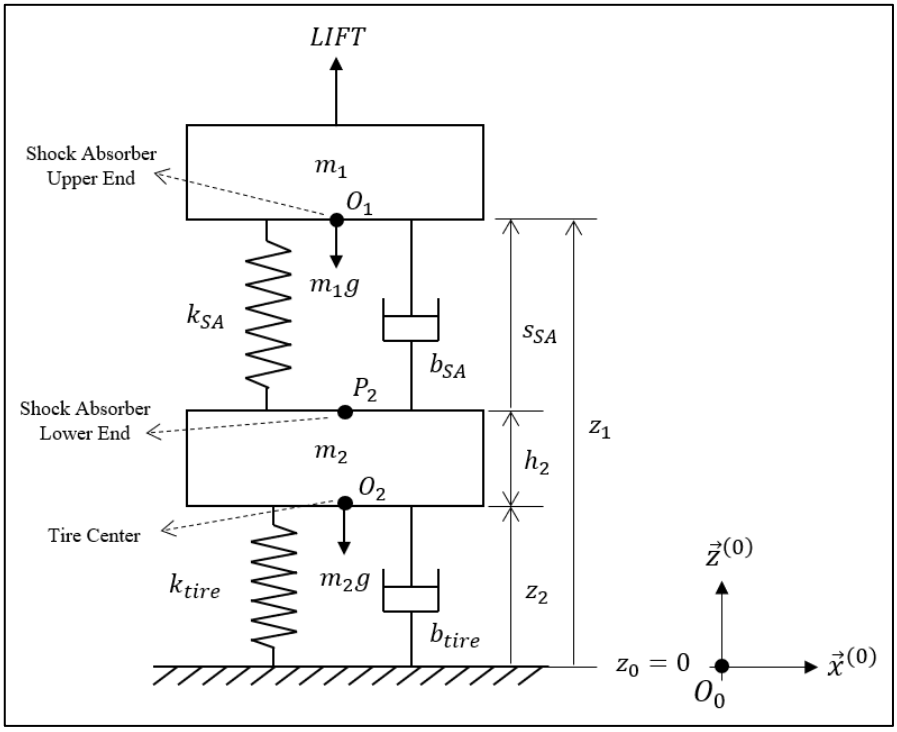

Figure 4.3. Simplified 2 DoF representation of landing gear drop test

The elements of the mass-spring-damper system above are explained as follows.

m_1 : The upper mass that represents the aircraft load on the landing gear and mass of upper assembly of the shock absorber

m_2 : The lower mass that represents the unsprung mass of the landing gear

k_{SA} : The spring coefficient of the shock absorber

b_{SA} : The damping coefficient of the shock absorber

k_{tire} : The spring coefficient of the tire

b_{tire} : The damping coefficient of the tire

$LIFT$: Force acting on the upper mass due to wing lift

There are 4 points taken as reference on the shock absorber, as presented in Figure 4.3. Shock absorber upper end, O_1, is the point where one end of the SA spring and damper is attached. On the other hand, shock absorber lower end, P_2, is the other end of the SA spring, and the damper is attached. The third reference point is attached at the tire center as O_2. Earth fixed reference frame, $\mathcal{F}_0$, is attached to the ground surface with an origin at O_0. Dimensions measured from these reference points are explained as follows.

$$z_1 = \overrightarrow{O_0O_1} \cdot \vec{k} \tag{4.1}$$

$$z_2 = \overrightarrow{O_0O_2} \cdot \vec{k} \tag{4.2}$$

$$h_2 = \overrightarrow{O_2P_2} \cdot \vec{k} \tag{4.3}$$

$$s_{SA} = \overrightarrow{O_2O_1} \cdot \vec{k} \tag{4.4}$$

It shall be noted that the damping properties of the tire are neglected during the evaluation of shock absorber characteristics because the damping forces of aircraft tires are in the order of 0.1% of the spring forces. A typical damping coefficient of a tire can be assumed as follows [27].

$$b_{tire} = k_{tire}/(1000/s) \tag{4.5}$$

Thus, taking equation (4.5) into account, the effect of tire damping is negligible. The equations of motion for the system in Figure 4.3 are derived in Section 4.1.2 as follows.

4.1.2 Equations of Motion for 2 DoF Mass Spring Damper Model

The equation of motion that is specific to the scope of the thesis is defined in this section.

The free-body diagram of the upper mass is presented in Figure 4.4. The total force acting on the upper mass due to shock absorber is defined as

$$F_{SA} = F_{SA,spr} + F_{SA,dmp} \tag{4.6}$$

where

$F_{SA,spr}$: Spring force of the shock absorber

$F_{SA,dmp}$: Damper force of the shock absorber

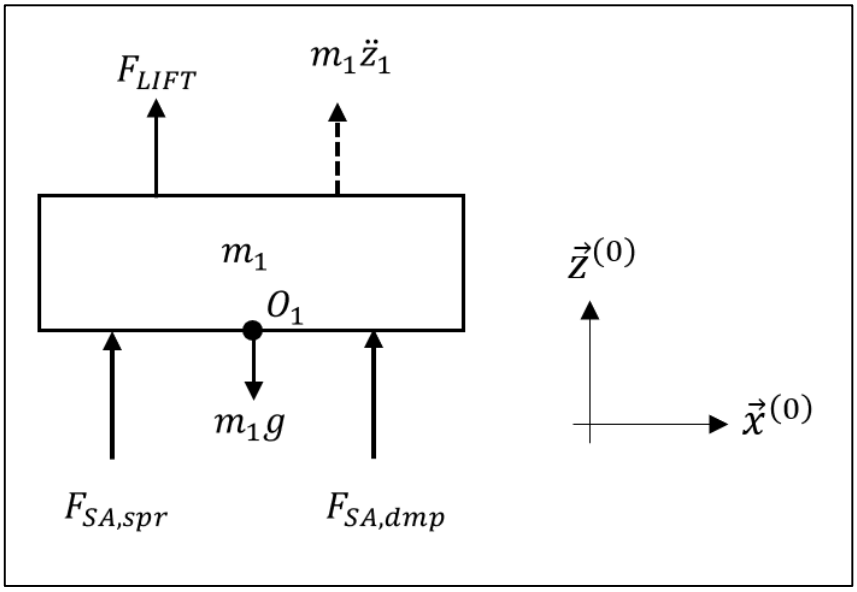

Figure 4.4. Free-body diagram of the upper mass

With respect to the assumption, the force exerted on the upper mass due to wing lift is defined as

$$F_{LIFT} = (m_1 + m_2)g \tag{4.7}$$

The spring and damper forces exerted by the shock absorber are defined as

$$F_{SA,spr} = k_{SA}\left(l_{0,SA} - s_{SA}\right) \tag{4.8}$$

$$F_{SA,dmp} = -b_{SA}\dot{s}_{SA} \tag{4.9}$$

where

$l_{0,SA}$: Length of the shock absorber at the initial contact

s_{SA} : Stroke length of the shock absorber

$\dot{s}_{SA}$: Stroke velocity of the shock absorber

The initial length of the shock absorber is length related to the arrangement of the shock absorber assembly and is measured as the length at the initial contact. The stroke length and the velocity of the shock absorber are defined as follows.

$$s_{SA} = z_1 - z_2 - h_2 \tag{4.10}$$

$$\dot{s}_{SA} = \dot{z}_1 - \dot{z}_2 \tag{4.11}$$

Thus, the equation of motion for the upper mass can be written as

$$m_1 \ddot{z}_1 = F_{LIFT} + F_{SA,spr} + F_{SA,dmp} - m_1 g \tag{4.12}$$

which yields

$$m_1 \ddot{z}_1 = F_{LIFT} + k_{SA}\left(l_{0,SA} + h_2 + z_2 - z_1\right) - b_{SA}(\dot{z}_1 - \dot{z}_2) - m_1 g \tag{4.13}$$

The free-body diagram of the lower mass is presented in Figure 4.5. The forces acting on the lower mass come from the inertial load of the mass and the forces exerted by the shock absorber and the tire to the mass. The description of these forces is as follows.

$F_{tire,spr}$: Spring force of the tire

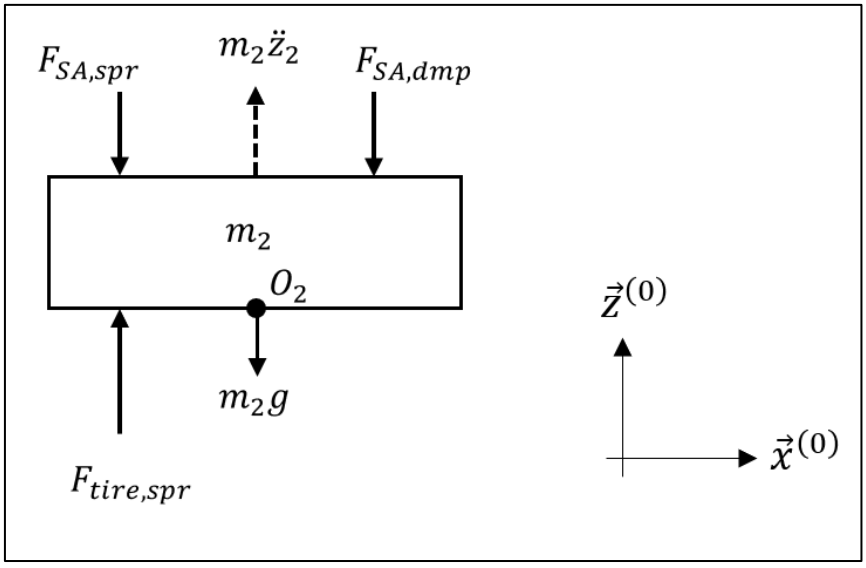

Figure 4.5. Free-body diagram of the lower mass

The force exerted on the lower mass by the tire is defined as;

$$F_{tire,spr} = k_{tire} s_{def} \tag{4.14}$$

where

s_{def} : Deflection of the tire from the initial contact

The deflection of the tire is a measure defined with the outer radius of the tire and is defined as follows.

$$s_{def} = r_{tire} - z_2 \tag{4.15}$$

where

r_{tire} : Outer radius of the tire

Thus, the equation of motion for the lower mass can be written as

$$m_2 \ddot{z}_2 = -F_{SA,spr} - F_{SA,dmp} - m_2 g + F_{tire,spr} \tag{4.16}$$

which yields

$$m_2 \ddot{z}_2 = -k_{SA}\left(l_{0,SA} + h_2 + z_2 - z_1\right) + b_{SA}(\dot{z}_1 - \dot{z}_2) - m_2 g + k_{tire}(r_{tire} - z_2) \tag{4.17}$$

Using the equations of motion in (4.13) and (4.17), a Simulink model is prepared, and the results of the 2 DoF Model are compared to test results given in NACA TN 2755.

4.1.3 Validation of 2 DoF Model w.r.t Test Results

In NACA TN 2755, a landing gear drop test has been performed and mathematically modeled. As presented in Figure 4.6, the landing gear in the test is vertically mounted, and several measurements have been taken from the test setup.

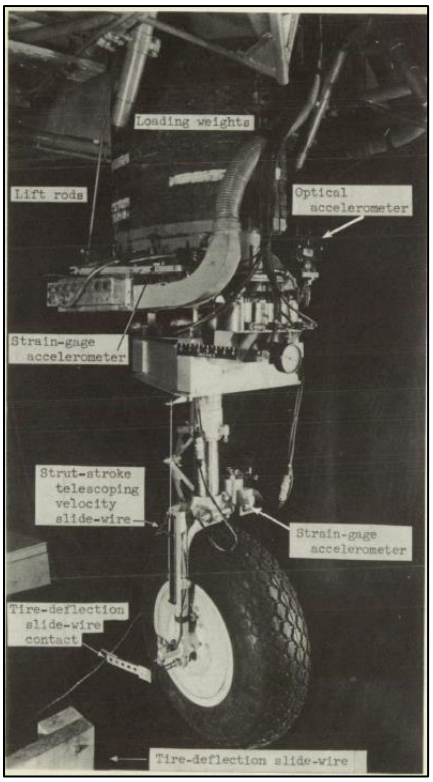

Figure 4.6. Landing gear drop test setup used for validation [15]

The type and accuracy of these test measurements are defined in Table 4.1 [15].

Table 4.1. Accuracy of test measurements

Measurement Type	*Unit*	*Accuracy*
Upper mass acceleration ($\ddot{z}_1$)	g	± 0.2
Force on upper mass (F_{SA})	N	± 2224
Lower mass acceleration ($\ddot{z}_2$)	g	± 0.3
Vertical velocity at ground contact (V_V)	m/s	± 0.03048
Upper mass velocity during impact ($\dot{z}_1$)	m/s	± 0.1524
Upper mass displacement (z_1)	m	± 0.01524
Lower mass displacement (z_2)	m	± 0.00914
Shock absorber stroke (s_{SA})	m	± 0.00914
Shock absorber velocity ($\dot{s}_{SA}$)	m/s	± 0.01524
Time after contact	s	± 0.003

The test setup properties are defined in Table 4.2.

Table 4.2. Test setup parameters

Parameter	*Value*	*Unit*
Upper mass (m_1)	1093.61	kg
Lower mass (m_2)	59.42	kg
Vertical velocity at ground contact (V_V)	2.7	m/s
The outer radius of tire (r_{tire})	0.3429	m

Sign and conventions in NACA TN 2755 landing gear model are different from their use in this thesis study. Signs and conventions of mass spring damper model used in NACA TN 2755 can be seen in Figure 4.7.

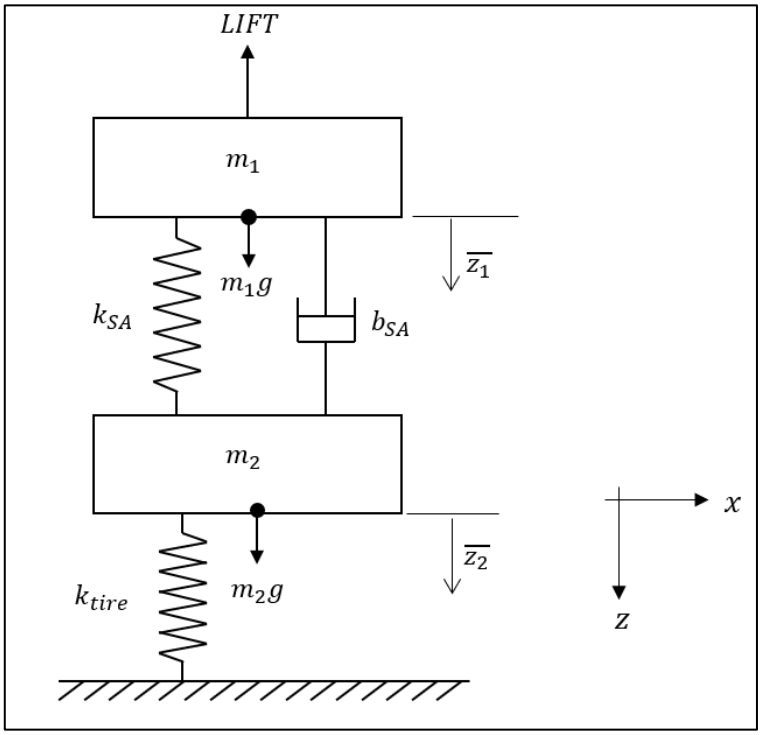

Figure 4.7. NACA TN 2755 mass spring damper model [15]

The sign and conventions used in NACA Model are related with the signs and conventions used in Thesis Model as follows.

$$\overline{z_1} = (z_1)_0 - z_1 \tag{4.18}$$

$$\overline{z_2} = (z_2)_0 - z_2 \tag{4.19}$$

$$\dot{\overline{z_1}} = -\dot{z}_1 \tag{4.20}$$

$$\dot{\overline{z_2}} = -\dot{z}_2 \tag{4.21}$$

Since the variables of the system are defined differently from the definitions used in the thesis study, the initial conditions of NACA model are defined independently from dimensions of the system as $\overline{z_1} = 0$ and $\overline{z_2} = 0$ such that only the change in the parameters has been taken into consideration. Also, there is not any additional information on the dimensions of the test setup as well.

The initial conditions of the NACA Model are defined in Table 4.3.

Table 4.3. Initial conditions NACA Model

Parameter	*Initial Condition*	*Unit*
$\overline{z_1}$	0	m
$\overline{z_2}$	0	m
$\dot{\overline{z_1}}$	2.7	m/s
$\dot{\overline{z_2}}$	2.7	m/s

Thus, by taking the initial conditions defined in Table 4.3, and by using equations (4.18), (4.19), (4.20) and (4.21), the initial conditions of the Thesis Model simulation are presented in Table 4.4.

Table 4.4. Initial conditions of Thesis Models

Parameter	*Initial Condition*	*Unit*
z_1	$(z_1)_0$	m
z_2	$(z_2)_0$	m
$\dot{z}_1$	-2.7	m/s
$\dot{z}_2$	-2.7	m/s

The initial conditions used for z_1 and z_2 in Thesis Model are defined as arbitrary constants, i.e., $(z_1)_0$ and $(z_2)_0$. This definition does not have any effect on the results because the evaluation of the results is performed with respect to change in the parameters.

To perform an adequate assessment with respect to the analysis and test results presented in NACA TN 2755, evaluation parameters are defined with respect to signs and conventions used in Figure 4.3 and initial conditions defined in Table 4.4. In general, the negative of a change in a parameter after initial contact (t_0) is defined with designation with a hat (ˆ) on top of the parameter. The reason for taking the negative of the change is to correlate the results from the Thesis Model with NACA Model on the same domain.

$$\hat{z}_1 = (z_1)_0 - z_1 \tag{4.22}$$

$$\hat{z}_2 = (z_2)_0 - z_2 \tag{4.23}$$

$$\hat{s}_{SA} = (z_1)_0 - (z_2)_0 - h_2 - s_{SA} \tag{4.24}$$

where

$\hat{z}_1$: Upper mass displacement

$\hat{z}_2$: Lower mass displacement

$\hat{s}_{SA}$: Shock absorber stroke displacement

Sign and conventions used for velocity and acceleration of the system are based on the same initial conditions. Thus, a further definition is not required.

A drop test analysis has been performed with 2 DoF Model using the same parameters defined in NACA TN 2755 (see Table 4.2) with respect to initial conditions defined in Table 4.4. The results of the test are in the time domain, in which the time of the test and simulation is from $t_0 = 0\ s$ to $t = 0.16\ s$. For the analysis, the shock absorber characteristics of the NACA shock absorber are defined used. Since the shock absorber forces used in NACA are not defined same as the spring and damper forces defined in equations (4.8) and (4.9), equations of motion in (4.12) and (4.16) have been used, instead of equations (4.13) and (4.17). Thus, the spring force and damper force of NACA shock absorber are defined as

$$F_{SA,spr,NACA} = p_{a_0} A_a \left(\frac{v_0}{v_0 - A_a \hat{s}_{SA}}\right)^{n_p} \tag{4.25}$$

$$F_{SA,dmp,NACA} = \frac{\dot{s}_{SA}}{|\dot{s}_{SA}|} \frac{\rho A_h^3}{2(C_d A_n)^2} \dot{s}_{SA}^2 \tag{4.26}$$

where the definition and values of the parameters are listed in Table 4.5.

Table 4.5. NACA shock absorber parameters [15]

Parameter	*Value*	*Unit*
Air pressure in strut when $\hat{s}_{SA} = 0$ (p_{a_0})	299922	N/m^2
Air volume in strut when $\hat{s}_{SA} = 0$ (v_0)	0.001	m^3
Pneumatic area (A_a)	0.0054	m^2
Polytropic constant (n_p)	1.12	
Damper fluid density (ρ)	869.15	kg/m^3
Hydraulic area (A_h)	0.0044	m^2
Coefficient of discharge (C_d)	0.9	
Net orifice area (A_n)	5.187×10^{-5}	m^2

The shock absorber spring and damper characteristics of NACA test setup defined with equations (4.25) and (4.26) is calculated with the parameters listed in Table 4.5 and presented in Figure 4.8.

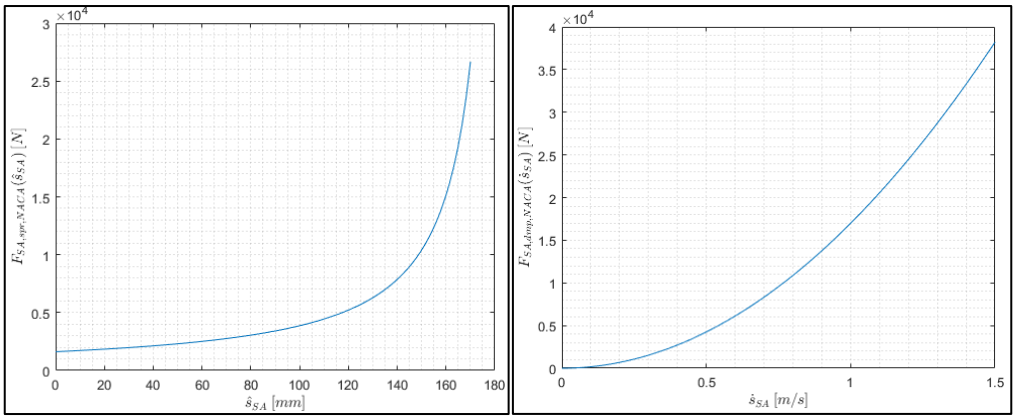

Figure 4.8. NACA test setup shock absorber characteristics

Furthermore, the tire spring stiffness used in the NACA Model and the Thesis Model is defined as follows.

$$k_{tire} = 283380\ N/m \tag{4.27}$$

Test results, NACA Model analysis results, and Thesis Model analysis results are compared to check the validity of the thesis model in Figure 4.9, Figure 4.10, Figure 4.11, and Figure 4.12. Results of the test are defined as discrete point data (not continuous) in the reference documentation [15]. The test results are presented as scattered data in figures. Since the reference documentation consists of mathematical modeling of the drop test and analysis results of this mathematical model (NACA Model), the analysis result is included in figures with a dashed-dotted line ($-\cdot$). Furthermore, the results of the analysis performed with the 2 DoF Model (Thesis Model), which is used in this thesis, are presented in figures with a continuous line.

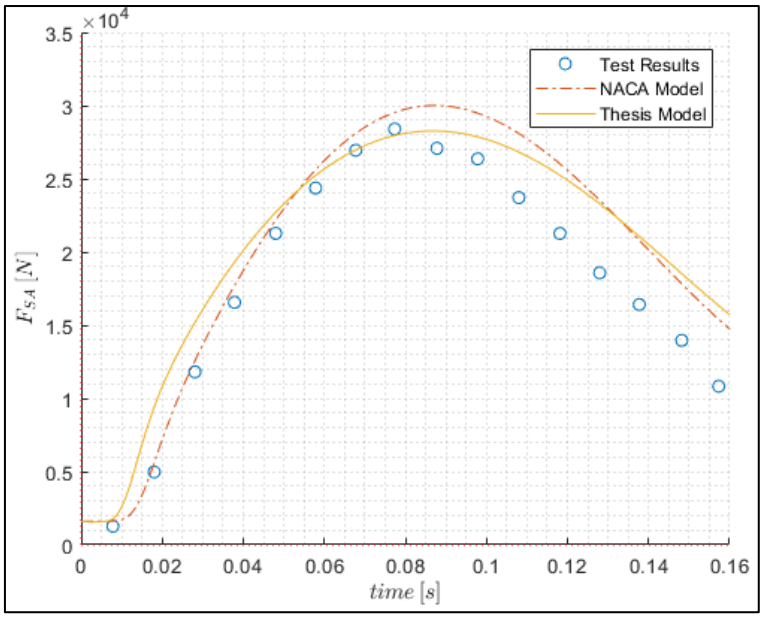

Figure 4.9. Comparison of F_{SA} between Test Results, NACA Model and Thesis Model

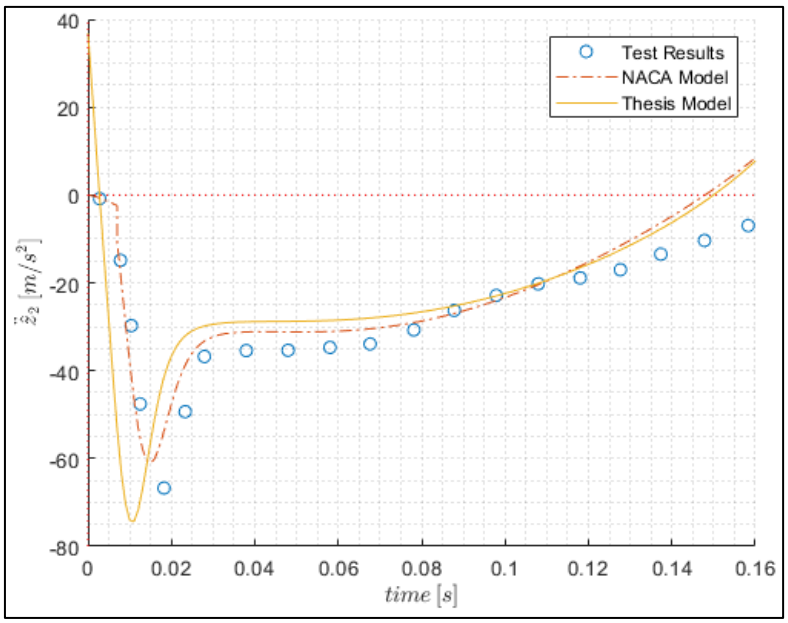

Figure 4.10. Comparison of $\ddot{z}_2$ between Test Results, NACA Model and Thesis Model

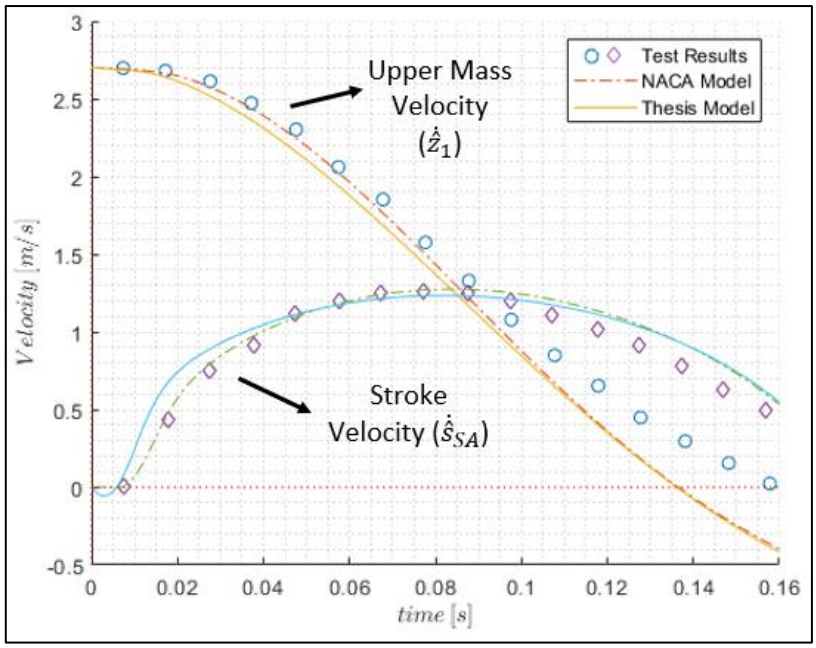

Figure 4.11. Comparison of $\dot{\hat{s}}_{SA}$ and $\dot{\hat{z}}_1$ between Test Results, NACA Model and Thesis Model

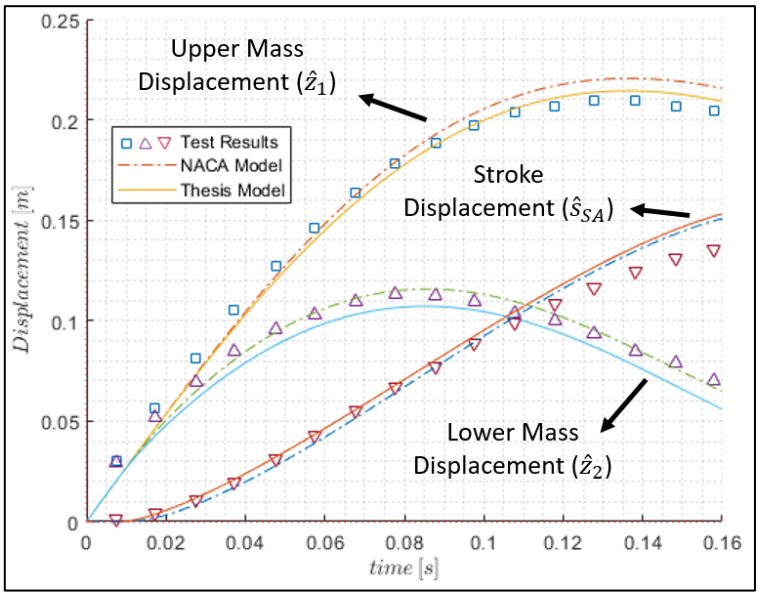

Figure 4.12. Comparison of $\hat{s}_{SA}$, $\hat{z}_1$ and $\hat{z}_2$ between Test Results, NACA Model and Thesis Model

The comparison of NACA test results, NACA Model results, and Thesis Model results show that the model used in the thesis qualitatively yields the same result.

The data presented above are not processed as criteria in this thesis. Thus, an error calculation is not performed for those parameters one by one. However, the error of the model is evaluated with respect to the scope of the optimization.

As it will be explained further in Section 4.2.1, F_{SA} vs. $\hat{s}_{SA}$ between t_0 to t_f is the scope of the optimization in this thesis. The test results are only available for the time from $t_0 = 0\ s$ to $t_f = 0.16\ s$. However, the scope of optimization in 4.2.1 requires t_f to be higher than $0.16\ s$. Thus, comparison of NACA Model and Thesis Model is performed with respect to the scope of optimization.

NACA Model and Thesis Model have been run from $t_0 = 0\ s$ to $t = 0.25\ s$. Thus, using the NACA Model results and Thesis Model results which have been presented in Figure 4.13, the error between NACA Model and Thesis Model has been calculated. The error calculation is performed by taking NACA Model results as the reference.

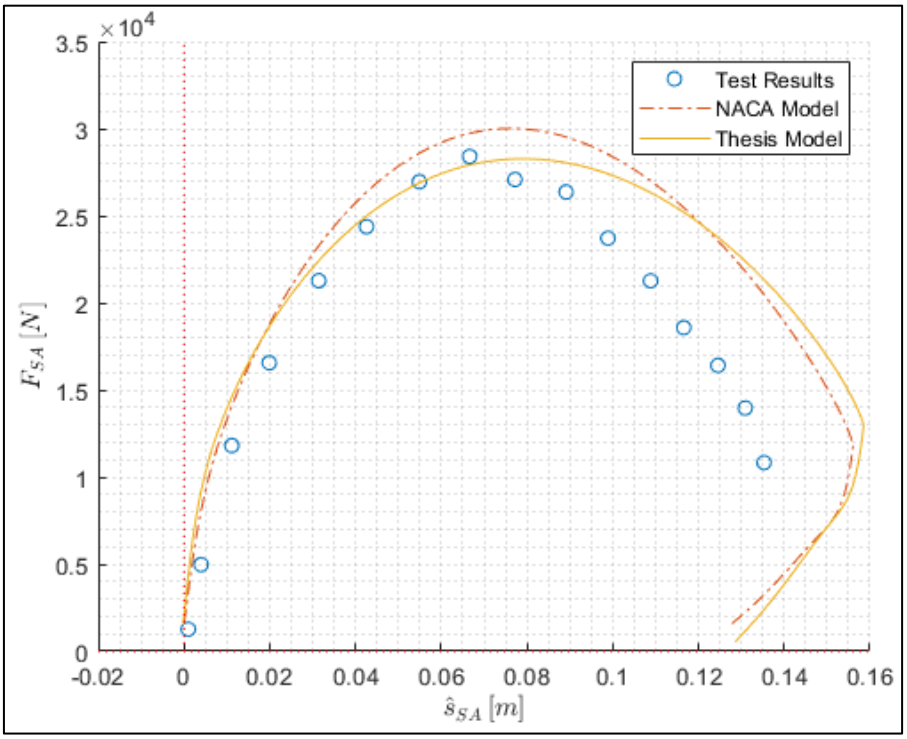

Figure 4.13. NACA Model and Thesis Model results of F_{SA} vs. $\hat{s}_{SA}$ in $t = [0,0.25]$ and test result of F_{SA} vs. $\hat{s}_{SA}$ in $t = [0,0.16]$

As it is explained later in Section 4.2.1, efficiency calculated from the results is the scope of this thesis study. Thus, efficiencies calculated both in NACA Model and Thesis Model are compared as follows.

$$\eta_{NACA} = \%78.26 \tag{4.28}$$

$$\eta_{Thesis} = \%80.92 \tag{4.29}$$

Taking the NACA Model as the reference, the relative error can be calculated as follows.

$$\varepsilon_{Relative} = \frac{|80.92-78.26|}{78.26} \times 100 = \%3.4 \tag{4.30}$$

4.2 2 DoF Model Response Optimization

A landing gear drop test is modeled using test results from NACA TN 2755 in Section 4.1. So, using the same test conditions, optimization has been performed to find the optimum shock absorber spring, $F_{SA,spr}$, and damper, $F_{SA,dmp}$, characteristics. The methods of approach to the optimization are described, and the selection of optimization algorithm is explained. The optimum spring and damper characteristics are presented at the end of the section.

The optimization study is performed using the "Thesis Model" in Section 4.1. The equations of motion were determined for the system previously. The dynamic behavior of the mass-spring-damper system is implicitly dependent on the position, velocity, and acceleration of the system. Also, the objective is purely dependent on the dynamic response of the system. Thus, the optimization of this problem is called as response optimization.

The optimization is based on the parameters defined in Table 4.6. Since the problem is non-linear and the response of the system defines the objectives, search-type optimization methods are used as means for this problem, which is later explained in Section 4.2.2.2. Search type optimization requires the search region to be bounded;

otherwise, there are infinite parameters to evaluate for the optimization. The previously designed shock absorber characteristics, which were used in the test, are also known. The boundaries of the parameter search pool are defined using the known parameters of the legacy shock absorber in NACA TN 2755 for the initial determination. Different optimization methods require different ways to determine the boundaries. Thus, the determination of boundaries is explained for each method for the selection of parameters in 4.2.2.1.

Table 4.6. Optimization reference parameters

Parameter	*Value*	*Unit*
m_1	1093.61	kg
m_2	59.42	kg
r_{tire}	0.3429	m
k_{tire}	283380	N/m
F_{LIFT}	11307	N
$(z_1)_0$	$(z_1)_0$	m
$(z_2)_0$	$(z_2)_0$	m
$(\dot{z}_1)_0$	-2.7	m/s
$(\dot{z}_2)_0$	-2.7	m/s

4.2.1 The objective of the optimization

There is a single objective within the scope of this thesis study.

- Maximize the shock absorber efficiency (η_{SA})

A typical drop test result is explained under Section 1.3. Introduction to Landing Gear Drop Test. The shock absorber force evaluated during the optimization is defined, previously in equation (4.6), as follows.

$$F_{SA} = F_{SA,spr} + F_{SA,dmp} \tag{4.6}$$

The total change in the shock absorber stroke is another parameter to evaluate the shock absorber efficiency. Displacement of the shock absorber stroke is previously defined in equation (4.24) as follows.

$$\hat{s}_{SA} = (z_2)_0 + h_2 - s_{SA} \tag{4.24}$$

The efficiency of the shock absorber is dependent on the parameters of F_{SA} and $\hat{s}_{SA}$. The maximum value of F_{SA} and $\hat{s}_{SA}$ are limited by constraints independent from the efficiency. Shock absorber efficiency is generally a requirement on the design and is defined with the following equation [9].

$$\eta_{SA} = \frac{\int_0^{\hat{s}_{SA,max}} F_{SA} d\hat{s}_{SA}}{\hat{s}_{SA,max} F_{SA,max}} \tag{4.31}$$

The efficiency of the shock absorber is a means to determine how much of the total energy is absorbed by the shock absorber at the first oscillation of the drop. This is the energy under the load-deflection curve. The first oscillation is limited by $[t_0, t_f]$, where

t_0 : Time at the tire contacts to the ground ($t_0 = 0$ for this study)

t_f : Final time (the stroke displacement, $\hat{s}_{SA}$, reaches its maximum)

Knowing the two properties $F_{SA,max}$, $\hat{s}_{SA,max}$ and having the results as $F_{SA}(t)$ and $\hat{s}_{SA}(t)$, one can obtain the efficiency of a shock absorber by dividing the energy absorbed by the shock absorber (blue hatch) with the theoretical total energy absorption capability (yellow hatch) in Figure 4.14.

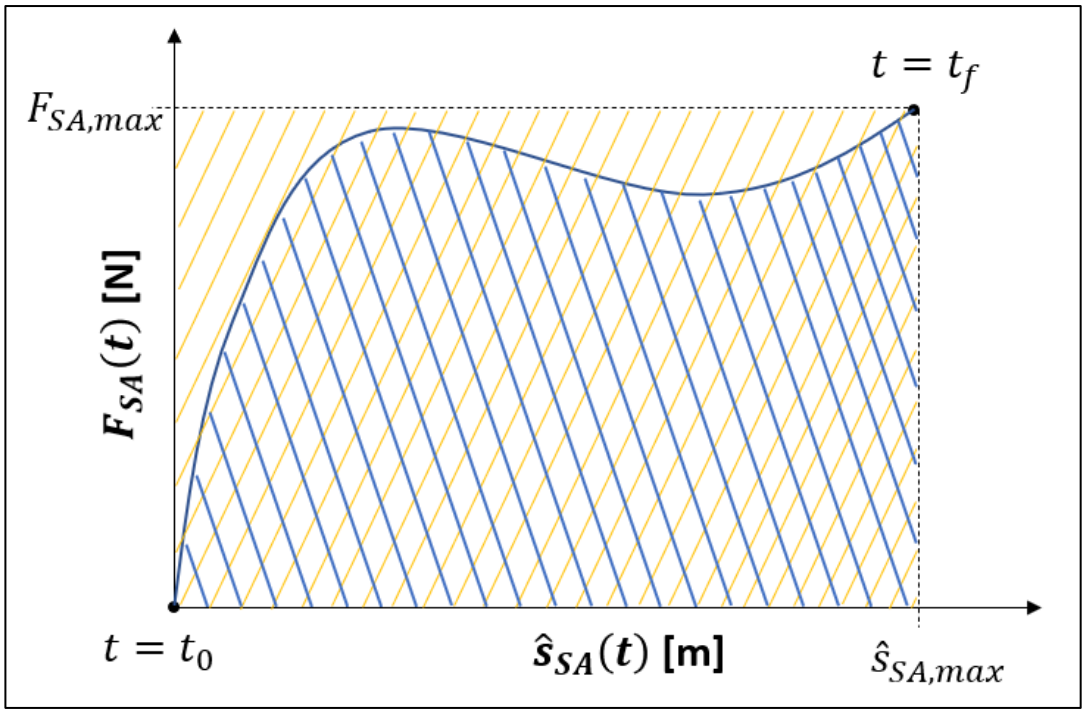

Figure 4.14. Efficiency evaluation of a drop test result

The single objective function used in the thesis, which is designated with J, is defined as follows.

$$J[F_{SA}, \hat{s}_{SA}] = \eta_{SA} \tag{4.32}$$

The efficiency of the previous shock absorber used in NACA TN 2755 is calculated using equation (4.31) as follows.

$$\eta_{SA,NACA} = \%78.26 \tag{4.33}$$

This value will be taken as the reference to evaluate the effectivity of optimization in Section 4.3.

4.2.2 Methods used in the optimization

The selection of decision variables and optimization search methods are explained in this section. Method for selection of decision variables affects the size of the search pool for the variables. The optimization search method, on the other hand,

does heavily influence the cost of the optimization (i.e., time, CPU power) and the effectiveness of finding the optimum solution. Comparison and the selection of the methods used in this thesis study are described in the following sections.

The optimization of the response is based on finding the optimum damper and spring characteristics that give the best objective result. The optimum damper and spring characteristics are found by fitting a damper and spring characteristics for every optimization iteration and evaluating the system's response. The approach for the determination of those characteristics is explained in the following section.

4.2.2.1 Selection of Decision Variables

The selection of decision variables for this problem is investigated from two different aspects: effect on optimization time and simplicity for determination of search region. Three different approaches to select the decision variables have been investigated. Method 1 and Method 2 are based on fitting a polynomial, $P[x]$, to determine the optimum spring and damper characteristics, where

$P[x] = k_{SA}[\hat{s}_{SA}]$ for spring as $x = \hat{s}_{SA}$

and

$P[x] = b_{SA}[\dot{s}_{SA}]$ for damper as $x = \dot{s}_{SA}$ for Optimization Approach 1 and

$P[x] = b_{SA}[\hat{s}_{SA}]$ for damper as $x = \hat{s}_{SA}$ for Optimization Approach 2

Method 3 is based on defining a piecewise linear function, $F[x]$, for optimum spring and damper characteristics similar to Methods 1 and 2, except it is not a polynomial but a piecewise linear curve.

4.2.2.1.1 Method 1: Decision Variables of c_i

In this method, coefficients of polynomials are selected as decision variables. The procedure for an optimization using these variables is presented in Figure 4.15 as follows.

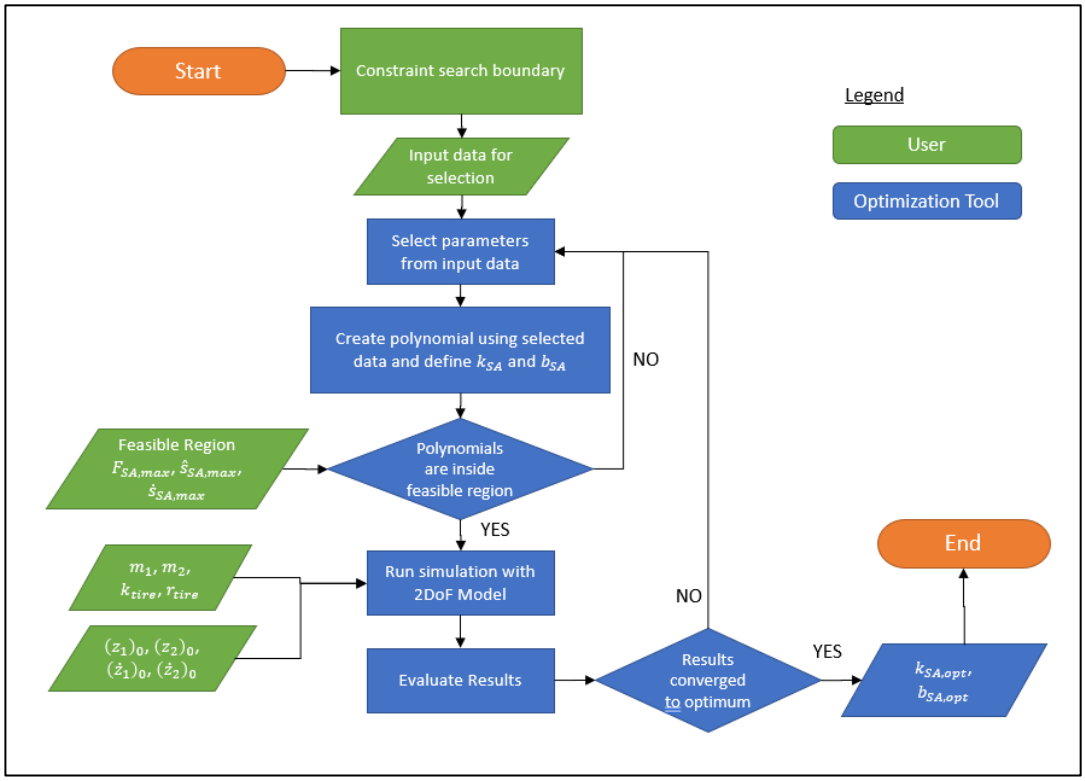

Figure 4.15. Optimization procedure using c_i as decision variables

In this method, the search pool is very large as

$$c_i = -1 \times 10^6 - 1 \times 10^6$$

$$|c_i| = 1 \times 10^{-13} - 1 \times 10^6$$

Using the search pool, a polynomial is constructed, such as

$$P[x] = c_3x^3 + c_2x^2 + c_1x + c_0$$

In this procedure, as presented in Figure 4.15, firstly "n+1" number of coefficients are selected from the search pool, and an n^{th} order polynomial is defined using c_i's.

Then, the polynomial is checked if it is inside the feasible region. The feasible region, on the other hand, is defined based on the $F_{SA,max}$ and $\hat{s}_{SA,max}$ values determined with the test results. $P[x]_{max}$ is manually defined in relation with $F_{SA,NACA,max}$ and $\hat{s}_{SA,max}$ or $\dot{s}_{SA,max}$. As presented in Figure 4.16, the optimization proceeds with a polynomial inside the feasible region while a polynomial outside the feasible region is eliminated, and a new polynomial is defined.

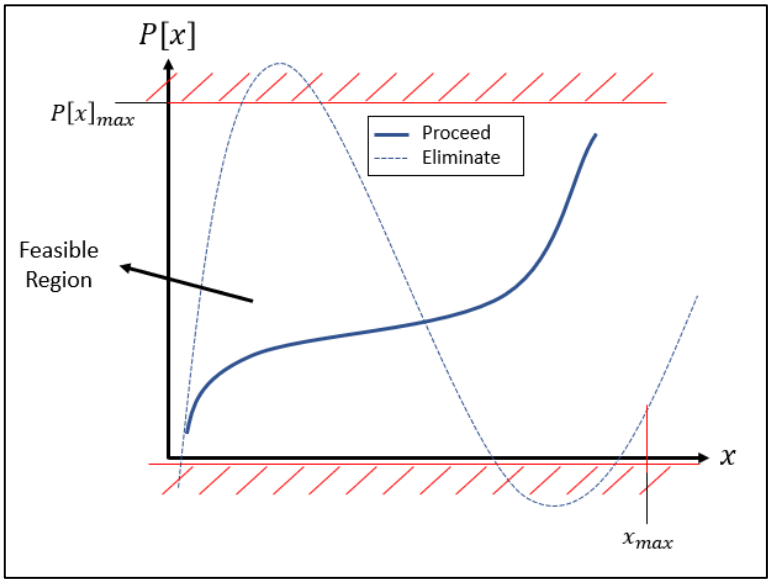

Figure 4.16. Polynomial feasibility check

The drawback of this procedure is the necessity of checking a very large number of polynomials against the feasible region and the difference of the order of magnitude between the polynomial coefficients. Thus, the method is inefficient in terms of finding a feasible solution and the cost of time.

4.2.2.1.2 Method 2: Decision Variables of y_i (using "polyfit" command)

In this method, y coordinates of points, which a polynomial will be fitted through, are defined as decision variables. The "polynomial curve fitting" command of the MATLAB tool is used for this method. The procedure for an optimization using these variables is presented in Figure 4.17 as follows.

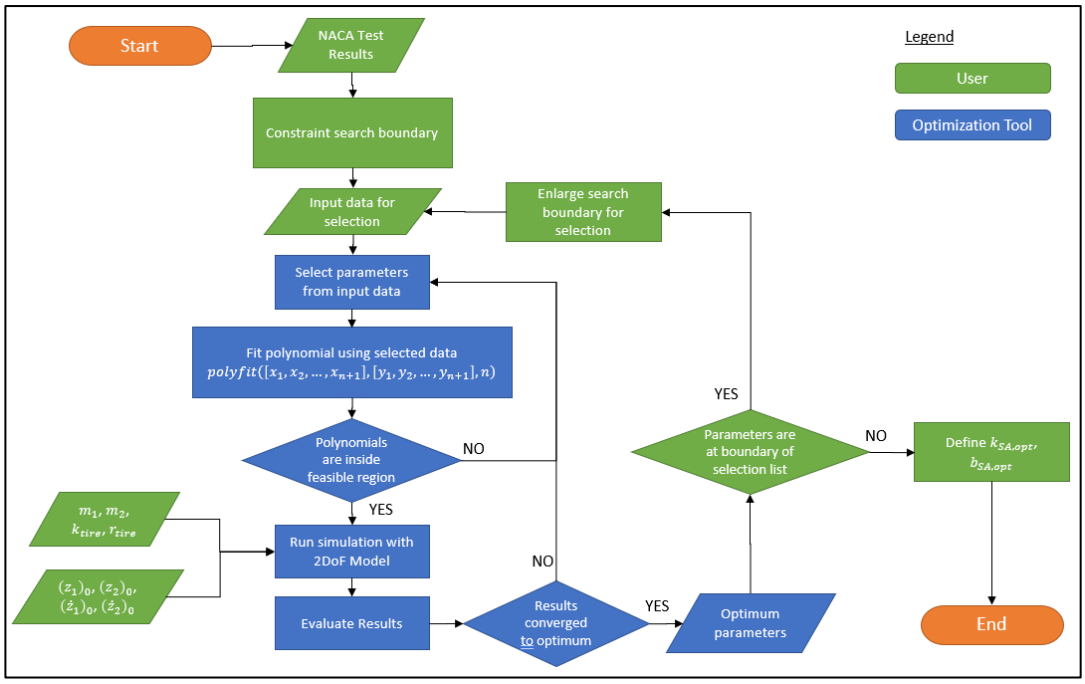

Figure 4.17. Optimization procedure using y_i as decision variables for "polyfit"

In this procedure, x coordinates for "n+1" points are defined by the user (x coordinates are evenly distributed in this study). Then, y_i's are selected by optimization algorithm from corresponding search pool of each. The search pool is initially manually defined with the NACA shock absorber characteristics using the results in the report. In the next step, the optimization will fit an nth order polynomial using user selected x_i and algorithm selected y_i values as follows.

$$P[x] = polyfit([x_1, x_2, \dots, x_{n+1}], [y_1, y_2, \dots, y_{n+1}], n)$$

Then, the polynomial is checked if it is inside the feasible region. The feasible region, on the other hand, is defined based on the $F_{SA,max}$ and $\hat{s}_{SA,max}$ values determined with the test results. $P[x]_{max}$ is manually defined in relation with $F_{SA,NACA,max}$ and $\hat{s}_{SA,max}$ or $\dot{s}_{SA,max}$ as presented in Figure 4.18.

The optimization proceeds with a polynomial inside the feasible region while a polynomial outside the feasible region is eliminated, and a new polynomial is defined.

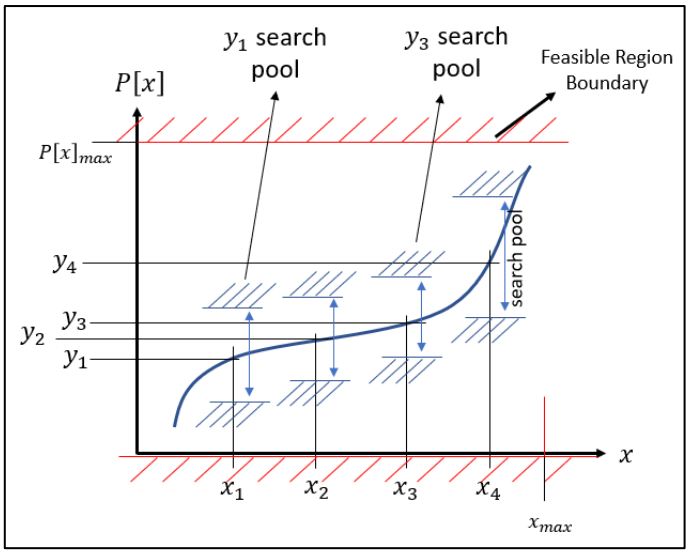

Figure 4.18. Polynomial feasibility check

After the maximization of the efficiency, the search pool is checked against the optimum y_i parameters. If any of y_i parameters coincide with the boundary of its own search pool; then, the search pool is re-defined manually by user, as presented in Figure 4.19.

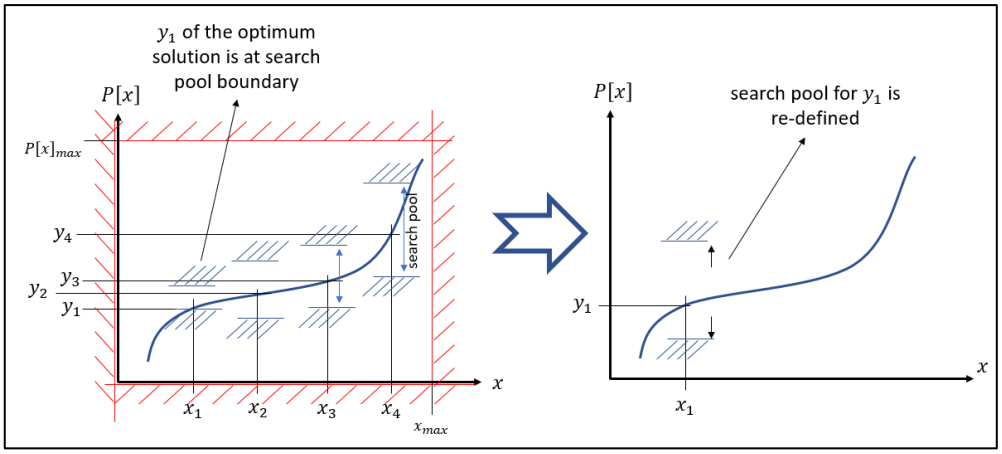

Figure 4.19. Re-defining search pool for y_i

There is only a minor drawback of this method compared to Method 3: the polynomial sometimes goes out of the feasible region. However, the occurrence of this instance is rare compared to Method 1. Method 2 is the most feasible approach for selecting the parameters quickly and with an average cost of time.

4.2.2.1.3 Method 3: Decision Variables of y_i (using "piecewise" command)

In this method, y coordinates of points, which a piecewise linear function will be created with, are defined as decision variables. The "piecewise function" command of the MATLAB tool is used for this method. The procedure for an optimization using these variables is presented in Figure 4.20 as follows.

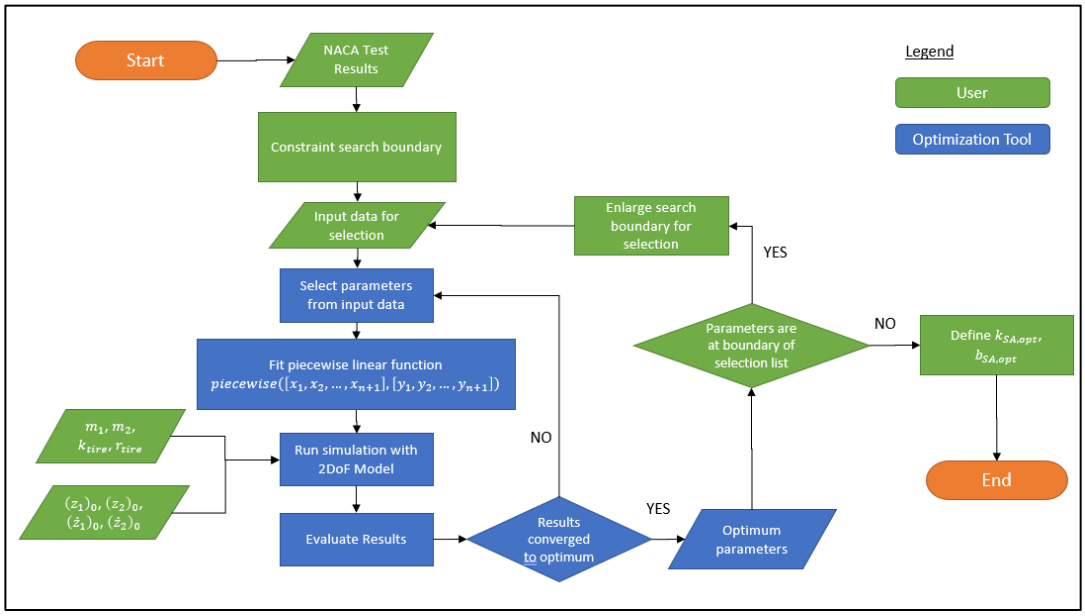

Figure 4.20. Optimization procedure using y_i as decision variables for "piecewise"

In this procedure, x coordinates for "n+1" points are defined by the user (x coordinates are evenly distributed in this study). Then, y_i's are selected by optimization algorithm from corresponding search pool of each. The search pool is initially manually defined with the NACA shock absorber characteristics using the results in the report. In the next step, the optimization code will create piecewise linear function using user selected x_i and algorithm selected y_i values as follows.

$$F[x] = piecewise([x_1, x_2, \dots, x_4], [y_1, y_2, y_3, y_4])$$

After the maximization of the efficiency, the search pool is checked against the optimum y_i parameters. If any of y_i parameters coincide with the boundary of its

own search pool; then, the search pool is re-defined manually by user, as presented in Figure 4.21.

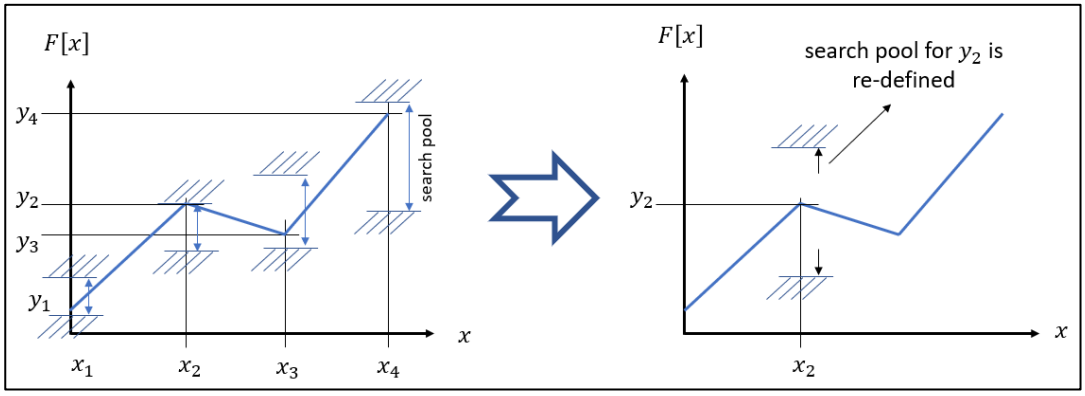

Figure 4.21. Re-defining search pool for y_i

This method provides the advantage of a reduction in computation time; however, the discontinuity of the curves defined in this method requires a polynomial to be fitted at the end of the solution, which results in a deviation from the optimum solution.

Comparing all methods, Method 2 is the most viable approach for this optimization problem; because the time and CPU power required for Method 2 are better than Method 1. Method 3 also processes the optimization in a short time, but since it is not a proper way to define spring and damper characteristics, a polynomial fit after the optimization is required, which deviates from the optimum solution.

4.2.2.2 Optimization search method

The optimization problem in this study is a single objective non-linear response optimization. Before starting the optimization case, an evaluation is performed against the effectiveness of different optimization methods on this type of problem and objective function.

Using objective function defined in equation (4.32), and the Thesis Model with parameters defined in Table 4.6. Optimization reference parameters, an optimization

is performed. Method 2: Decision Variables of $\boldsymbol{y_i}$ (using "polyfit" command) in Section 4.2.2.1 used as a method for selection of parameters for the optimization. The best pair of y_i values were searched that, a first order polynomial (a linear curve) is fit through.

The evaluation is performed using the Response Optimization tool in Simulink, which is a part of the Global Optimization Toolbox of MATLAB/Simulink. The result and time of different optimization search methods have been compared in Table 4.7.

Table 4.7. Comparison of search methods and algorithms

Optimization Method	Algorithm/ Search Method	*Objective (Higher is better)*	*Time*
Gradient-Descent	Active Set	0.8487	37 sec
	Interior Point	0.8479	15 min
	Sequential Quad. Programming	0.8487	43 sec
Pattern Search	Positive Basis N+1	0.8686	16 min
	Positive Basis 2N	0.8718	20 min
	Genetic Algorithm	0.8869	1 hour
Simplex Search	Simplex Search	0.8542	15 min

The comparison of three different optimization methods shows that Pattern Seach is better than the other optimization methods in finding the best solution for the problem defined in this thesis study. Pattern Search in MATLAB/Simulink has three different search algorithm to achieve the solution. The first two methods are the modified versions of the fundamental basis of the pattern search: Positive Basis N+1 and Positive Basis 2N [28]. The Genetic Algorithm (GA) is a deviation from traditional pattern search methods as it is a metaheuristic inspired by the natural selection which the selection of the parameters is performed by the method itself

inside the search region [29]. However, the selection method for the parameters is defined by the user, such as population, mutation, and crossover.

The evaluation of these optimization methods has been performed for a very large search region. Thus, it is normal for the GA to perform a first-order polynomial optimization in 1 hour. In previous studies on landing gear shock absorber response optimization, the effectiveness of genetic algorithm optimization was also acknowledged as the most efficient response optimization method [22].

In summary, the Genetic Algorithm is selected as the search method for this optimization problem.

4.2.3 The constraints of the optimization

Any optimization problem has its own constraints in terms of finding a solution. Those constraints can be the design limitations of the problem, physical limitations, and boundary improvement to reduce the time required to achieve the best solution.

The constraints used for the optimization problem in this study are defined as follows.

Physical Constraints:

- The change in the stroke of the shock absorber shall not have negative values for all t values. The intent of the constraint is to prevent the shock absorber from going beyond the extended position, which physically is not possible.

$$\hat{s}_{SA}(t) > 0 \quad for \quad [t_0, t_s]$$

where

t_s : Settling time (the time which drop test system settles, i.e., $\dot{s}_{SA} = 0$)

- The force at the damper shall have positive values for positive velocity values, negative values for negative velocity values. The constraint intends

to limit the design such that the solution is physically possible, that it does not store energy, and does not do positive work against the environment.

$$F_{SA,dmp}(t) > 0 \quad for \quad \dot{s}_{SA}(t) > 0$$

$$F_{SA,dmp}(t) < 0 \quad for \quad \dot{s}_{SA}(t) < 0$$

Design Constraints:

- The total force at the shock absorber shall be smaller than $30\,kN$. The constraint intends to limit the maximum force that can be exerted from the shock absorber to the aircraft. The results in NACA Model have been used as the reference [NACA TN 2755].

$$|F_{SA}(t)| < 30000\,N \quad for \quad [t_0, t_s]$$

- The total change on the shock absorber stroke shall be smaller than 165 mm. The constraint intends to limit the total landing gear length for installation purposes during the gear retracts into the aircraft fuselage. The results in NACA Model have been used as the reference [NACA TN 2755].

$$\hat{s}_{SA}(t) < 160\,mm \quad for \quad [t_0, t_s]$$

- There shall be a preload at the shock absorber spring when the shock absorber stroke is zero. This is a rule of thumb for a landing gear design to prevent the stiction of the shock absorber surface during the initial rebound [9]. Previous shock absorber design is used as a reference.

$$F_{SA,spr}(t) \geq 1500\,N \quad for \quad \hat{s}_{SA}(t) = 0$$

Search Improvement Constraints:

- The shock absorber stroke shall have an increasing value from the initial contact to the maximum stroke. The dynamic response of the system shall be single-valued for the time of interest of the objective. Any indeterminate motion of the system between this time of interest is not considered to be

acceptable. This constraint has been implemented to prevent the improper solutions which have been encountered at the initial optimization runs.

$$\dot{s}_{SA}(t) > 0 \quad for \quad [t_0, t_f]$$

4.3 Optimization Approaches and Results

The optimization is performed with the fitting of polynomials with different orders using Method 2 described in Section 4.2.2.1. Two different approaches to the optimization of the problem are explained. Results for different approaches and different orders of polynomial fittings are compared. The order of the polynomial, n, has been increased for both optimization approaches as long a better objective result is obtained. The drop test simulation results of the Thesis Model, which was presented in Section 4.1.3, are used as a reference to present the success of the optimization. These results are designated as "Reference" in optimization results.

4.3.1 Optimization Approach 1: b_{SA} as function of $\dot{s}_{SA}$

Shock absorbers are mechanical components which the coefficient of damping of these components is generally a function of the velocity [30]. Thus, the first approach to this optimization problem has assumed the damping coefficient of the damper to be a function of the velocity, i.e., $b_{SA}(\dot{s}_{SA})$. Referring to Method 2: Decision Variables of $\boldsymbol{y_i}$ (using "polyfit" command) in Section 4.2.2.1, the optimum polynomial that represents the spring and damper characteristics is tried to be found by changing the coordinates that the polynomial passes through.

Decision variables of the optimization:

$$y_1, y_2, \dots, y_{n+1}$$

used in

$$P[x] = polyfit([x_1, x_2, \dots, x_{n+1}], [y_1, y_2, \dots, y_{n+1}], n)$$

where

$P[\,] = k_{SA}[\,]$ and $x = \hat{s}_{SA}$ for spring

$P[\,] = b_{SA}[\,]$ and $x = \dot{s}_{SA}$ for damper

$n = 1,2,3$

$x_i = i \times \frac{x_{n+1}}{n}$

where

$x_{n+1} = 0.16\ m$ for spring

$x_{n+1} = 3\ m/s$ for damper

Objective function:

$$J[F_{SA}, \hat{s}_{SA}] = \max(\eta_{SA}) \tag{4.34}$$

Optimization input parameters

$m_1, m_2, r_{tire}, F_{LIFT}, (z_1)_0, (z_2)_0, (\dot{z}_1)_0, (\dot{z}_2)_0$ as defined in Table 4.6.

4.3.1.1 Optimization Approach 1: Results for $n = 1$

Fitting a polynomial passing through 2 points results in, $n = 1$, a 1st order polynomial. Optimum damping coefficient, $b_{SA}(\dot{s}_{SA})$, and optimum spring coefficient, $k_{SA}(\hat{s}_{SA})$, obtained with the 1st order polynomial fitting are presented in Figure 4.22.

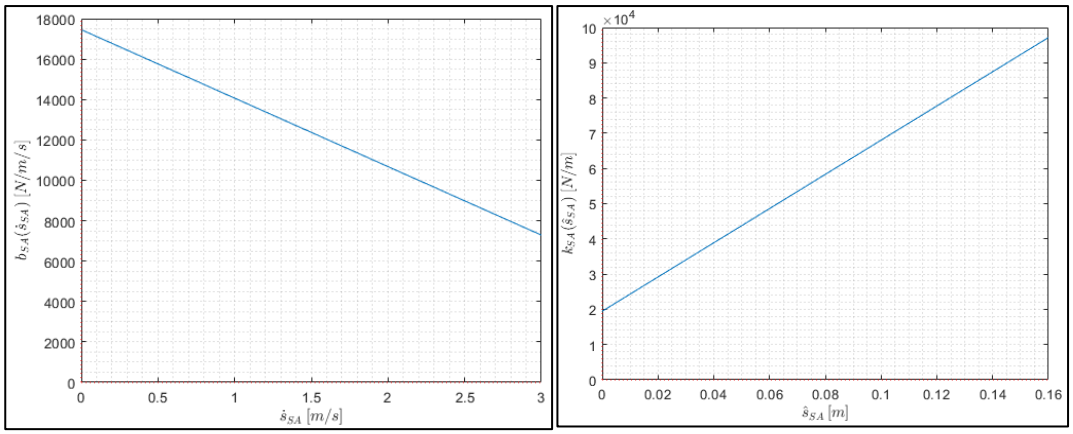

Figure 4.22. 1st order polynomial fitting of; $b_{SA}(\dot{s}_{SA})$ (left), $k_{SA}(\hat{s}_{SA})$ (right)

Effectivity of the optimization is evaluated with a comparison of a "drop test in Thesis Model with optimum spring/damper characteristics" with respect to a "drop test in Thesis Model with spring/damper characteristics defined in NACA TN 2755". The available test results of NACA TN 2755 are also presented in this comparison, as presented in Figure 4.23.

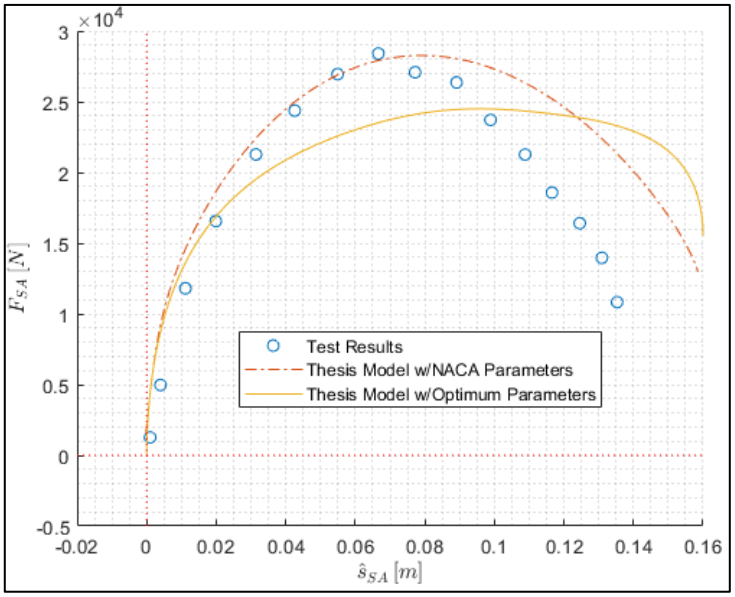

Figure 4.23. Thesis Model drop test simulation with NACA SA characteristics, and optimum SA characteristics for $n = 1$

The efficiency of the shock absorber using the optimum spring/damper characteristics is calculated using equation (4.31) as follows.

$$\eta_{SA,OA_1 n_1} = \%86.9 \tag{4.35}$$

where

OA_i : Optimization Approach i

n_i : i[th] order polynomial

4.3.1.2 Optimization Approach 1: Results for $n = 2$

Fitting a polynomial passing through 3 points results in, $n = 2$, a 2[nd] order polynomial. Optimum damping coefficient, $b_{SA}(\dot{s}_{SA})$, and optimum spring coefficient, $k_{SA}(\hat{s}_{SA})$, obtained with the 2[nd] order polynomial fitting are presented in Figure 4.24.

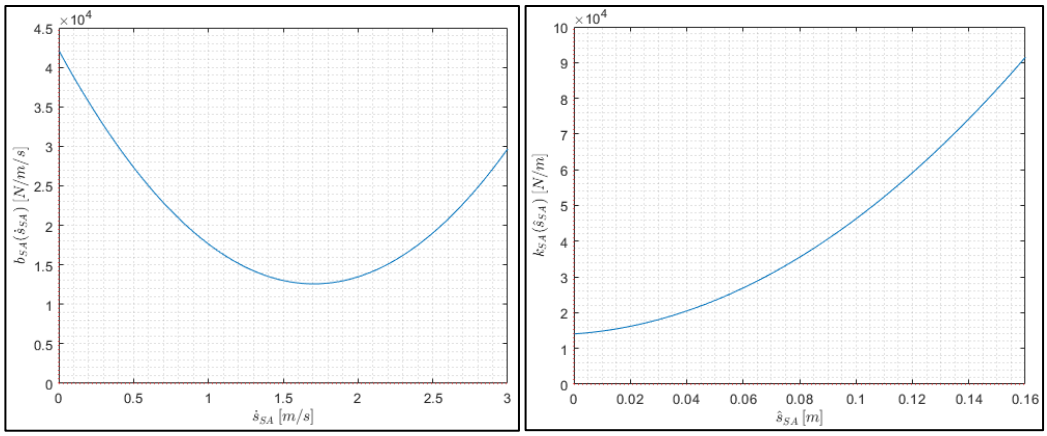

Figure 4.24. 2[nd] order polynomial fitting of; $b_{SA}(\dot{s}_{SA})$ (left), $k_{SA}(\hat{s}_{SA})$ (right)

Effectivity of the optimization is evaluated with a comparison of a "drop test in Thesis Model with optimum spring/damper characteristics" with respect to a "drop test in Thesis Model with spring/damper characteristics defined in NACA TN 2755". The available test results of NACA TN 2755 are also presented in this comparison, as presented in Figure 4.25.

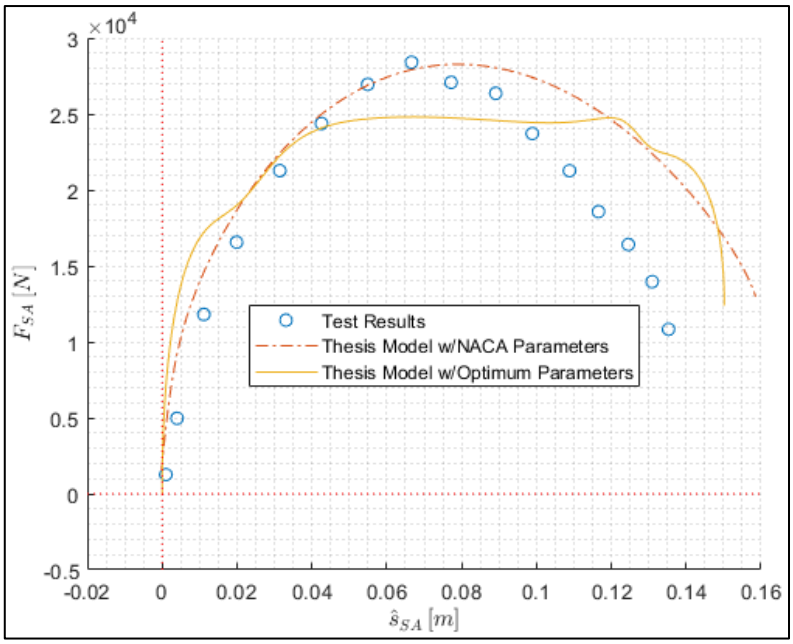

Figure 4.25. Thesis Model drop test simulation with NACA SA characteristics, and optimum SA characteristics for $n = 2$

The efficiency of the shock absorber using the optimum spring/damper characteristics is calculated using equation (4.31) as follows.

$$\eta_{SA,OA_1 n_2} = \%90.44 \tag{4.36}$$

4.3.1.3 Optimization Approach 1: Results for $n = 3$

Fitting a polynomial passing through 4 points results in, $n = 3$, a 3rd order polynomial. Optimum damping coefficient, $b_{SA}(\dot{s}_{SA})$, and optimum spring coefficient, $k_{SA}(\hat{s}_{SA})$, obtained with the 3rd order polynomial fitting are presented in Figure 4.26.

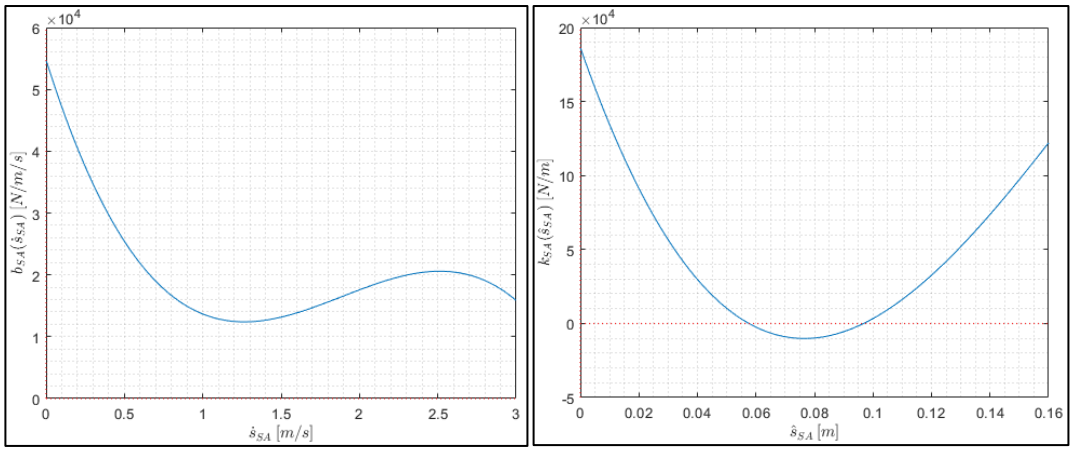

Figure 4.26. 3rd order polynomial fitting of; $b_{SA}(\dot{s}_{SA})$ (left), $k_{SA}(\hat{s}_{SA})$ (right)

Effectivity of the optimization is evaluated with a comparison of a "drop test in Thesis Model with optimum spring/damper characteristics" with respect to a "drop test in Thesis Model with spring/damper characteristics defined in NACA TN 2755". The available test results of NACA TN 2755 are also presented in this comparison, as presented in Figure 4.27.

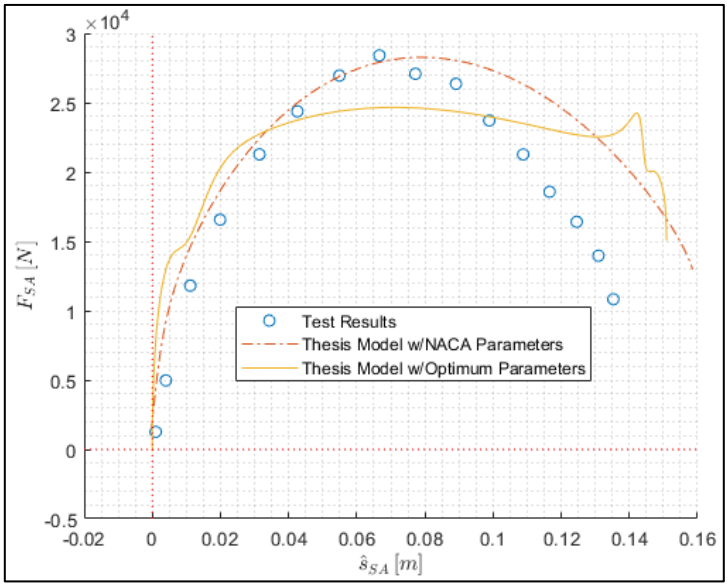

Figure 4.27. Thesis Model drop test simulation with NACA SA characteristics, and optimum SA characteristics for $n = 3$

The efficiency of the shock absorber using the optimum spring/damper characteristics is calculated using equation (4.31) as follows.

$$\eta_{SA,OA_1 n_3} = \%90.37 \quad (4.37)$$

4.3.2 Optimization Approach 2: b_{SA} as function of $\hat{s}_{SA}$

As mentioned in the previous section, the coefficient of damping is usually a function of velocity. However, there are such dampers that their coefficient of damping are a function of displacement and velocity at the same time or function of displacement only [9]. Since MFG design is suitable to define the coefficient of damping as a function of displacement, an optimization approach has been followed by taking both k_{SA} and b_{SA} as function of displacement, i.e. $k_{SA}(\hat{s}_{SA})$, $b_{SA}(\hat{s}_{SA})$. Referring to Method 2: Decision Variables of $\boldsymbol{y_i}$ (using "polyfit" command) in Section 4.2.2.1, the optimum polynomial that represents the spring and damper characteristics is tried to be found by changing the coordinates that the polynomial passes through.

Decision variables of the optimization:

$$y_1, y_2, \dots, y_{n+1}$$

used in

$$P[x] = polyfit([x_1, x_2, \dots, x_{n+1}], [y_1, y_2, \dots, y_{n+1}], n)$$

where

$P[\,] = k_{SA}[\,]$ and $x = \hat{s}_{SA}$ for spring

$P[\,] = b_{SA}[\,]$ and $x = \hat{s}_{SA}$ for damper

$n = 1,2,3$

$$x_i = i \times \frac{x_{n+1}}{n}$$

where

$x_{n+1} = 0.16\ m$ for spring and damper

Objective function:

$$J[F_{SA}, \hat{s}_{SA}] = \max(\eta_{SA}) \tag{4.38}$$

Optimization input parameters

$m_1, m_2, r_{tire}, F_{LIFT}, (z_1)_0, (z_2)_0, (\dot{z}_1)_0, (\dot{z}_2)_0$ as defined in Table 4.6.

4.3.2.1 Optimization Approach 2: Results for $n = 1$

Fitting a polynomial passing through 2 points results in, $n = 1$, a 1st order polynomial. Optimum damping coefficient, $b_{SA}(\hat{s}_{SA})$, and optimum spring coefficient, $k_{SA}(\hat{s}_{SA})$, obtained with the 1st order polynomial fitting are presented in Figure 4.28.

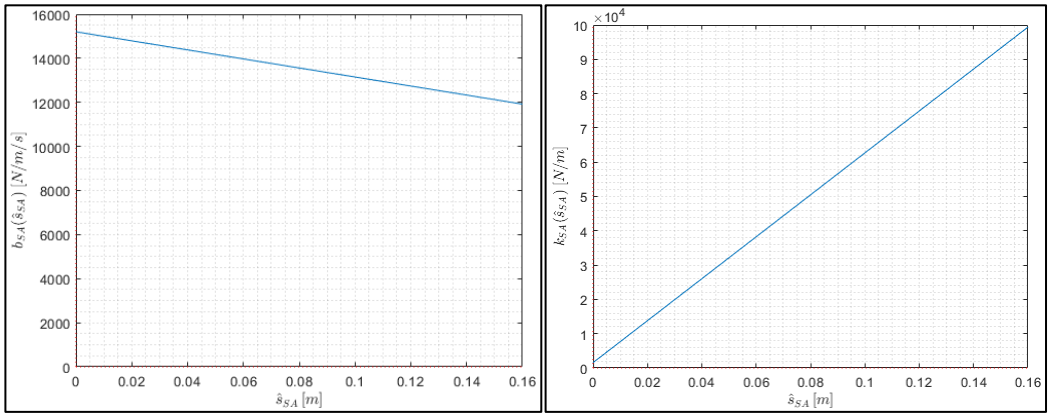

Figure 4.28. 2nd order polynomial fitting of; $b_{SA}(\hat{s}_{SA})$ (left), $k_{SA}(\hat{s}_{SA})$ (right)

Effectivity of the optimization is evaluated with a comparison of a "drop test in Thesis Model with optimum spring/damper characteristics" with respect to a "drop test in Thesis Model with spring/damper characteristics defined in NACA TN 2755". The available test results of NACA TN 2755 are also presented in this comparison, as presented in Figure 4.29.

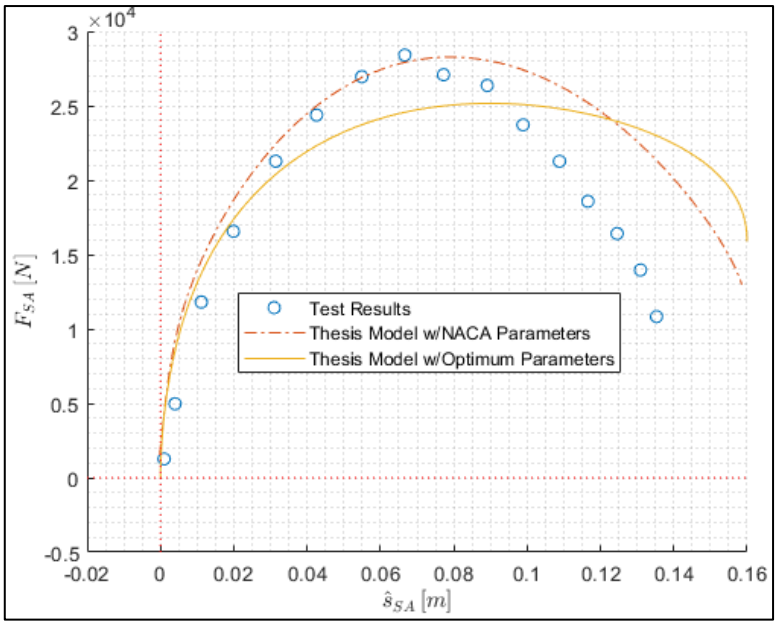

Figure 4.29. Thesis Model drop test simulation with NACA SA characteristics, and optimum SA characteristics for $n = 1$

The efficiency of the shock absorber using the optimum spring/damper characteristics is calculated using equation (4.31) as follows.

$$\eta_{SA,OA_2n_1} = \%86.33 \tag{4.39}$$

4.3.2.2 Optimization Approach 2: Results for $n = 2$

Fitting a polynomial passing through 3 points results in, $n = 2$, a 2nd order polynomial. Optimum damping coefficient, $b_{SA}(\hat{s}_{SA})$, and optimum spring coefficient, $k_{SA}(\hat{s}_{SA})$, obtained with the 2nd order polynomial fitting are presented in Figure 4.30.

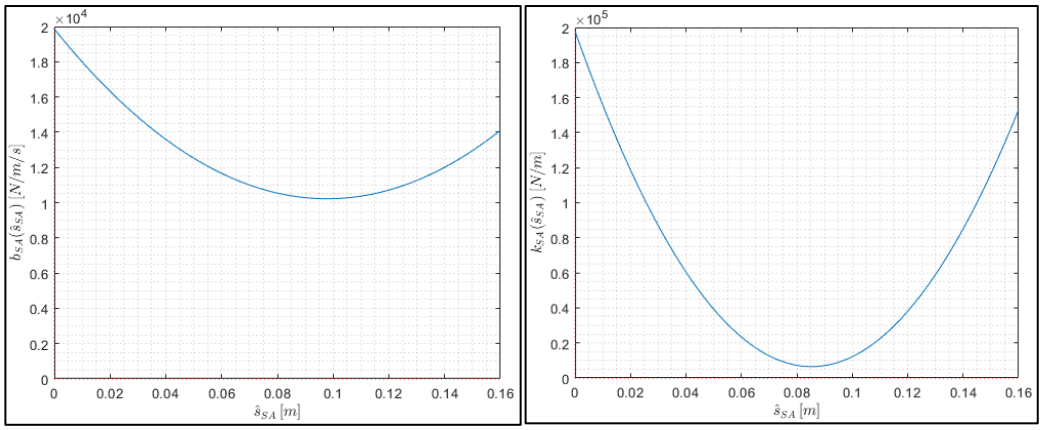

Figure 4.30. 2nd order polynomial fitting of; $b_{SA}(\hat{s}_{SA})$ (left), $k_{SA}(\hat{s}_{SA})$ (right)

Effectivity of the optimization is evaluated with a comparison of a "drop test in Thesis Model with optimum spring/damper characteristics" with respect to a "drop test in Thesis Model with spring/damper characteristics defined in NACA TN 2755". The available test results of NACA TN 2755 are also presented in this comparison, as presented in Figure 4.31.

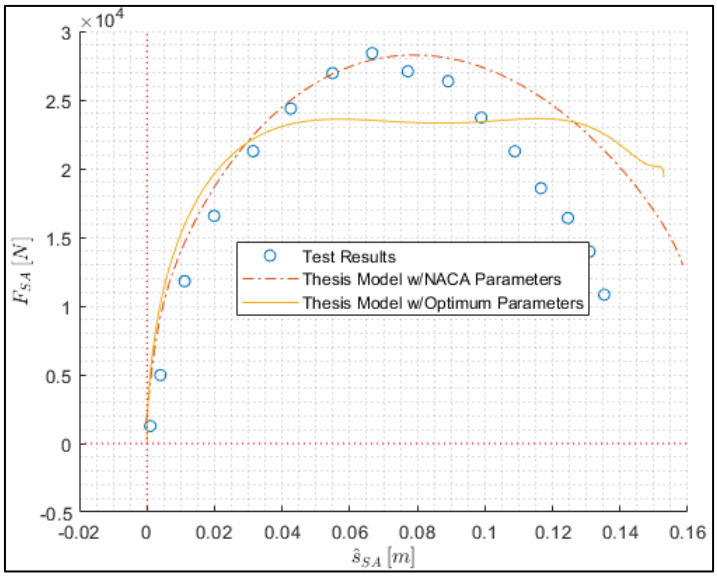

Figure 4.31. Thesis Model drop test simulation with NACA SA characteristics, and optimum SA characteristics for $n = 2$

The efficiency of the shock absorber using the optimum spring/damper characteristics is calculated using equation (4.31) as follows.

$$\eta_{SA,OA_2n_2} = \%91.82 \tag{4.40}$$

4.3.2.3 Optimization Approach 2: Results for $n = 3$

Fitting a polynomial passing through 4 points results in, $n = 3$, a 3rd order polynomial. Optimum damping coefficient, $b_{SA}(\hat{s}_{SA})$, and optimum spring coefficient, $k_{SA}(\hat{s}_{SA})$, obtained with the 3rd order polynomial fitting are presented in Figure 4.32.

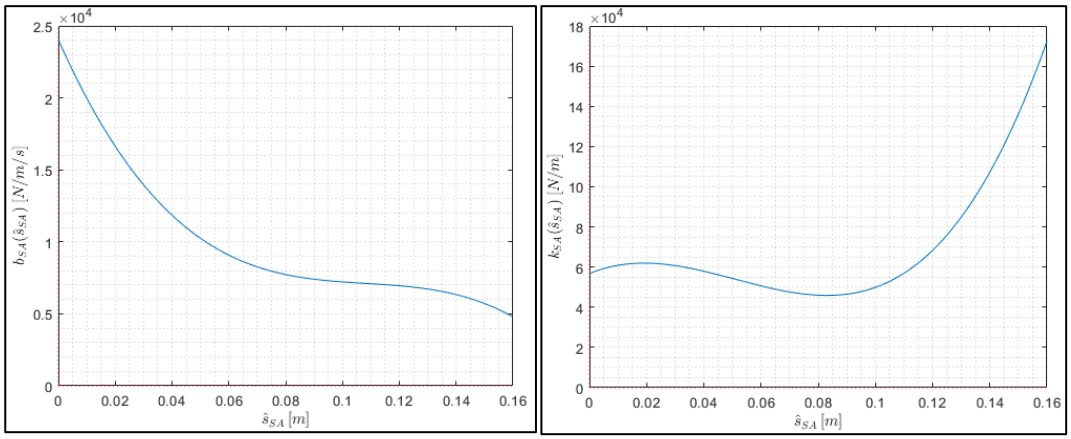

Figure 4.32. 3rd order polynomial fitting of; $b_{SA}(\hat{s}_{SA})$ (left), $k_{SA}(\hat{s}_{SA})$ (right)

Effectivity of the optimization is evaluated with a comparison of a "drop test in Thesis Model with optimum spring/damper characteristics" with respect to a "drop test in Thesis Model with spring/damper characteristics defined in NACA TN 2755". The available test results of NACA TN 2755 are also presented in this comparison, as presented in Figure 4.33.

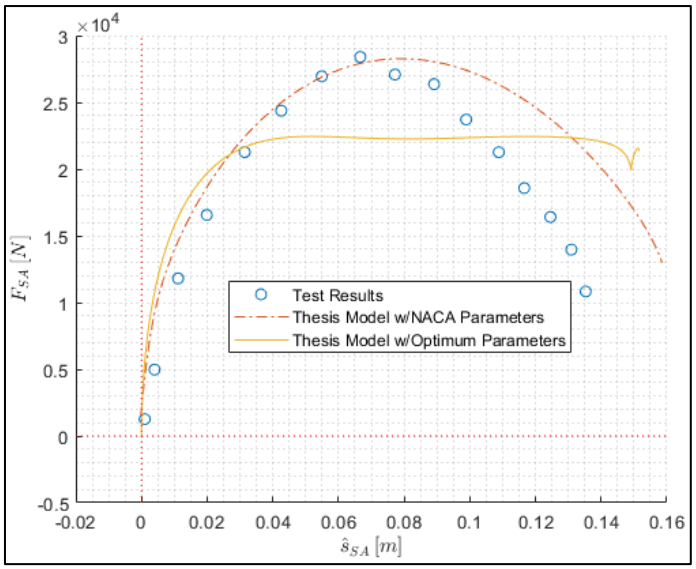

Figure 4.33. Thesis Model drop test simulation with NACA SA characteristics, and optimum SA characteristics for $n = 3$

The efficiency of the shock absorber using the optimum spring/damper characteristics is calculated using equation (4.31) as follows.

$$\eta_{SA,OA_2 n_3} = \%94.05 \tag{4.41}$$

4.3.2.4 Optimization Approach 2: Results for $n = 4$

Fitting a polynomial passing through 5 points results in, $n = 4$, a 4th order polynomial. Optimum damping coefficient, $b_{SA}(\hat{s}_{SA})$, and optimum spring coefficient, $k_{SA}(\hat{s}_{SA})$, obtained with the 4th order polynomial fitting are presented in Figure 4.34

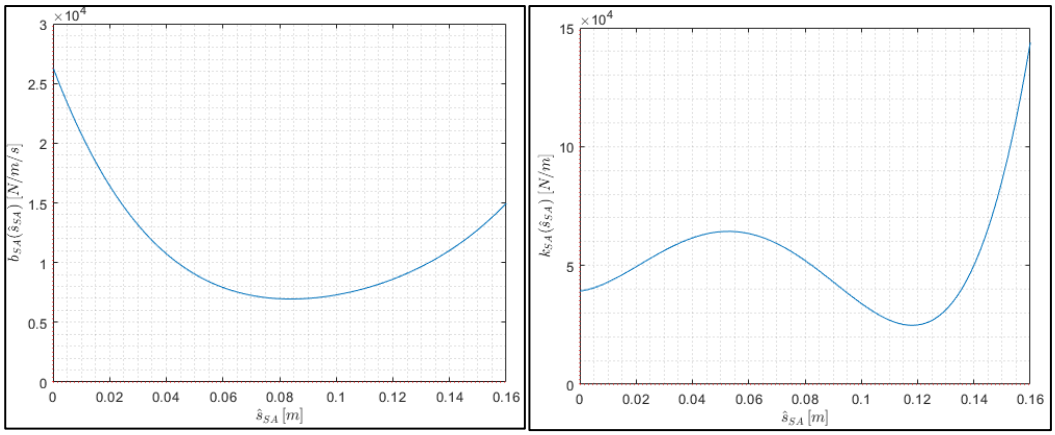

Figure 4.34. 4th order polynomial fitting of; $b_{SA}(\hat{s}_{SA})$ (left), $k_{SA}(\hat{s}_{SA})$ (right)

Effectivity of the optimization is evaluated with a comparison of a "drop test in Thesis Model with optimum spring/damper characteristics" with respect to a "drop test in Thesis Model with spring/damper characteristics defined in NACA TN 2755". The available test results of NACA TN 2755 are also presented in this comparison, as presented in Figure 4.35.

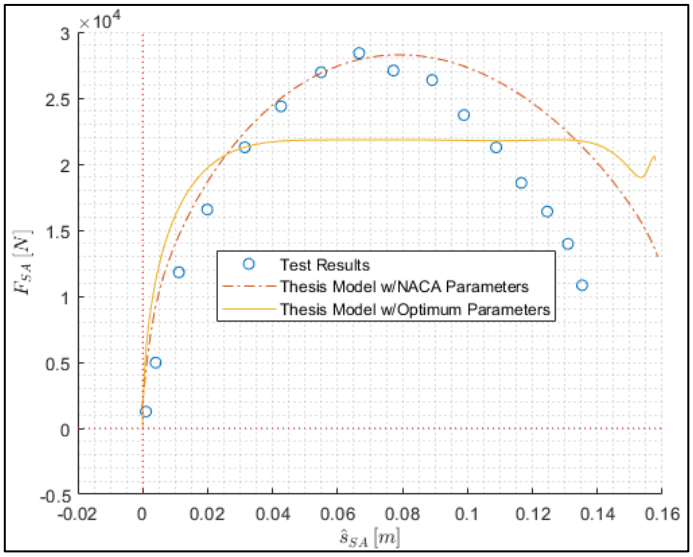

Figure 4.35. Thesis Model drop test simulation with NACA SA characteristics, and optimum SA characteristics for $n = 4$

The efficiency of the shock absorber using the optimum spring/damper characteristics is calculated using equation (4.31) as follows.

$$\eta_{SA,OA_2 n_4} = \%94.45 \tag{4.42}$$

4.3.3 Comparison of Optimization Approches

Two different optimization approaches are described in Sections 4.3.1 and 4.3.2. The same objective is aimed at both approaches. Both approaches are performed under the same optimization constraints.

The objective function, η_{SA}, i.e., efficiency, is evaluated based on $\hat{s}_{SA}$ as defined below.

$$\eta_{SA} = \frac{\int_0^{\hat{s}_{SA,max}} F_{SA} d\hat{s}_{SA}}{\hat{s}_{SA,max} F_{SA,max}} \tag{4.31}$$

The results of two optimization approaches are listed in Table 4.8.

Table 4.8. Optimization Approach comparison

Approach	*Objective Function* $[\eta_{SA}]$	*Increase w.r.t.* $\eta_{SA,NACA}(\%78.26)$
OA1, $n = 1$	%86.9	%11.04
OA1, $n = 2$	%90.44	%15.56
OA1, $n = 3$	%90.37	%15.47
OA2, $n = 1$	%86.33	%10.31
OA2, $n = 2$	%91.82	%17.33
OA2, $n = 3$	%94.05	%20.18
OA2, $n = 4$	%94.45	%20.69

As seen in Table 4.8, OA 2 is better than OA 1 in terms of giving a better solution for the objective. In OA 1, there is not any further increase in the efficiency after $n = 2$, where the increase for the OA 2 stop at $n = 3$. In general one may expect the efficiency to go %100 if the order of the polynomial goes infinity. However, this is not applicable to the definition of this problem; because to achieve a %100

efficiency, the F_{SA} is required to be equal to $F_{SA,max}$ for $t > 0$. Thus, it means F_{SA} is defined as step result in time domain, and this requires b_{SA} or k_{SA} to be defined as step functions (or infinity at $t = 0$). Furthermore, it does not necessarily mean for the efficiency to be increasing with the increasing order of the polynomial. Even with the use of an active damping system, the efficiency of the shock absorber was increased to $\%94.5$ [20]. Thus, it is not expected from a passive design to have better efficiency than an active design.

In summary, referring to Table 4.8, spring/damper characteristics for Optimization Approach 2 for $n = 4$ is found as the optimum solution to the problem.

CHAPTER 5

APPLICATION OF MFG ON LANDING GEAR SHOCK ABSORBER

The use of MFG on a landing gear shock absorber is investigated in this chapter. The design of MFGS and MFGD for a given condition was previously described in Section 3. Separately, an optimization is performed on existing landing gear design inputs to obtain the optimum spring and damper characteristics. Thus, MFGs will be designed to act as a non-linear spring and a non-linear damper with the optimum characteristics.

The application of MFG on landing gear is evaluated from two aspects: theoretical achievability of the solution and feasibility of the MFG installation on a landing gear.

5.1 Design Concept

MFG is a mechanism that consists of planar motion. The landing gear shock absorber also performs planar displacement. The initial idea of the application of MFG on a landing gear shock absorber is realized by allowing the MFG's displacement in z-direction inside the shock absorber, in which the shock absorber also performs displacement in the same direction. The initial concept is depicted in Figure 5.1.

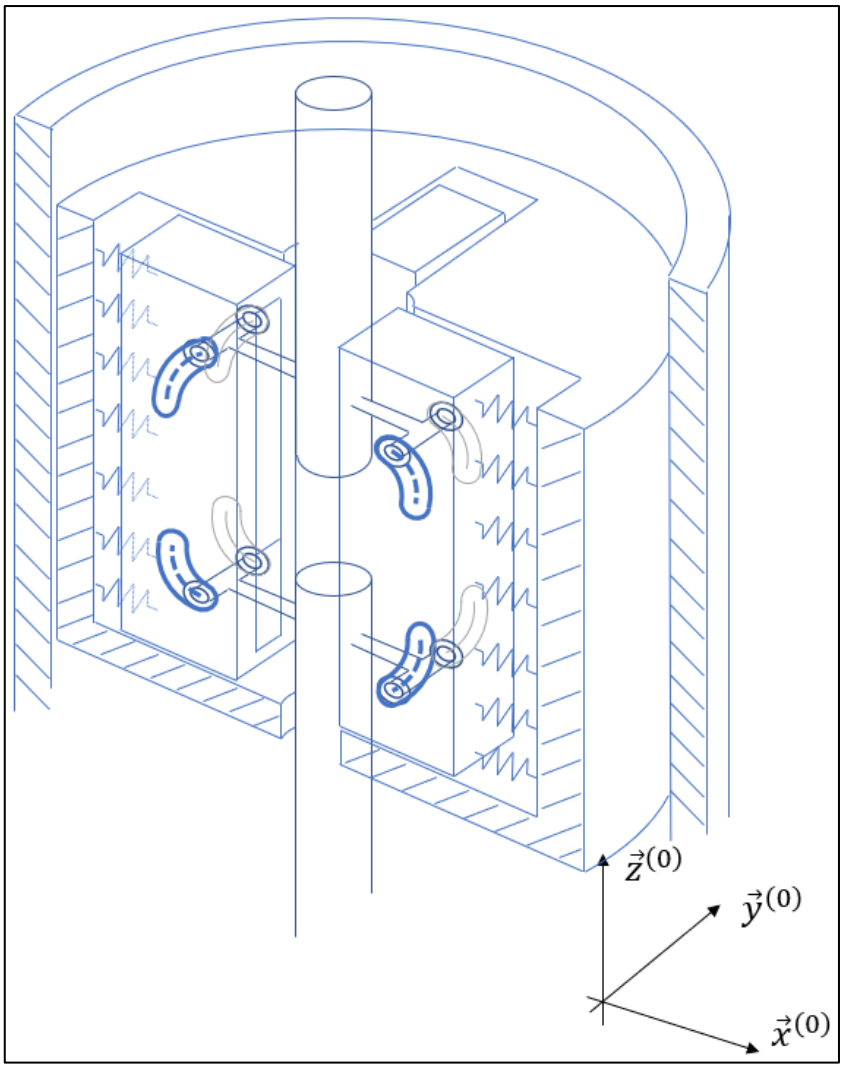

Figure 5.1. Sketch of the installation of MFG on landing gear

A landing gear shock absorber has a cylindrical design for its easy production, low friction, and better hydraulic fluid sealing properties. Thus, the initial application concept causes inefficient use of a cross-sectional area of the shock absorber. To use the circular cross-section of the shock absorber more efficiently, a new concept of MFG installation is introduced, in which there are two MFGs using the same input links. The application of two MFGs at the same time is illustrated in Figure 5.2.

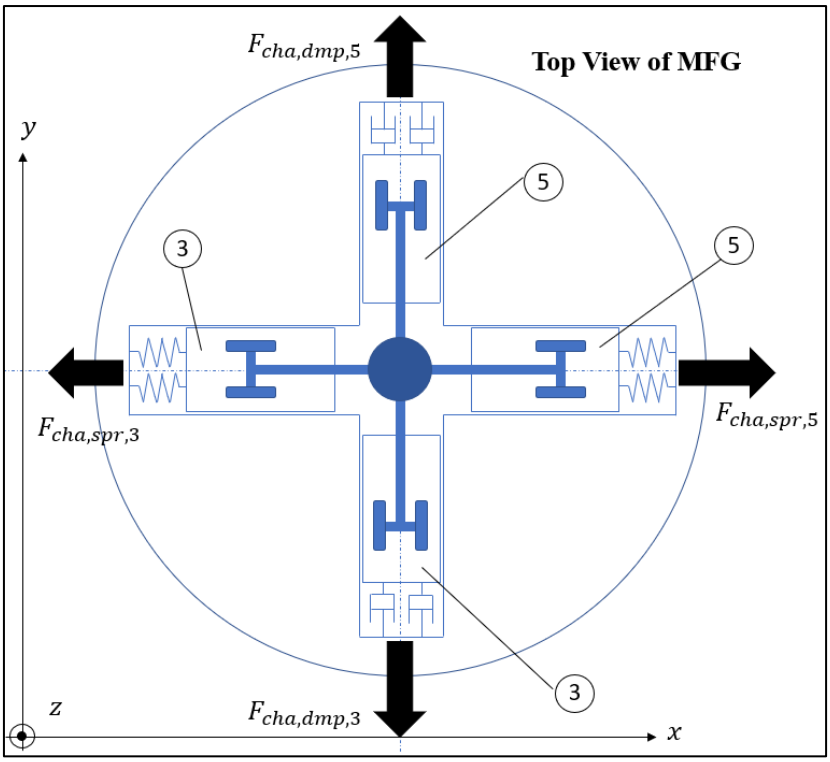

Figure 5.2. Installation of MFGS and MFGD at the same MFG

This application has the benefits of reducing the load on an MFG and using the MFGs for different purposes at the same time, such as one is MFGS, and the other is MFGD.

With the design concepts introduced above, different options are evaluated in the following sections.

An MFG system with optimum spring and damper characteristics determined in Section 4.3 is designed in this section.

Let the optimum spring and damper characteristics be presented here as follows.

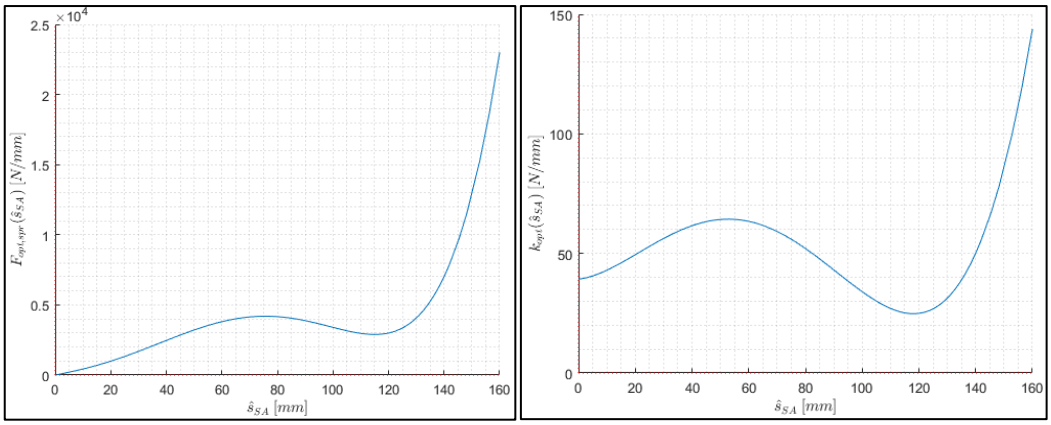

Figure 5.3. Optimum spring force and spring coefficient

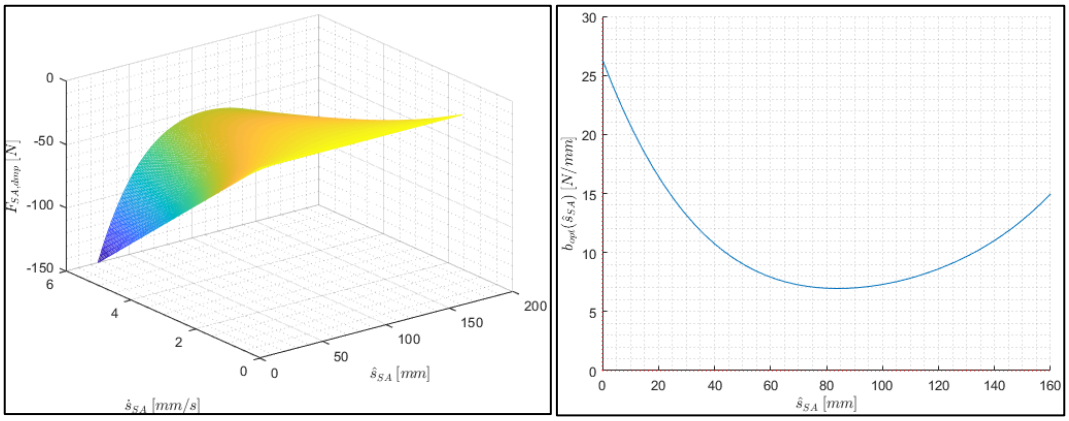

Figure 5.4. Optimum damper force and damping coefficient

The design of the MFGs will be handled separately for spring and damper.

5.2 Design of MFGS

The optimum spring characteristic of the shock absorber (see Figure 5.3) is defined as follows.

$$k_{SA}[\hat{s}_{SA}] = 2.43 \times 10^{-6}\hat{s}_{SA}^4 - 4.45 \times 10^{-4}\hat{s}_{SA}^3 \ldots$$

$$+2.83 \times 10^{-2}\hat{s}_{SA}^2 + 0.146\hat{s}_{SA} + 39.21\ N/mm \qquad (5.1)$$

$$F_{SA,spr} = k_{SA}[\hat{s}_{SA}]\hat{s}_{SA} \qquad (5.2)$$

Firstly, the spring for the chamber of this MFGS shall be selected. Requirements of this chamber spring shall be specified, so a correct selection can be performed. The spring inside the chamber shall store the same amount of potential energy that will be stored at the MFG, which means the potential energy stored at the SA spring. This can be determined via the energy graph of the shock absorber spring, which obtained via

$$E_{SA,spr}[\hat{s}_{SA}] = \int_0^{\hat{s}_{SA}} F_{SA,spr}[\hat{s}_{SA}] d\hat{s}_{SA} \tag{5.3}$$

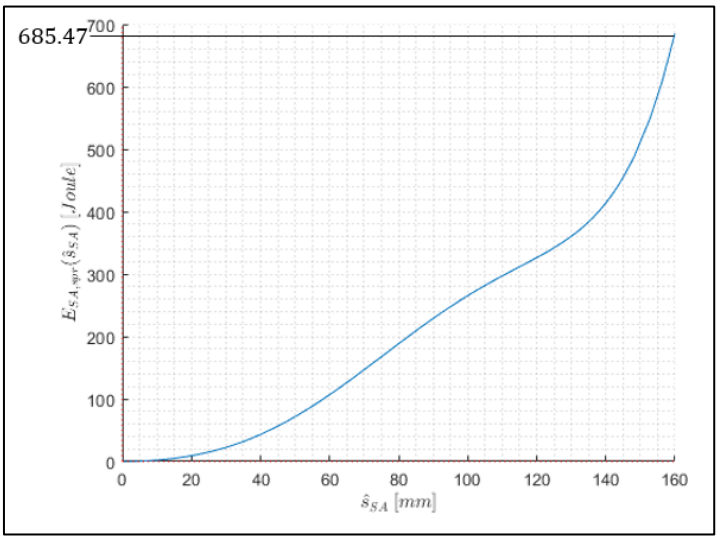

Figure 5.5. Energy stored at shock absorber spring

Evaluating equation (5.3) for $\hat{s}_{SA} = 160mm$, one will find that the energy stored at the SA spring is equal to $E_{SA,spr}[160] = 685.47\ Joule$ as presented in Figure 5.5.

Since the MFG consists of two chambers that store energy, the energy needs to be stored in one chamber is defined as follows.

$$E_{MFG,spr,cha} = \frac{E_{SA,spr}[\hat{s}_{SA}]}{2} = \frac{E_{MFG,spr}[s_{MFG}]}{2} \tag{5.4}$$

Thus, the following condition shall be satisfied for the selected spring of compression type as

$$E_{MFG,spr,cha}[l_{spr,min}] = \frac{1}{2} k_{cha} (l_{spr,min} - l_{f,spr})^2 > 342.75\ Joule \tag{5.5}$$

and for a selected spring of tension type as

$$E_{MFG,spr,cha}[l_{spr,max}] = \frac{1}{2}k_{cha}(l_{spr,max} - l_{f,spr})^2 > 342.75\,Joule \quad (5.6)$$

where

$l_{spr,min}$: Minimum length of a compression spring (catalog value)

$l_{spr,max}$: Maximum length of a tension spring (catalog value)

$l_{f,spr}$: Free length of the selected spring (catalog value)

k_{cha} : Spring constant of the chamber

Here, it should be noted that, k_{cha} may not be the spring constant of one spring. The chamber may consist set of springs that work in parallel. Which yields

$$k_{cha} = n_{spr}k_{spr} \quad (5.7)$$

where

n_{spr} : Quantity of springs in a chamber

k_{spr} : Spring constant

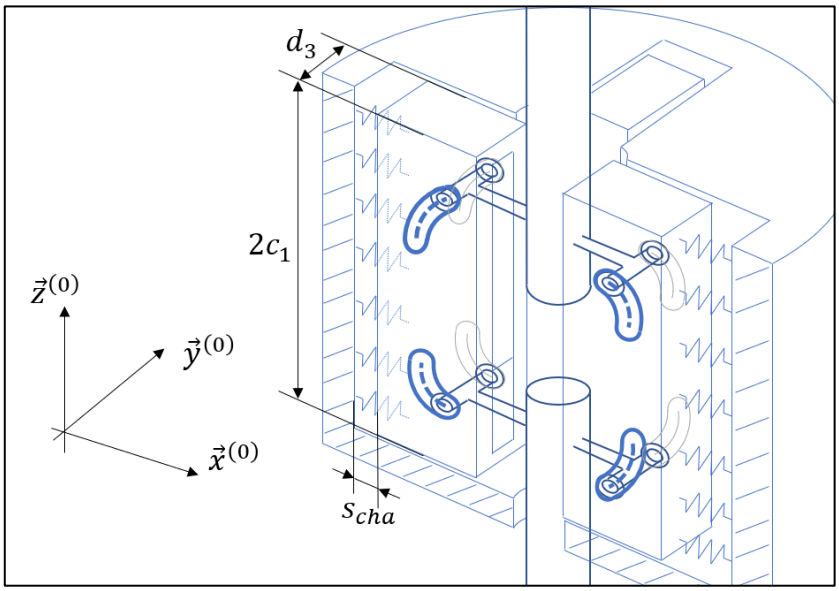

Figure 5.6. Dimensions of a chamber volume

As presented in Figure 5.6, a set of springs can be installed inside the chamber. The installation of these spring in parallel is performed such that the maximum number of springs are installed inside the chamber as presented in Figure 5.7.

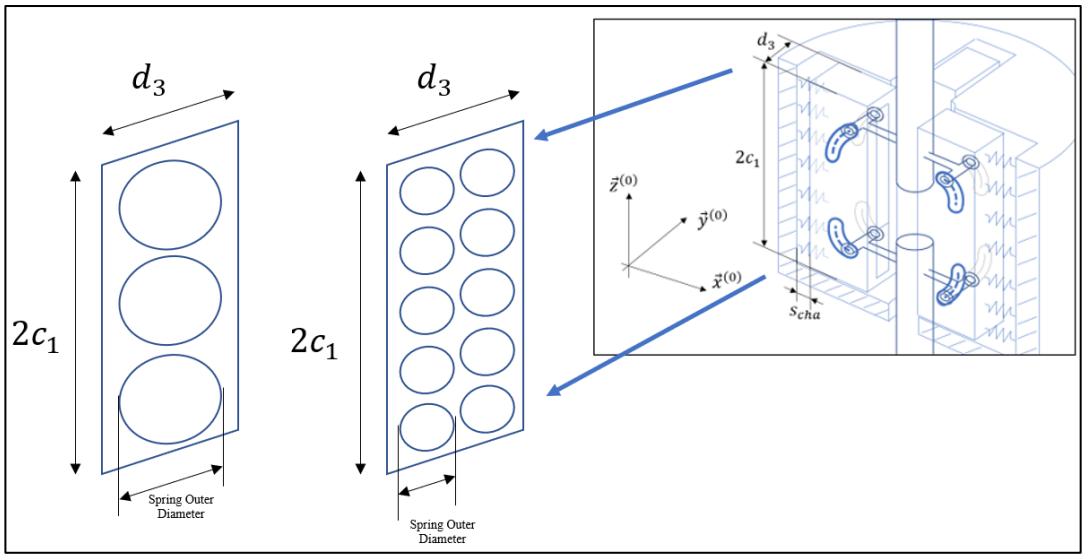

Figure 5.7. Example of determination number of springs inside the chamber

The number of springs is taken into account during the selection of the spring w.r.t. equation (5.5) or equation (5.6). For the application of the optimum SA design, some of the dimensions for the MFGs, which have been identified in Figure 5.6 and Figure 3.5, are determined to start the design. According to the satisfaction of the design, the dimensions are adjusted.

$$c_1 = 200\ mm \tag{5.8}$$

$$d_3 = 50\ mm \tag{5.9}$$

The compression type of spring is thought to be the initial preference due to the small installation envelope requirement. A spring may be designed for given requirements; however, springs in the market, which have been already produced, are searched from the internet [31]. The stock numbers of these springs can be found in Appendix C. The candidate springs and their properties are presented in Table 5.1.

Table 5.1. Candidate spring properties

Spring ID	*Outer Diameter [mm]*	$l_{f,spr}$ *[mm]*	k_{spr} *[N/mm]*	*Max Deflection [mm]*	n_{spr}	k_{cha} *[N/mm]*	$E_{spr}[l_{spr,min}]$ *[Joule]*
CS1	48.412	65.786	426.83	7.872	8	3414.64	105.8
CS2	31.344	50.8	373.13	7.059	12	4477.56	111.56
CS3	41.275	41.402	526.61	6.403	9	4739.49	97.16
CS4	24.994	62.738	414.21	6.078	32	13254.7	244.8
CS5	37.287	55.626	1385.57	4.28	10	13855.7	126.91
CS6	33.325	28.702	547	3.693	12	6564	44.76
CS7	45.237	36.576	338.22	4.143	8	2705.76	23.22

Considering the energy storage capabilities, CS4 stands out as a potential candidate compared to the other springs, but it still does not satisfy the criterion given in equation (5.5). Thus, an adjustment on the dimensions is required. Previously given in equation (5.8) and equation (5.9), c_1 and d_3 dimensions are defined as follows.

$$c_1 = 200\ mm \tag{5.10}$$

$$d_3 = 75\ mm \tag{5.11}$$

Thus, equation (5.5) can be calculated for CS4 as follows

$$E_{spr,CS4}[l_{spr,min}] = \frac{1}{2}(48 \times 414.2)(56.66 - 62.738)^2 = 367.2\ Joule \tag{5.12}$$

Let an MFGS be designed using the spring selected above. It shall be noted that the shock absorber and the MFG displacements shall be related to each other correctly to design against the correct requirements. The total displacement of the shock absorber is defined as $160\ mm$. Thus the total displacement between Link 2 and Link 4 of the MFGs shall be $160\ mm$ as

$$s_{2/4,max} - 2d_{cle} = 160\ mm \tag{5.13}$$

which yields

$$s_{MFG,max} - d_{cle} = s_{2/4,max}/2 - d_{cle} = 80\ mm \tag{5.14}$$

If one evaluates the dimensions of the MFGS, one can observe that the total displacement of Link 2 and Link 4 would be small with respect to c_1 as presented in Figure 5.8.

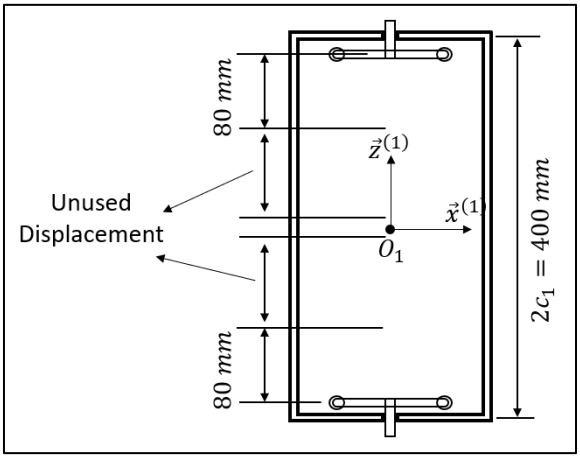

Figure 5.8. Evaluation of total displacement of MFG w.r.t. SA

This is mainly due to requirement of storing high amount of energy inside small installation envelope.

First, the spring coefficient and force defined in equation (5.1) and equation (5.2) shall be re-defined in s_{MFG} domain, instead of $\hat{s}_{SA}$, to allow a design inside the allowable region. If one selects the clearance parameters as

$$d_{cle} = 10\ mm \tag{5.15}$$

then

$$s_{MFG,min} \geq d_{cle} = 10\ mm \tag{5.16}$$

Thus, a change needs to be performed on $\hat{s}_{SA}$ to design the MFG. The following change will satisfy the requirement to stay inside the allowable region.

$$\hat{s}_{SA} = 160 - \left(s_{2/4} - 2d_{cle}\right) = 160 - (2s_{MFG} - 2d_{cle}) \tag{5.17}$$

which yields

$$\hat{s}_{SA} = 180 - 2s_{MFG} \tag{5.18}$$

If the equation (5.18) is plugged in equation (5.2), one obtains the spring force as

$$F_{MFG,spr}[s_{MFG}] = k_{MFG}[s_{MFG}](s_{MFG} - 90) \tag{5.19}$$

where

$$k_{MFG}[s_{MFG}] = -1.94 \times 10^{-5}{s_{MFG}}^4 + 4.81 \times 10^{-3}{s_{MFG}}^3 \ldots$$
$$-0.412{s_{MFG}}^2 + 13.952s_{MFG} - 174.856\ N/mm \tag{5.20}$$

The spring force of the MFGS defined in equations (5.19) and (5.20) is presented in Figure 5.9.

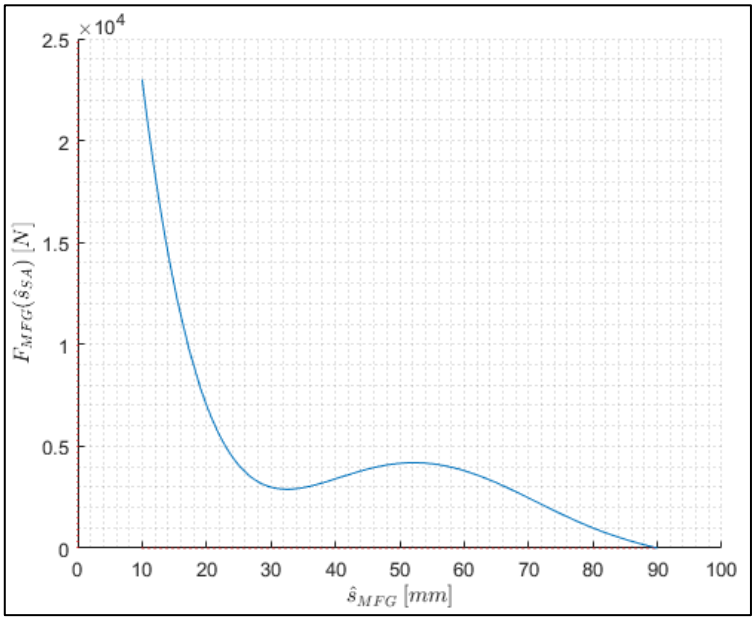

Figure 5.9. MFGS force of optimum shock absorber spring

Furthermore, one needs to decide on the other dimensions of the MFGS. Knowing the spring's maximum deflection property, the width of Link 3 (b_3) can be defined as presented in Figure 5.10.

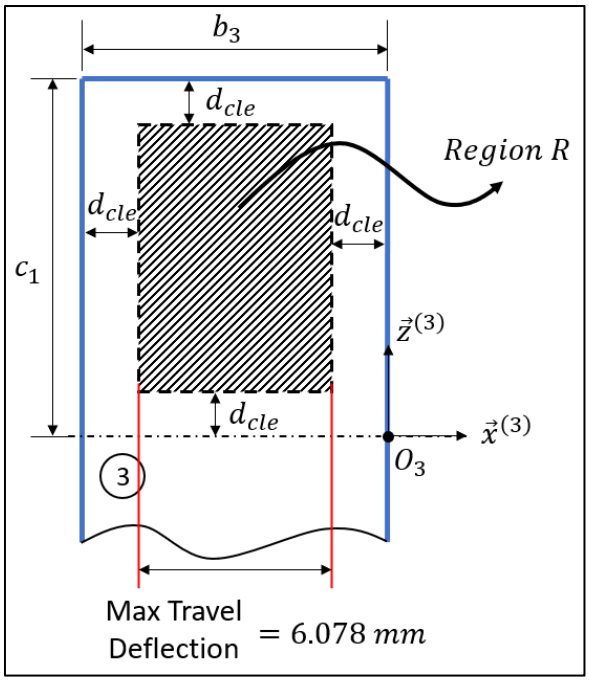

Figure 5.10. Determination of required b_3

Taking the total travel deflection into consideration, since the clearance value is selected as $d_{cle} = 10\ mm$, one obtains b_3 as

$$b_3 = 26.078\ mm \tag{5.21}$$

The free length of the spring is known from Table 5.1 as

$$l_{f,spr} = 62.738\ mm \tag{5.22}$$

If minimum space allocation is desired from the MFGS, b_1 can be determined in relation with $l_{f,spr}$ as long as the selections of integral limits (see Page 40) are performed to benefit the most out of the allowable region. Thus, referring to Page 40 and Figure 5.11 ($s_{cha} = l_{f,spr}$), b_1 may be defined as

$$b_1 = l_{f,spr} + b_3 - d_{cle} + b_2 \tag{5.23}$$

or

$$b_1 = l_{f,spr} + d_{cle} + b_2 \tag{5.24}$$

Note that any selection of b_1 in accordance with equation (5.23) or equation (5.24) restricts the selection of integral limits for equation (3.55).

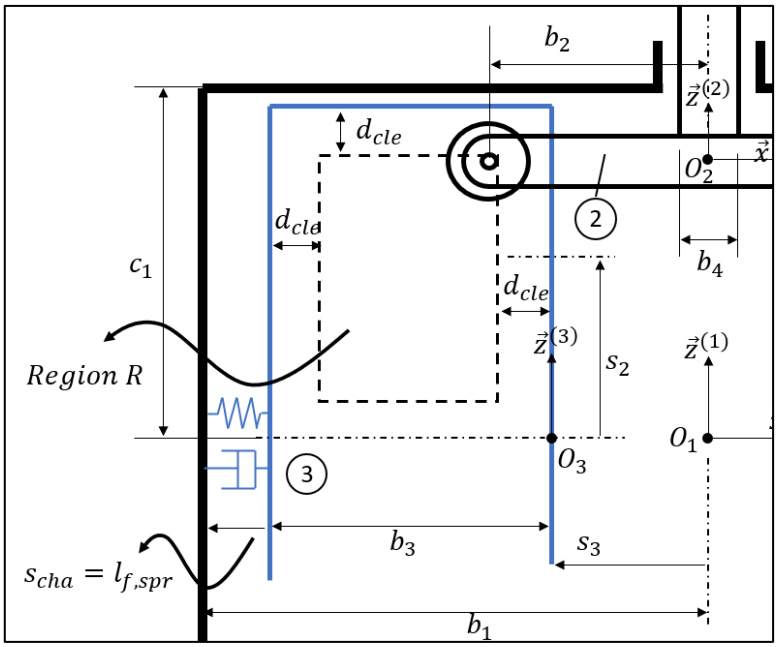

Figure 5.11. Determination b_1 in relation with $l_{f,spr}$

Referring to equation (5.23), b_1 is defined as

$$b_1 = 62.738 + 26.078 - 10 + b_2 = 78.816 + b_2 \quad (5.25)$$

Lastly, the length of the arm of Link 2 should be determined. If one takes the movement of Link 3 into account, referring to Figure 5.11 and Figure 5.10, one can define b_2 as follows

$$b_2 = b_3 - d_{cle} + b_4/2 \quad (5.26)$$

where

b_4 : Diameter of Link 2

Determination of b_4 diameter requires further strength analysis/calculation and material information; however, this is out of the scope of this thesis study. Thus, b_4 is assumed as

$$b_4 = 10\ mm \quad (5.27)$$

Referring to equation (5.26) and equation (5.27), one can define b_2 and effectively b_1 (see equation (5.25)) as

$$b_2 = 26.078 - 10 + 10/2 = 21.078\, mm \tag{5.28}$$

$$b_1 = 78.816 + 21.078 = 99.894\, mm \tag{5.29}$$

With respect to dimensions given in equations (5.10), (5.15), (5.21), (5.28) and (5.29), the MFGS is plotted in MATLAB environment as assembled. The layout of the MFGS is presented in Figure 5.12.

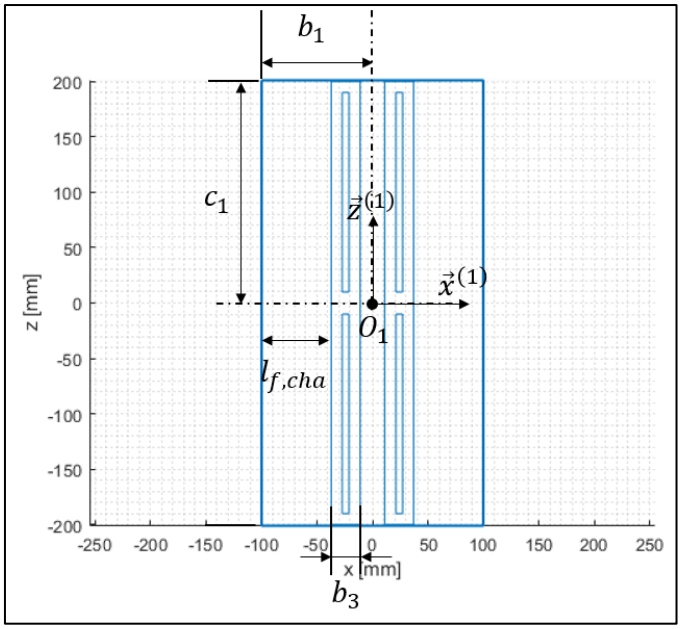

Figure 5.12. MFGS installation layout

Given the dimensions, the allowable region is defined as presented in Figure 5.13.

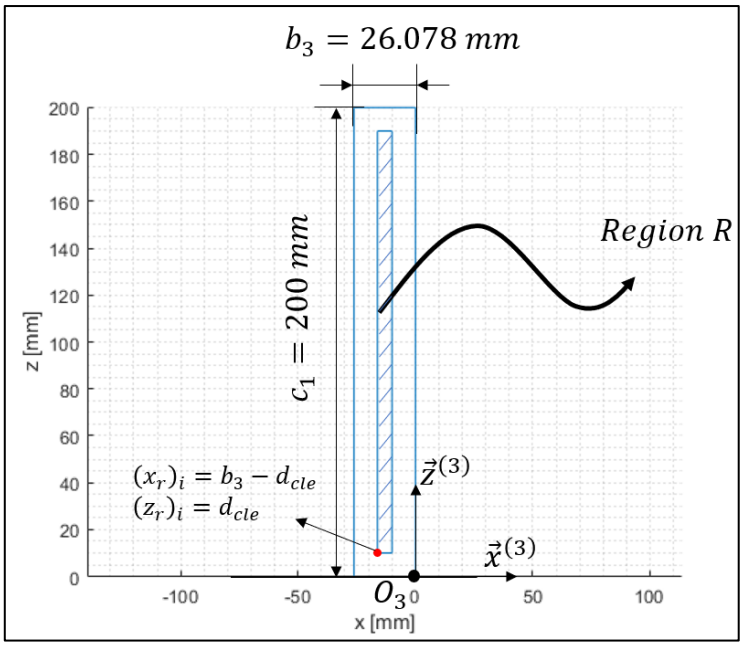

Figure 5.13. Allowable region R on Link 3

Thus, given the dimensions and spring chamber properties referring to the solution derived in Section 3.2.1, the solution is found for this MFGS design. As previously described while using equation (5.23) for the dimensions of the MFGS, the point that slot shape centerline passes through is selected as described on Page 40. As a reminder, the selection of the point, as presented in Figure 5.13, yields

$$(x_r)_i = 16.078\ mm \tag{5.30}$$

$$(z_r)_i = 10\ mm \tag{5.31}$$

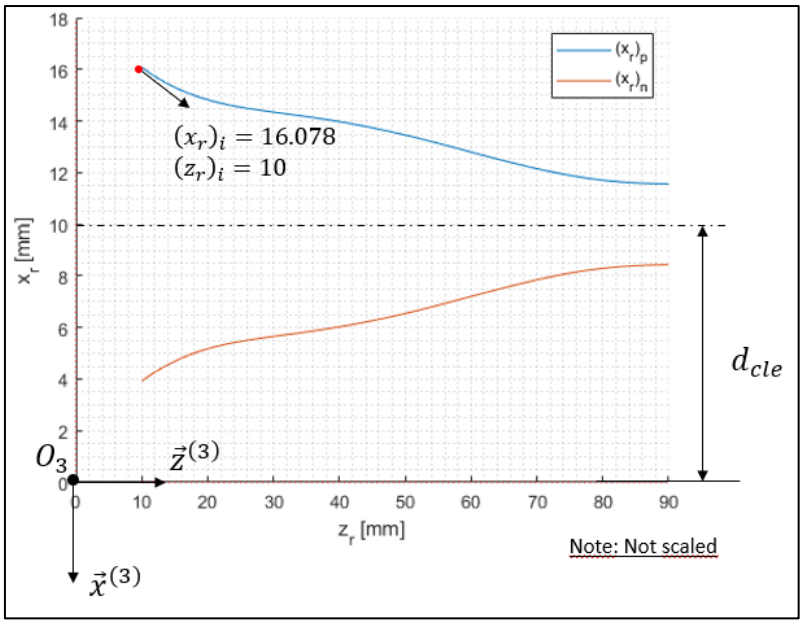

Figure 5.14. Solutions for $(x_r)_p$ and $(x_r)_n$ (for $(x_r)_i = 16.078$, $(z_r)_i = 10$)

As presented in Figure 5.14, $(x_r)_p$ is the solution for this problem. Thus, taking $(x_r)_p$ as the solution, the position analysis is performed as presented in Figure 5.15.

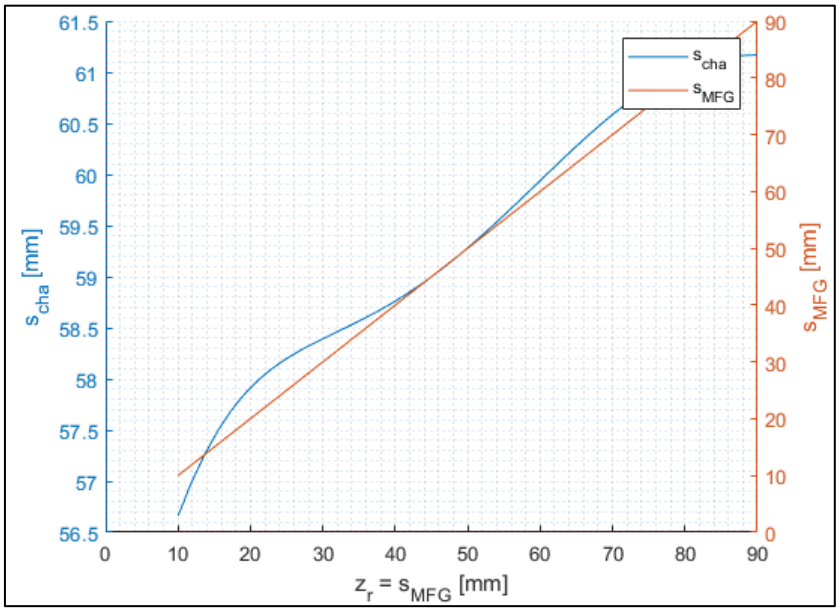

Figure 5.15. Position analysis of MFGS design

$\dot{s}_{cha}$ and $\dot{s}_{MFG}$ evaluated with respect to z_r with taking $\dot{s}_{MFG}$ as unit velocity ($\dot{s}_{MFG} = 1\ mm/s$) in Figure 5.16.

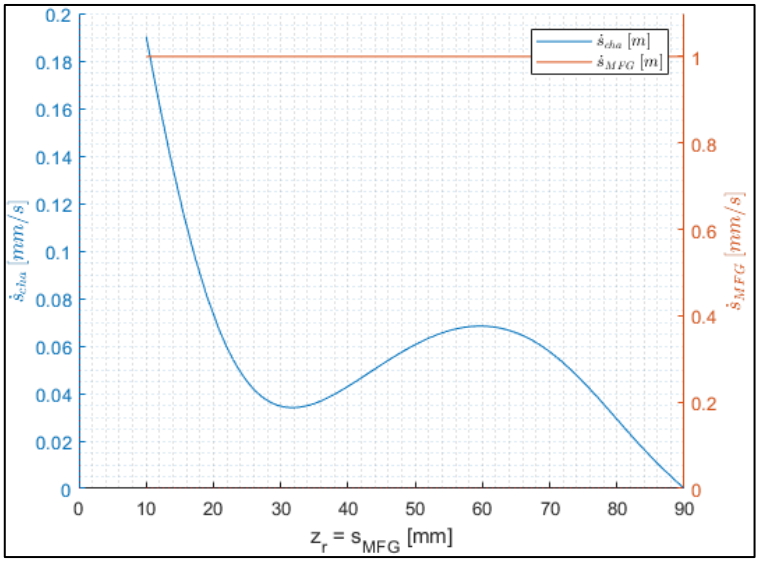

Figure 5.16. Velocity analysis of MFGS design

Finally, $F_{MFG,spr}$ and $-F_{cha,spr}$ are presented in Figure 5.17 with respect to s_{MFG}. $\dot{s}_{cha}$ was also presented in Figure 5.16 with respect to s_{MFG} (note that $\dot{s}_{MFG} = 1\ mm/s$).

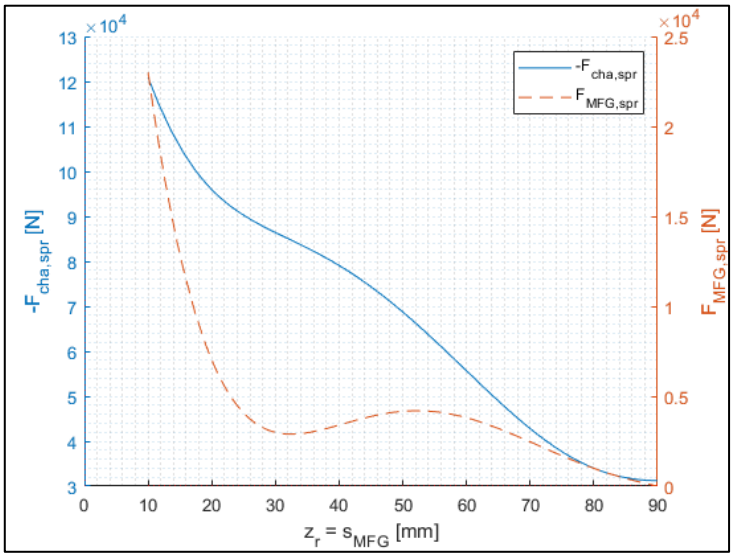

Figure 5.17. $F_{MFG,spr}$ and $-F_{cha,spr}$ w.r.t. s_{MFG}

Referring to equation (3.48), if "$-F_{cha,spr}$ in Figure 5.17" is multiplied with "$\dot{s}_{cha}$ in Figure 5.16", "$F_{MFG,spr}$ in Figure 5.17" will be obtained (remember that $\dot{s}_{MFG} = 1\ mm/s$).

5.3 Design of MFGD

The optimum damper characteristic of the shock absorber (see Figure 5.3) is defined as follows.

$$b_{SA}[\hat{s}_{SA}] = 9.35 \times 10^{-8}\hat{s}_{SA}^4 - 3.92 \times 10^{-5}\hat{s}_{SA}^3 \ldots$$

$$+7.35 \times 10^{-3}\hat{s}_{SA}^2 - 0.627\hat{s}_{SA} + 26.34\ N/mm/s \quad (5.32)$$

$$F_{SA,dmp} = -b_{SA}[\hat{s}_{SA}]\dot{s}_{SA} \quad (5.33)$$

For the design of MFGD, some of the dimensions determined in Section 5.2 are used. The dimensions that were determined previously and which will be used in MFGD design are defined as follows.

$$c_1 = 200\ mm \quad (5.34)$$

$$b_1 = 99.894\ mm \quad (5.35)$$

Dampers are not standard elements such as springs. The design of a damper changes according to its application [30]. Thus, the damping coefficient inside the chamber will be determined as the outcome of the MFGD design. So, the remaining dimensions of the MFGD are "carefully" determined by own choice to have a sensible design, in which the links do not clash with each other.

Firstly, the clearance of the allowable region is selected the same with MFGS as

$$d_{cle} = 10\ mm \quad (5.36)$$

Similarly to MFGS, the damping constant and damper force shall be re-defined in s_{MFG} domain, instead of $\hat{s}_{SA}$, to allow a design inside the allowable region. Thus, referring to equation (3.32), the following condition shall be satisfied.

$$s_{MFG,min} \geq d_{cle} = 10\ mm \tag{5.37}$$

Thus, a change needs to be performed on $\hat{s}_{SA}$ to design the MFG. The following change will satisfy the requirement to stay inside the allowable region.

$$\hat{s}_{SA} = 160 - \left(s_{2/4} - 2d_{cle}\right) = 160 - (2s_{MFG} - 2d_{cle}) \tag{5.38}$$

which yields

$$\hat{s}_{SA} = 180 - 2s_{MFG} \tag{5.39}$$

Since the damping force is function of velocity, the velocity of shock absorber damper, $\dot{s}_{SA}$, must be related to the velocity of MFGD input link, $\dot{s}_{MFG}$. This relationship is defined as follows.

$$\dot{s}_{SA} = 2\dot{s}_{MFG} \tag{5.40}$$

If equations (5.39) and (5.40) are plugged in equation (5.33), one obtains the damping force as

$$F_{MFG,dmp} = -b_{MFG}[s_{MFG}]\dot{s}_{MFG} \tag{5.41}$$

where

$$b_{MFG}[s_{MFG}] = 2.99 \times 10^{-6}{s_{MFG}}^4 - 4.5 \times 10^{-4}{s_{MFG}}^3 \ldots$$

$$+3.5 \times 10^{-2}{s_{MFG}}^2 - 1.568 s_{MFG} + 42.54\ N/(mm/s) \tag{5.42}$$

The spring used in MFGS limits the dimensions of the chamber. Since the damper is not a standard component, the minimum and maximum dimensions of the damper inside the chamber are defined by the author for MFGD design. Yet, the realization of this damper design is out of scope in this thesis study. The minimum and maximum dimensions of the damper are defined as

$$50\ mm \geq s_{cha} \geq 25\ mm \tag{5.43}$$

If minimum space allocation is desired from the MFGD, b_3 can be determined in relation to the total length change of the chamber, as

$$\Delta s_{cha} = 25\ mm \tag{5.44}$$

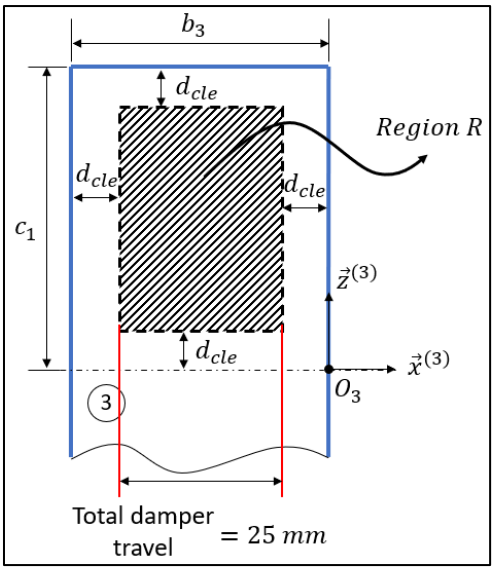

Figure 5.18. Determination of required b_3

Taking the total damper travel into consideration and referring to Figure 5.18, since the clearance value is selected as $d_{cle} = 10\ mm$, one obtains b_3 as

$$b_3 = 45\ mm \tag{5.45}$$

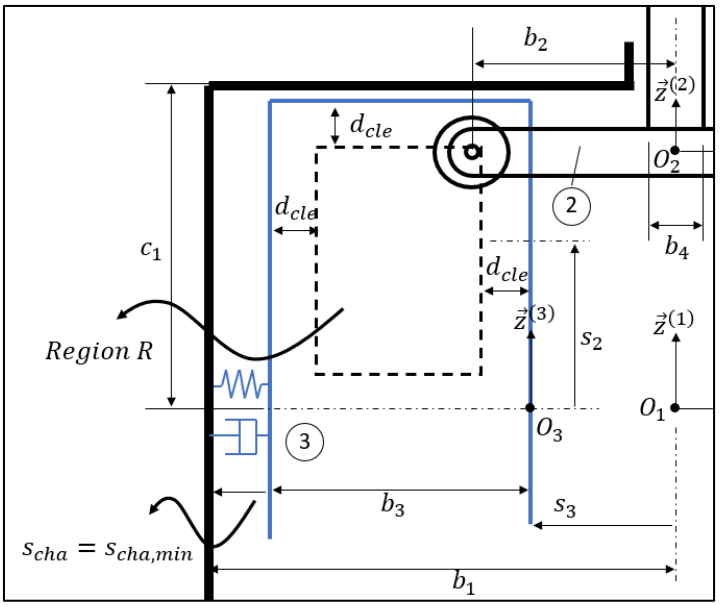

Figure 5.19. Determination b_2 in relation with $s_{cha,min}$ position

Lastly, the length of the arm of Link 2 should be determined. If one takes the movement of Link 3 into account, referring to Figure 5.19 and Figure 5.18, one can define b_2 as follows

$$b_2 = b_3 - d_{cle} + b_4/2 \tag{5.46}$$

where, same as MFGS,

$$b_4 = 10\ mm \tag{5.47}$$

Referring to equation (5.46) and equation (5.47), one can define b_2 as

$$b_2 = 45 - 10 + 10/2 = 40\ mm \tag{5.48}$$

With respect to dimensions given in equations (5.34), (5.35), (5.36), (5.45) and (5.48), the MFGD is plotted in MATLAB environment as assembled. The layout of the MFGD is presented in Figure 5.20.

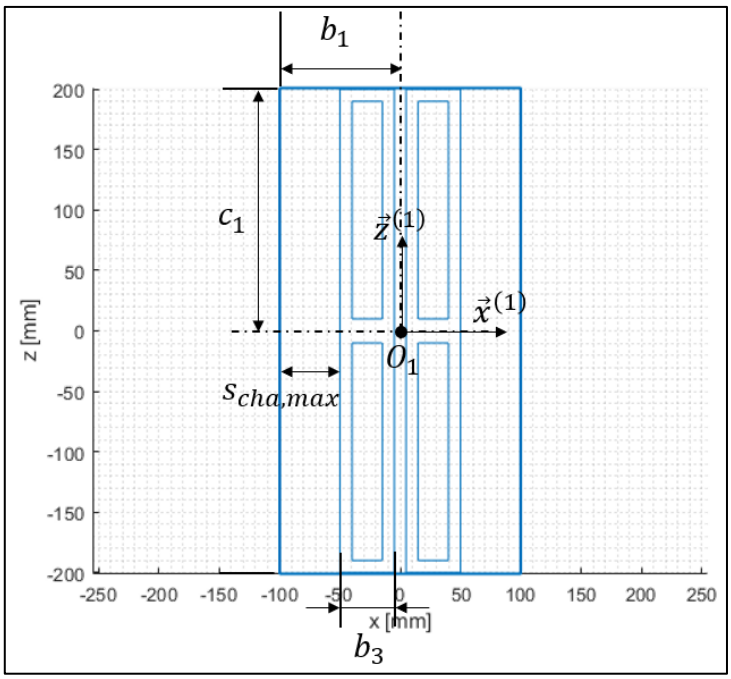

Figure 5.20. MFGD installation layout

Given the dimensions, the allowable region is defined as presented in Figure 5.21.

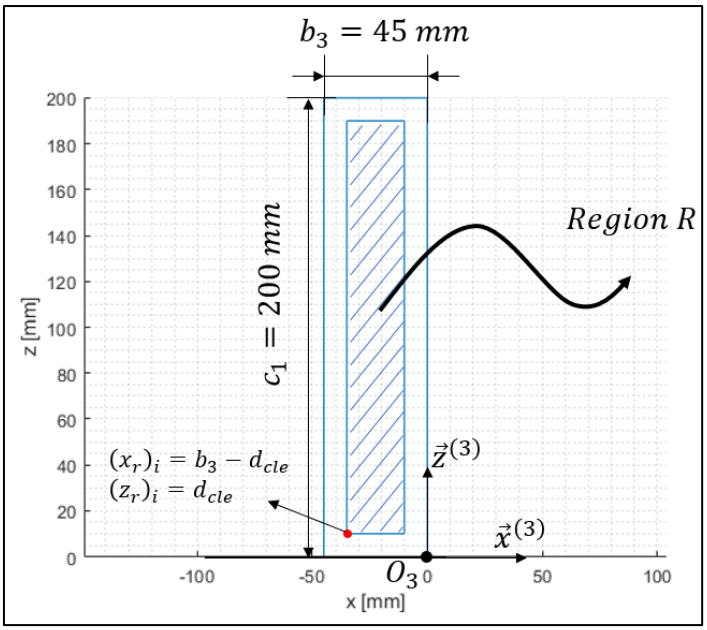

Figure 5.21. Allowable region R on Link 3

The point that slot shape centerline passes through is selected as described on Page 55. As a reminder, the selection of the point, as presented in Figure 5.21, yields

$$(x_r)_i = 35\ mm \tag{5.49}$$

$$(z_r)_i = 10\ mm \tag{5.50}$$

Before starting to design a slot shape, the last necessary parameter is the damping coefficient of the chamber. Since the energy absorption of the chamber damper is a function of not only the position but also the velocity, the damper requirements inside the chamber could not be determined, such as spring. Thus, using the selections in equations (5.49) and (5.50), with trial and error, the damper coefficient inside the chamber is determined as

$$b_{cha} = 108.9\ N/(mm/s) \tag{5.51}$$

The damper coefficient is determined such that all working envelope of the damper, defined in equation (5.43), will be used.

Thus, given the dimensions and damper chamber properties referring to a solution derived in Section 3.3.1, the solution is found for this MFGD design.

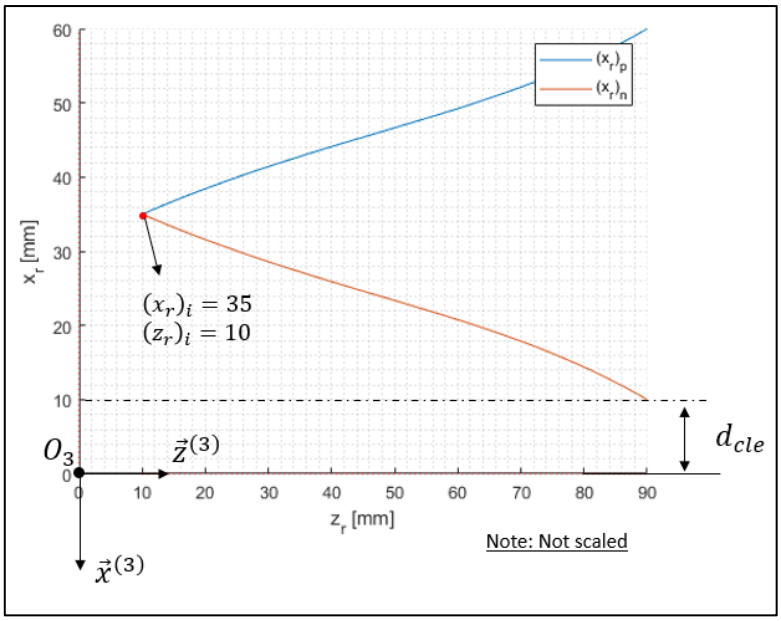

Figure 5.22. Solutions for $(x_r)_p$ and $(x_r)_n$ (for $(x_r)_i = 45$, $(z_r)_i = 10$)

Referring to equation (3.102) and as presented in Figure 5.22, $(x_r)_n$ is the solution for this problem. Thus, taking $(x_r)_n$ as the solution, the position analysis is performed as presented in Figure 5.23.

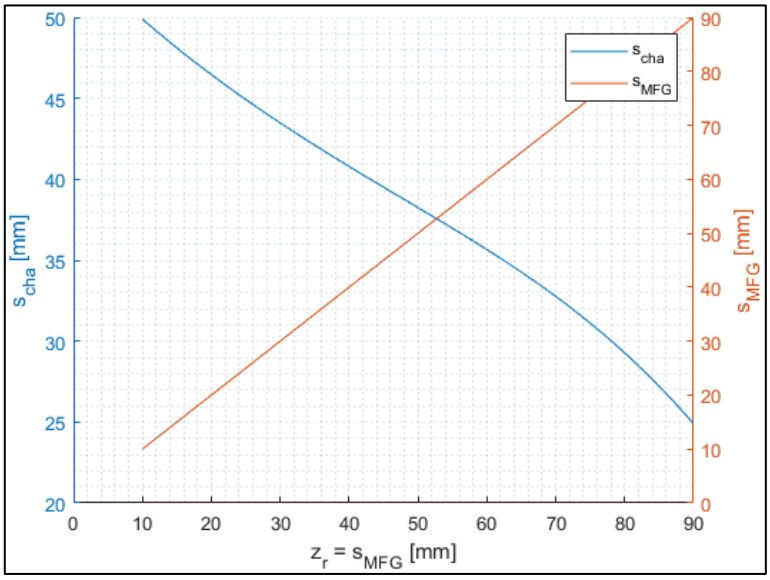

Figure 5.23. Position analysis of MFGD design

$\dot{s}_{cha}$ and $\dot{s}_{MFG}$ are evaluated with respect to z_r with taking $\dot{s}_{MFG}$ as unit velocity ($\dot{s}_{MFG} = 1\ mm/s$) in Figure 5.24.

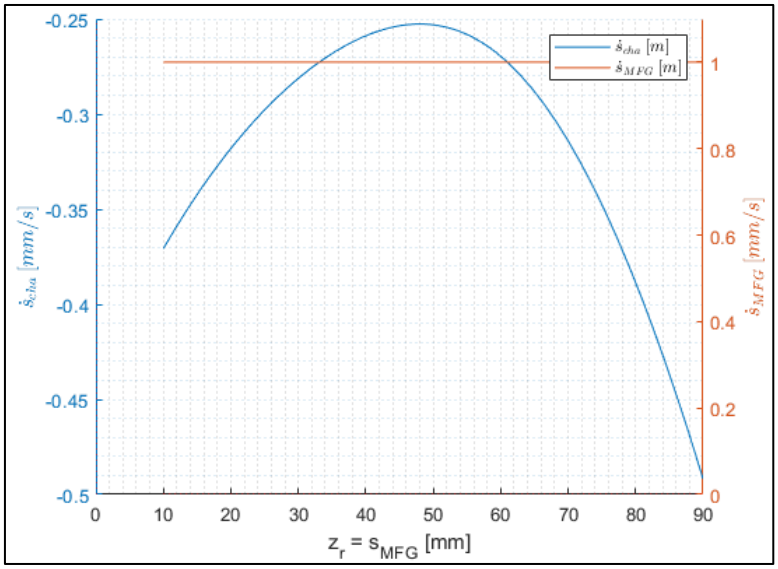

Figure 5.24. Velocity analysis of MFGD design

Finally, $F_{MFG,dmp}$ and $-F_{cha,dmp}$ are presented in Figure 5.25 with respect to s_{MFG}. $\dot{s}_{cha}$ was also presented in Figure 5.24 with respect to s_{MFG} (note that $\dot{s}_{MFG} = 1\ mm/s$).

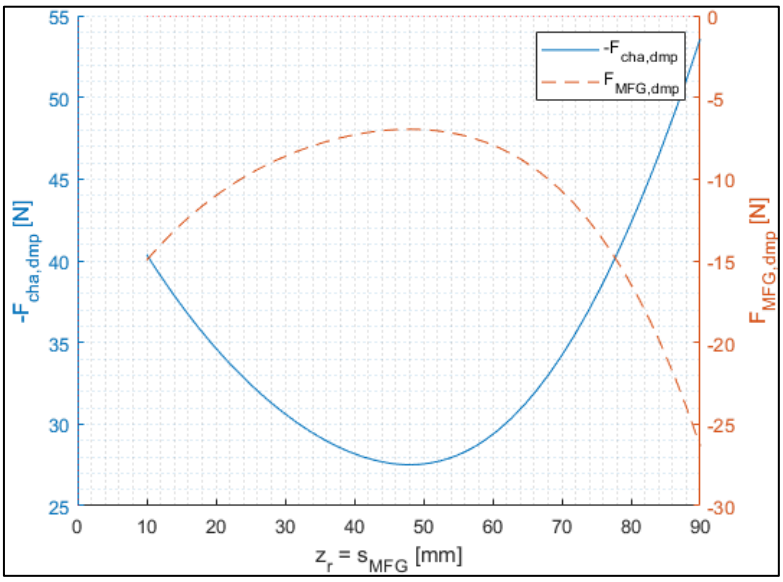

Figure 5.25. $F_{MFG,dmp}$ and $-F_{cha,dmp}$ w.r.t. s_{MFG}

Referring to equation (3.86), if "$-F_{cha,dmp}$ in Figure 5.25" is multiplied with "$\dot{s}_{cha}$ in Figure 5.24", "$F_{MFG,spr}$ in Figure 5.25" will be obtained (remember that $\dot{s}_{MFG} = 1\ mm/s$).

5.4 Comparison of Design with Previous Shock Absorber Design

The concept of using MFG for a shock absorber design is explained initially at the beginning of this chapter. An MFGS and an MFGD have been designed using the optimum shock absorber characteristics defined in section 4.3. Thus, taking the dimensions of the previous shock absorber (the shock absorber in NACA TN 2755 tests) as a reference, the dimensions of the MFGS and MFGD design will be evaluated compared.

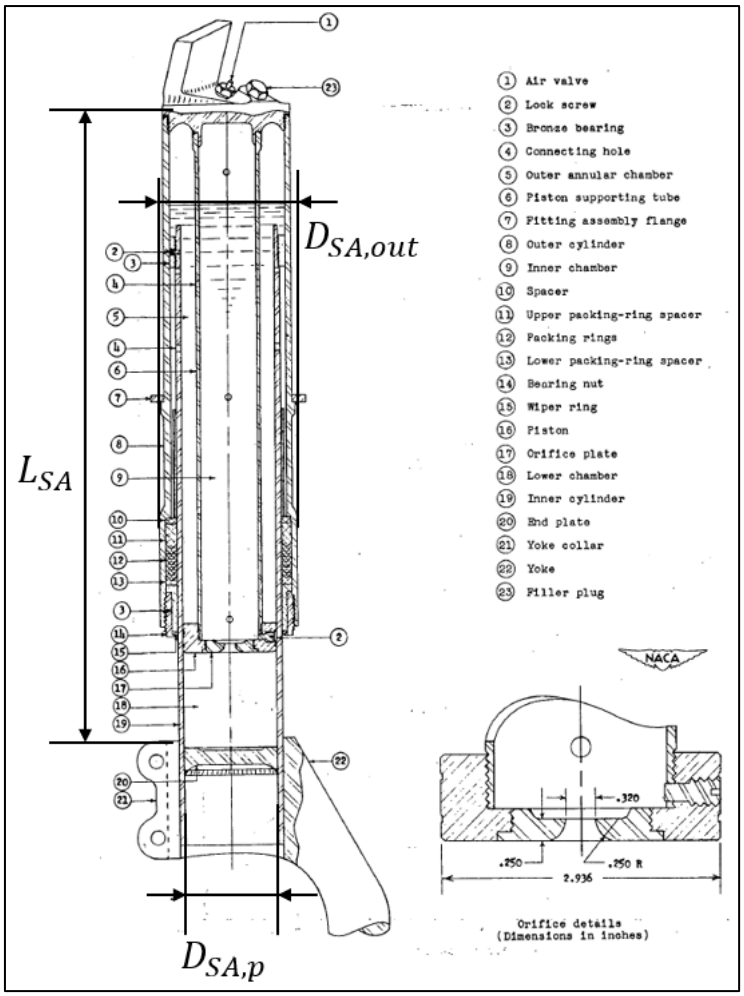

Figure 5.26. Shock absorber used in NACA tests [15]

Referring to Figure 5.26, the piston diameter of shock absorber assembly of NACA SA is given as

$$D_{SA,p,NACA} = 75.58\,mm \tag{5.52}$$

and outer diameter and length of the shock absorber assembly of NACA SA can be measured as

$$D_{SA,out,NACA} \cong 112\,mm \tag{5.53}$$

$$L_{SA,NACA} \cong 515\,mm \tag{5.54}$$

The installation of the MFGS and MFGD on the same link was previously explained in Section 5.1. Referring to Figure 5.2, the top view for the installation of MFGs with respect to dimensions determined previously is presented in Figure 5.27.

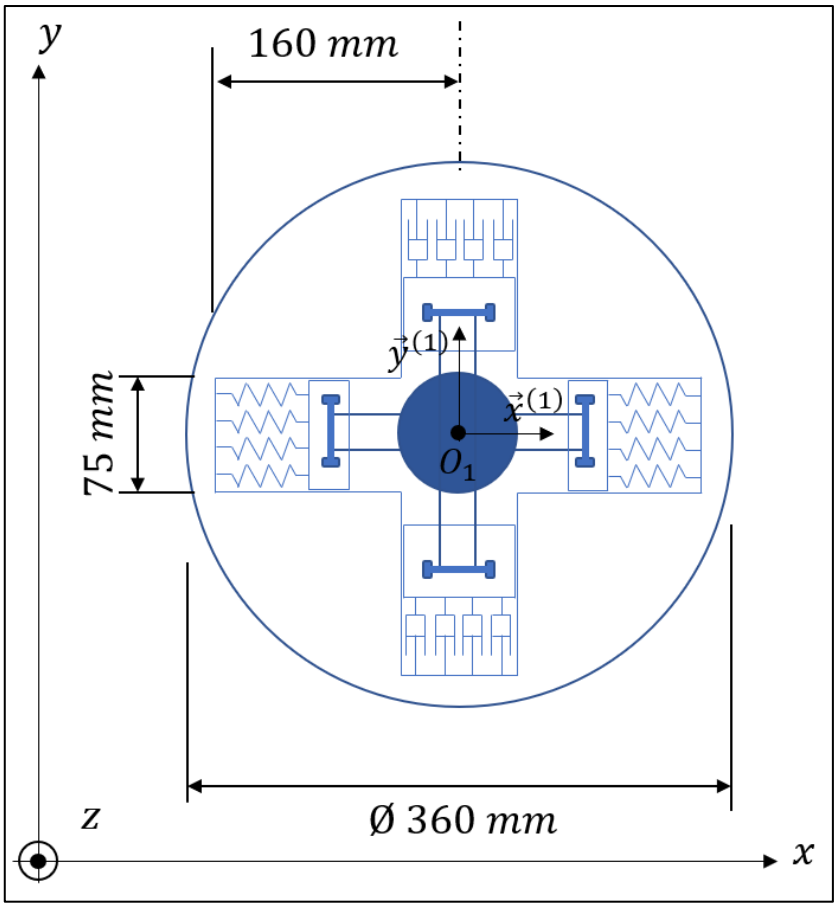

Figure 5.27. Installation of MFGS and MFGD, top view

During the installation of the mechanisms, some dimensions are required to be changed to prevent Link 3 of MFGS and Link 3 of MFGD from clashing. Thus, b_1 is changed as

$$b_1 = 160\ mm \tag{5.55}$$

and b_2 for MFGS and MFGD is changed accordingly.

The side view of the installation of MFGs is given in Figure 5.28.

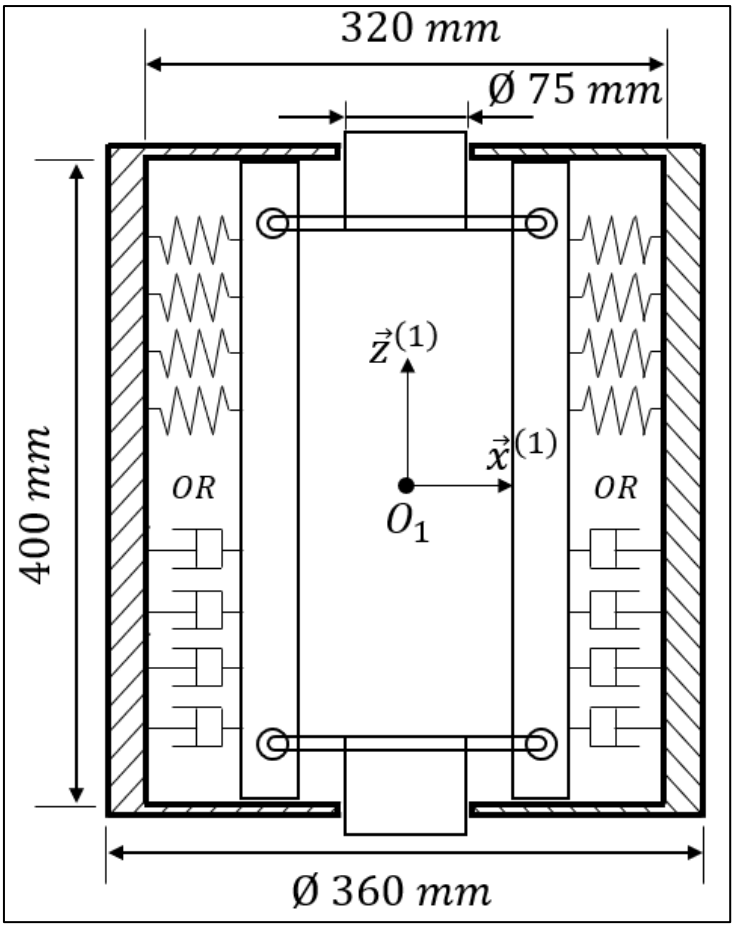

Figure 5.28. Installation of MFG, side view

Using the MFG assembly presented in Figure 5.27 and Figure 5.28, a landing gear assembly is prepared to compare with the shock absorber used in NACA. This assembly is presented in Figure 5.29.

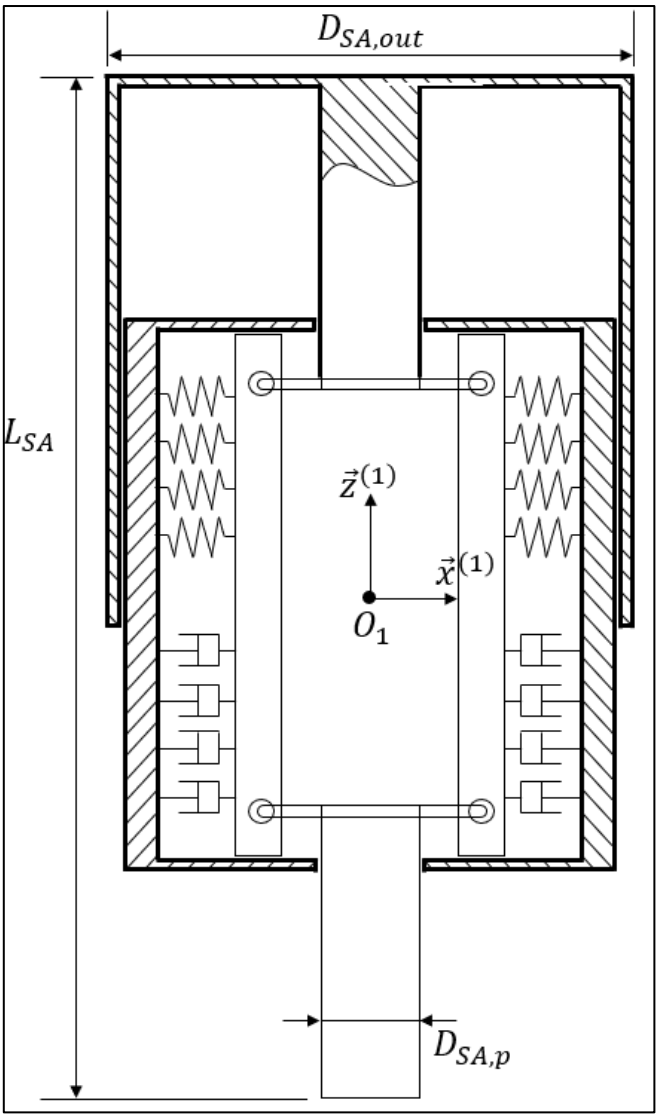

Figure 5.29. Shock absorber designed with MFG

Referring to Figure 5.29, the piston diameter of shock absorber assembly of shock absorber with MFG is defined as

$$D_{SA,p,MFG} = 75\ mm \tag{5.56}$$

and outer diameter and length of the shock absorber assembly with MFG is estimated (by giving credit to the thickness of structural parts) as

$$D_{SA,out,MFG} \cong 400\ mm \tag{5.57}$$

$$L_{SA,MFG} \cong 740\ mm \tag{5.58}$$

5.5 Dicussion on Design Outcome

At the beginning of this chapter, optimum shock absorber characteristics are taken as a reference to begin the design. Using a real spring, design of a real MFGS is aimed to check the feasibility and applicability of MFG's use on an aircraft landing gear. On the other hand, the damper design is aimed to be kept feasible.

After the design of the MFGS and MFGD, it has been observed that the travel of the MFG links (Link 3 and Link 5) are very small compared to the travel of the input links (Link 2 and Link 4). The main cause of this difference is keeping the shock absorber dimensions as small as possible to have a feasible shock absorber design that may fit inside the aircraft. The big difference between link travels causes the force transmission, from Links 3 and 5 to Links 2 and 4, to be very inefficient. Furthermore, inefficient force transmission may cause oversizing of components of MFG. On the other hand, even the smallest installation envelope is aimed, the shock absorber dimensions are resulted to be very big to install inside an aircraft.

CHAPTER 6

CONCLUSION

6.1 Summary

At the beginning of the thesis study, an introduction is performed to provide information about the general properties that are referred throughout the study. The Mechanical Force Generator and its particular properties are featured. Information on shock absorber design and aircraft landing gear design is introduced to give an understanding of the basis of the problem. The drop test procedure, which is widely used during the verification and modeling of aircraft landing gear design processes, is summarized. Guidance on the evaluation of the test results is performed.

Since shock absorber design of aircraft landing gear is a very specialized area, a literature review on shock absorber design is performed in Chapter 2. Being the commonly used design, the oleo-pneumatic type shock absorbers are described. Research is performed related to the problem defined at the beginning of the thesis study. Research studies on shock absorber efficiency are summarized and evaluated.

In Chapter 3, a design methodology for Mechanical Force Generator is developed. General properties and the components of a Mechanical Force Generator are described. Kinematic chains that will help the design of the slot shape of Mechanical Force Generators are defined. Loop closure equations are determined using these kinematic chains. Equations used in position and velocity analysis, which is applicable to any Mechanical Force Generator design, are defined. The use of Mechanical Force Generator as a non-linear spring and a non-linear damper are investigated. Two methods are introduced, for non-linear spring and non-linear damper, to determine the slot shape of the Mechanical Force Generator for any given parameters and force characteristics as a requirement. The assumptions used in these

methods are defined. The methods are mathematically presented step by step and clearly explained. As side information, the construction of a special spring, which may work both as a compression spring and a tension spring, is explained. Referring to the non-linear property of a Mechanical Force Generator Spring, properties of special spring cases with a quadratic coefficient are investigated. At the end of the chapter, examples of the slot shape determination are performed for Mechanical Force Generator Spring and Mechanical Force Generator Damper. For the given dimensions and force characteristics, the slot shapes are mathematically determined, the results and slot shapes are illustrated. With these examples, the mathematically derived methods are proven to be valid before their use in Chapter 5.

In Chapter 4, optimization of landing gear shock absorber characteristics is aimed. To perform this optimization, a spring mass damper model with 2 degrees of freedom is introduced. The validity of this model is evaluated with respect to a more detailed model prepared by the National Advisory Committee for Aeronautics which is prepared with test data. After the model and its equations of motion are explained, the objective of the optimization is defined. The optimization is sought to find the optimum spring coefficient and damper coefficient that will perform the best objective for the drop test conditions and parameters defined in the model used as a reference for model validation. Different methods to represent the non-linear characteristics of spring and damper are evaluated. As a result of this evaluation, "n^{th} order polynomial fitting passing through n+1 point" is chosen as the method. The constraints of the optimization are defined to limit the optimization for real and feasible solutions. At the end of the chapter, two different approaches to define the damper coefficient are followed: a damper coefficient as a function of velocity and a damper coefficient as a function of position. The results of different approaches are presented and evaluated. The definition of damper coefficient as a function of position gave better results and was taken as a reference for Mechanical Force Generator design for landing gear shock absorber.

In the last chapter, the design concept to install a Mechanical Force Generator Spring and a Mechanical Force Generator Damper on landing gear is introduced. Firstly,

using real springs, the spring part of the shock absorber was designed. Then, using the dimensions determined during spring design, the damper part of the shock absorber is designed. At the end of the chapter, the design of the shock absorber is compared with the shock absorber previously used in the reference documentation of the optimization. Evaluating the design of Mechanical Force Generators in this chapter and comparing the shock absorber design with the previous design, it is observed that the use of Mechanical Force Generator is not feasible for aircraft landing gear. Due to the very limited installation area of aircraft landing gear, the design ended up in very small force transmission angles, which causes inefficient use of space envelope. On the other hand, even the smallest installation envelope is aimed, the dimensions of the shock absorber resulted in larger than the previous shock absorber.

6.2 Conclusion and Recommendation

The Mechanical Force Generators are very flexible in terms of obtaining the desired spring and damper characteristics. Throught the study, it has been observed that these mechanisms are so flexible in design so that the system behaviour is not similar to usual springs or usual dampers. It is recommended for the future studies that the mechanical force generator itself does not require a fictitious property such as spring constant. So, the system design can purely focus on the force input and output to the mechanism.

On the other hand, when assembled, the mechanism required very large space envelope to operate for the shock absorber application. Space envelope is one of the major constraints of air vehicle design. Besides, a mechanical system with large number of component is not preferred in aeropace application due to their reliability and maintainability requirements. Thus, application of Mechanical Force Generator on landing gear shock absorbers is not feasible.

Referring to special spring cases described in Section 3.4.1, there may be different a uses of Mechanical Force Generators istead of aerospace industry. Since the mechanism requires large space envelope and large scaled systems such as construction or heavy duty machines can be good application fields of Mechanical Force Generators. Taking those application areas into consideration, evaluating Mechanical Force Generator as vibration isolators is a recommended field of study for future researches.

REFERENCES

[1] R. Soylu, “Mechanical force generator and related kinematic chains.,” *U.S. Pat. No. 10,738,863*, 2020.

[2] M. B. Ekinci, “Design and Experimental Analysis of Mechanical Force Generators for Performance Improvements of Machines,” *M. Sc. Thesis, Middle East Tech. Univ.*, no. August, 2019.

[3] U. Erdinç, “Dynamic Analysis, Design and Practical Applications of an Overconstrained Mechanical Force Generator,” *M. Sc. Thesis, Middle East Tech. Univ.*, vol. 4, no. December, pp. 9–15, 2017.

[4] H. Mencek, “Theoretical and Experimental Dynamic Performance Optimization of Planar Mechanisms Using Adjustment Systems and Mechanical Generators,” *Ph. D. Thesis, Middle East Tech. Univ.*, no. September, pp. 1–27, 2015.

[5] “Cessna 180 with conventional landing gear - shutterstock,” *Accessed on: Oct. 10, 2021. [Online]*. https://www.shutterstock.com/image-photo/cessna-180-skywagon-no-longer-produced-12933040

[6] “High-Quality Shots Of Unpainted Chinese J-20 Stealth Fighter Offer New Capability Insights,” *Accessed on: Jul. 5, 2021. [Online]*. https://www.thedrive.com/the-war-zone/22534/high-quality-shots-of-unpainted-chinese-j-20-stealth-fighter-offer-new-capability-insights

[7] J. Roskam, *Airplane Flight Dynamics and Automatic Flight Controls, Part II*. DARcorporation, 1998.

[8] Federal Aviation Administration, “Chapter 13 Aircraft Landing Gear Systems,” in *The Aviation Maintenance Technician Handbook – Airframe, Volume 2*, 2018.

[9] N. S. Currey, *Aircraft Landing Gear Design: Principles and Practices*. American Institute of Aeronautics and Astronautics, 1988.

[10] R. K. Schmidt, *The Design of Aircraft Landing Gear*. SAE International,

2021.

[11] A-5B Gears Struts and Couplings Commmitee, *Landing Gear Structural Requirements as Listed in the MIL-886X Series of Specifications, SAE AS8860A*. SAE International, 2012.

[12] European Aviation Safety Agency (EASA), “CS-25 certification specifications for large aeroplanes,” 2008.

[13] “Heroux Devtek - Landing Gear Drop Test Setup.” https://www.herouxdevtek.com/images/sections/sites_exploitation/st_hubert/DSC_0013.JPG

[14] Y. Li, J. Z. Jiang, S. A. Neild, and H. Wang, “Optimal inerter-based shock-strut configurations for landing-gear touchdown performance,” *J. Aircr.*, vol. 54, no. 5, pp. 1901–1909, 2017,

[15] B. Milwitzky and F. E. Cook, “Analysis of landing-gear behavior,” *Natl. Aeronaut. Sp. Adm. Washingt. DC*, 1953.

[16] J. R. McGehee and H. D. Carden, “A mathematical model of an active control landing gear for load control during impact and roll-out,” *Natl. Aeronaut. Sp. Adm.*, 1976.

[17] J. R. Mcgehee and R. C. Dreher, “Experimental Investigation of Active Loads Control for Aircraft Landing Gear,” *Natl. Aeronaut. Sp. Adm.*, 1982.

[18] G. L. Ghiringhelli, “Testing of semiactive landing gear control for a general aviation aircraft,” *J. Aircr.*, vol. 37, no. 4, pp. 606–616, 2000,

[19] J. H.-S. G. Mikulowski, “Adaptive Aircraft Shock Absorbers,” *AMAS Work. smart Mater. Struct. SMART*, vol. 3, pp. 63–72, 2003.

[20] C. Han, B. H. Kang, S. B. Choi, J. M. Tak, and J. H. Hwang, “Control of landing efficiency of an aircraft landing gear system with magnetorheological dampers,” *J. Aircr.*, vol. 56, no. 5, pp. 1980–1986, 2019,

[21] M. Z. Q. Chen, C. Papageorgiou, F. Scheibe, F. C. Wang, and M. Smith, “The missing mechanical circuit element,” *IEEE Circuits Syst. Mag.*, vol. 9,

no. 1, pp. 10–26, 2009,

[22] F. Shi, W. Isaac Anak Dean, and T. Suyama, “Single-objective Optimization of Passive Shock Absorber for Landing Gear,” *Am. J. Mech. Eng.*, vol. 7, no. 3, pp. 107–115, 2019,

[23] E. Söylemez, *Makina Teorisi - 1 Mekanizma Tekniği*. Birsen Yayınevi, 2000.

[24] A. Carrella, M. J. Brennan, and T. P. Waters, “Static analysis of a passive vibration isolator with quasi-zero-stiffness characteristic,” *J. Sound Vib.*, vol. 301, no. 3–5, pp. 678–689, 2007,

[25] A. Carrella, “Passive vibration isolators with high-static-low-dynamic-stiffness,” University of Southampton, 2008.

[26] A-5B Gears Struts and Couplings Committee, *Tests, Impact, Shock Absorber Landing Gear, Aircraft, SAE AS6053A*. SAE International, 2012.

[27] A. G. Barnes and T. J. Yager, “Enhancement of aircraft ground handling simulation capability,” *AGARD*, 1998, [Online]. Available: https://ntrs.nasa.gov/search.jsp?R=19990008563

[28] R. M. Lewis and V. Torczon, “Rank Ordering and Positive Bases In Pattern Search Algorithms,” no. 96, pp. 1–24, 1996, [Online]. Available: http://hdl.handle.net/2060/19970011189

[29] M. Mitchell, *An introduction to genetic algorithms*. MIT Press, 1998.

[30] J. C. Dixon, *The shock absorber handbook*. John Wiley & Sons, 2008.

[31] “Stock Compression Spring Catalogue,” *Accessed on: Oct. 5, 2021. [Online]*. https://www.thespringstore.com/media/download-pdf-entire/Stock-Compression-Spring-Catalog.pdf

APPENDICES

A. Spring Forces in MFGS when Link 4 is the Ground

Let MFG-4-gr denote the mechanism that is obtained from the MFG presented in Figure 3.1 by letting Link 1 to be free to move; and by making Link 4 to be the ground (i.e., Link 4 is not able to move). In other words, MFG-4-gr is obtained from MFG by using the method of kinematic inversion. Similar to MFGS, let 2 linear springs be attached between Links 1 and 3; and Links 1 and 5 of MFG-4-gr, yielding the mechanism which will be called to be MFGS-4-gr in this study. Similar to MFGS, MFGS-4-gr converts two real, linear, identical springs (with a constant stiffness) into an equivalent, virtual, nonlinear spring that is assumed to be attached between Links 2 and 4. Note that the virtual spring connects Link 2 to the ground (since Link 4 is fixed in MFGS-4-gr).

Furthermore, let the forces applied on Links 3 and 5 (by the 2 linear springs) be designated as $\vec{F}_{cha,spr,3}$ and $\vec{F}_{cha,spr,5}$ which are given by equations (3.33) and (3.34), respectively. Furthermore, let the force $\vec{F}_{MFG,spr,2,4-gr}$, applied on Link 2, be the force which is equivalent to the 2 spring forces $\vec{F}_{cha,spr,3}$ and $\vec{F}_{cha,spr,5}$. In other words, for rigid body mechanics purposes, one can delete the 2 spring forces $\vec{F}_{cha,spr,3}$, $\vec{F}_{cha,spr,5}$; and use the equivalent force $\vec{F}_{MFG,spr,2,4-gr}$ given by

$$\vec{F}_{MFG,spr,2,4-gr} = F_{MFG,spr,2,4-gr}\vec{k} \qquad \text{(A.1)}$$

instead (see Figure A.1). Here it should be noted that although the spring forces $\vec{F}_{cha,spr,3}$ and $\vec{F}_{cha,spr,5}$ are actual forces, the equivalent force $\vec{F}_{MFG,spr,2,4-gr}$ is fictitious.

In Figure A.1, m_L denotes the mass of a load that is placed on Link 2; and g denotes gravitational acceleration. L is the vertical distance between O_2 and m_L; and $s_{MFG,eq}$ is constant. H denotes a horizontal line attached rigidly to the ground. Note that, m_L,

g, L, $s_{MFG,eq}$ and H are not referred to in this Appendix. These symbols will be referred to in Section 3.4.1.4 while discussing spring case 4.

Neglecting gravitational, frictional and inertial effects, in order for the fictitious force $\vec{F}_{MFG,spr,2,4-gr}$ to be equivalent to the two spring forces $\vec{F}_{cha,spr,3}$ and $\vec{F}_{cha,spr,5}$, the instantaneous power due to $\vec{F}_{MFG,spr,2,4-gr}$ must be equal to the sum of the instantaneous powers due to $\vec{F}_{cha,spr,3}$ and $\vec{F}_{cha,spr,5}$ at all times, i.e.,

$$\vec{F}_{MFG,spr,2,4-gr} \cdot \vec{v}_2 = \vec{F}_{cha,spr,3} \cdot \vec{v}_3 + \vec{F}_{cha,spr,5} \cdot \vec{v}_5 \tag{A.2}$$

where $\vec{v}_2$, $\vec{v}_3$ and $\vec{v}_5$ are the absolute velocities of Links 2, 3 and 5, respectively, given by

$$\vec{v}_2 = \vec{v}_1 + \vec{v}_{2/1} \tag{A.3}$$

$$\vec{v}_3 = \vec{v}_1 + \vec{v}_{3/1} \tag{A.4}$$

$$\vec{v}_5 = \vec{v}_1 + \vec{v}_{5/1} \tag{A.5}$$

In equations (A.3) – (A.5), $\vec{v}_1$ denotes the absolute velocity of Link 1. Furthermore, $\vec{v}_{2/1}$, $\vec{v}_{3/1}$ and $\vec{v}_{5/1}$ are the relative velocities, with respect to Link 1, of Links 2, 3 and 5, respectively, where

$$\vec{v}_1 = \dot{s}_{MFG}\vec{k} \tag{A.6}$$

$$\vec{v}_{2/1} = \dot{s}_{MFG}\vec{k} \tag{A.7}$$

$$\vec{v}_{3/1} = \dot{s}_{cha}\vec{\imath} \tag{A.8}$$

$$\vec{v}_{5/1} = -\dot{s}_{cha}\vec{\imath} \tag{A.9}$$

Substituting equations (A.1), (3.33), (3.34) and equation (A.3) – (A.8) into equation (A.2), and simplifying, one obtains

$$-F_{cha,spr}\dot{s}_{cha} = F_{MFG,spr,2,4-gr}\dot{s}_{MFG} \tag{A.10}$$

Now, comparing equation (A.10) with equation (3.48), it follows that

$$F_{MFG,spr,2,4-gr} = F_{MFG,spr} \tag{A.11}$$

Hence, the design procedure (for determination of the slot shape for MFGS) presented in Section 3.2.1 is also applicable for the determination of the slot shape for MFGS-4-gr. In order to apply the design procedure in Section 3.2.1 for MFGS-4-gr, one needs to replace $F_{MFG,spr}$ in equation (3.40) with $F_{MFG,spr,2,4-gr}$. Indeed, the user defined function $k_{MFG}[s_{MFG}]$ and the user defined parameter $l_{0,MFG}$ that appear in equation (3.40) should be selected such that the equivalent spring force $F_{MFG,spr,2,4-gr}[s_{MFG}]$ is generated in the desired manner.

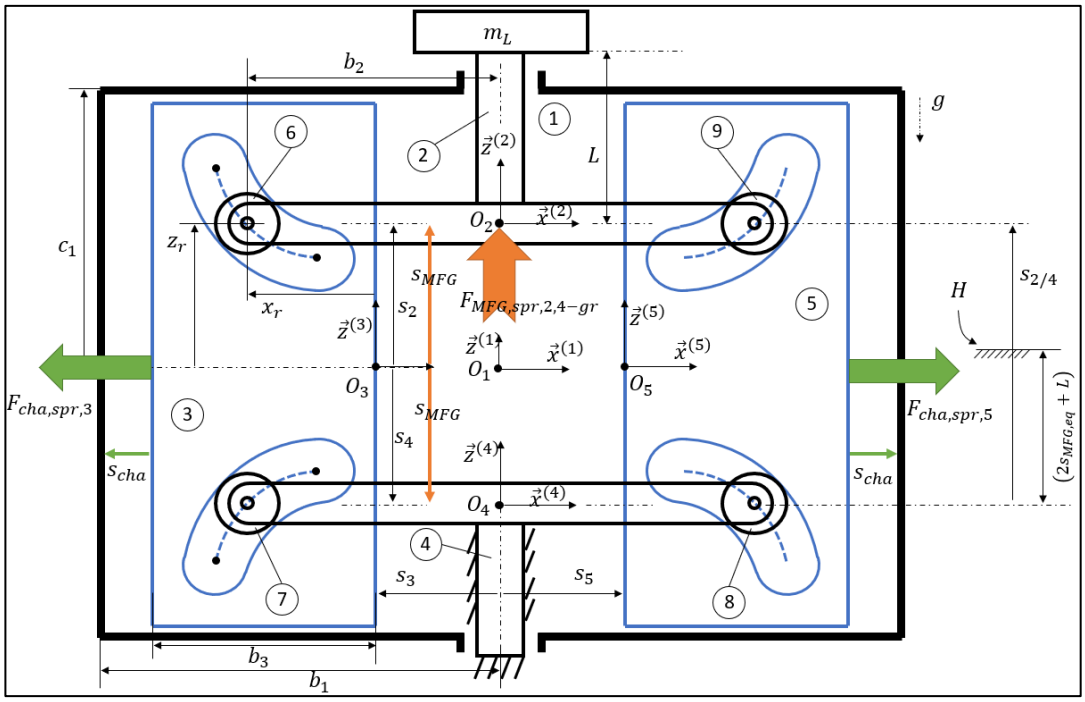

Figure A.1. Spring forces acting on MFGS-4-gr

B. Spring Forces in MFGS when there are no Grounded Links

Let MFG-no-gr denote the kinematic chain from which the MFG mechanism presented in Figure 3.1 is obtained. In other words, none of the links, including Link 1, is grounded in MFG-no-gr. Similar to MFGS, let two linear springs be attached between Links 1 and 3; and Links 1 and 5 of MFG-no-gr, yielding the kinematic chain which will be called to be MFGS-no-gr in this study. Similar to MFGS, MFGS-no-gr converts two real, linear, identical springs (with a constant stiffness) into an equivalent, virtual, nonlinear spring that is assumed to be attached between Links 2 and 4. Let the spring forces acting on MFGS-no-gr be as presented in Figure 3.5 where the definition of the forces $\vec{F}_{cha,spr,3}$, $\vec{F}_{cha,spr,5}$, $\vec{F}_{MFG,spr,2}$ and $\vec{F}_{MFG,spr,4}$ are identical with the definitions that are used in Section 3.2.

Neglecting gravitational, frictional and inertial effects, in order for the fictitious forces $\vec{F}_{MFG,spr,2}$ and $\vec{F}_{MFG,spr,4}$ to be equivalent to the two spring forces $\vec{F}_{cha,spr,3}$ and $\vec{F}_{cha,spr,5}$, the sum of the instantaneous powers due to the fictitious forces $\vec{F}_{MFG,spr,2}$ and $\vec{F}_{MFG,spr,4}$ must be equal to the sum of the instantaneous powers due to the real forces $\vec{F}_{cha,spr,3}$ and $\vec{F}_{cha,spr,5}$ at all times, i.e.,

$$\vec{F}_{MFG,spr,2} \cdot \vec{v}_2 + \vec{F}_{MFG,spr,4} \cdot \vec{v}_4 = \vec{F}_{cha,spr,3} \cdot \vec{v}_3 + \vec{F}_{cha,spr,5} \cdot \vec{v}_5 \quad \text{(B.1)}$$

where $\vec{v}_2$, $\vec{v}_3$, $\vec{v}_4$ and $\vec{v}_5$ are the absolute velocities of Links 2, 3, 4 and 5, respectively, given by

$$\vec{v}_2 = \vec{v}_1 + \vec{v}_{2/1} \quad \text{(B.2)}$$

$$\vec{v}_3 = \vec{v}_1 + \vec{v}_{3/1} \quad \text{(B.3)}$$

$$\vec{v}_4 = \vec{v}_1 + \vec{v}_{4/1} \quad \text{(B.4)}$$

$$\vec{v}_5 = \vec{v}_1 + \vec{v}_{5/1} \quad \text{(B.5)}$$

In equations (B.2) – (B.5), $\vec{v}_1$ denotes the absolute velocity of Link 1 which is not necessarily zero (as opposed to MFGS). Furthermore, $\vec{v}_{2/1}$, $\vec{v}_{3/1}$, $\vec{v}_{4/1}$ and $\vec{v}_{5/1}$ are

the relative velocities with respect to Link 1, of Links 2, 3, 4 and 5, respectively, where

$$\vec{v}_{2/1} = \dot{s}_{MFG}\vec{k} \tag{B.6}$$

$$\vec{v}_{3/1} = \dot{s}_{cha}\vec{\imath} \tag{B.7}$$

$$\vec{v}_{4/1} = -\dot{s}_{MFG}\vec{k} \tag{B.8}$$

$$\vec{v}_{5/1} = -\dot{s}_{cha}\vec{\imath} \tag{B.9}$$

Substituting equations (B.2) – (B.9) into equation (B.1), and simplifying, one obtains

$$-F_{cha,spr}\dot{s}_{cha} = F_{MFG,spr}\dot{s}_{MFG} \tag{B.10}$$

which is identical with equation (3.48). Hence, the design procedure (for determination of the slot shape for MFGS) presented in Section 3.2.1 is also applicable for the determination of the slot shape for MFGS-no-gr.

C. Spring Catalogue Detail Information

Spring Stock Part Numbers

Spring ID	*Stock Part Number*
CS1	PC9195-48412-4750-OT-65786-CG-N-MM
CS2	PC6858-31344-6000-MW-50800-CG-N-MM
CS3	PC7925-41275-4000-MW-41402-CG-N-MM
CS4	PC6350-24994-8000-MW-62738-CG-N-MM
CS5	PC9525-37287-4750-MW-55626-CG-N-MM
CS6	PC6350-33325-3500-MW-28702-CG-N-MM
CS7	PC6655-45237-3000-HD-36576-CG-N-MM